



universität
wien

MASTERARBEIT

Titel der Masterarbeit

„Characterization of Cell Populations in Ascites of
Ovarian Cancer Patients“

verfasst von

Katharina Auer BSc

angestrebter akademischer Grad

Master of Science (MSc)

Wien, 2013

Studienkennzahl lt. Studienblatt:

A 066 877

Studienrichtung lt. Studienblatt:

Masterstudium Genetik und Entwicklungsbiologie

Betreuer:

A.o.Univ.Prof.Dr. Wolfgang Mikulits

Preamble

A lot of data were generated in the course of this master thesis and therefore I would like to mention and thank the people that supported me in this study: Anna Bachmayr-Heyda, Stefanie Aust, and Dietmar Pils helped in processing the obtained biomaterials, Agnes Reiner generated the libraries for RNA-seq, Dietmar Pils furthermore annotated the sequencing data and showed and helped me with the functional annotations and the statistical calculations. Eva Schuster and Elisabeth Maritschnegg provided me with data about the mutation status of the patients' tumors and all other colleagues in the Molecular Oncology Group always supported me with everything I lost, broke, or forgot.

Katharina Auer

Table of Contents

1	Introduction	1
1.1	Overview	1
1.2	Ovarian cancer	1
1.3	Origin	3
1.4	Metastatic process and EMT.....	3
1.5	Cell surface markers	4
1.5.1	EpCAM.....	4
1.5.2	CD44.....	5
1.5.3	CD133 (prominin-1).....	5
1.5.4	L1CAM.....	6
1.5.5	CD45 (PTPRC).....	6
1.6	Mutation status.....	6
1.7	Molecular subclassification	7
1.8	Mode of tumor spread.....	8
1.9	Working hypothesis	9
1.10	Aim of the project	10
2	Material and Methods.....	11
2.1	Clinicopathological factors	11
2.2	Patients' material	11
2.2.1	Blood	11
2.2.2	Tumor tissue	11
2.2.3	Ascites	12
2.3	Embedding of ascites	12
2.4	Cryopreservation and thawing	13
2.5	Enrichment of tumor/ immune cells (Magnestat)	13
2.6	Isolation of RNA.....	14
2.7	RNA-Seq.....	15

2.7.1	Library preparation and sequencing	15
2.7.2	Statistical analysis and functional annotation.....	15
2.8	Flow Cytometry (FC).....	17
2.8.1	Antibodies.....	17
2.8.2	Antibody titration and condition testing.....	17
2.8.3	Disintegration of ascitic cell aggregates.....	18
2.8.4	Staining.....	19
2.8.5	Gating	19
2.8.6	Statistics.....	20
2.9	Immunofluorescence.....	20
2.9.1	Antibodies.....	20
2.9.2	Staining Procedure.....	21
3	Results	22
3.1	Overview.....	22
3.2	Processing of Ascites	23
3.3	Flow Cytometry	24
3.3.1	Gating	24
3.3.2	Correlations	27
3.3.3	Specimen and cell populations	28
3.3.4	Principal Component Analysis	35
3.3.5	Correlation of cell frequencies with presence of spheroids.....	37
3.3.6	Correlation with peritoneal tumor spread.....	41
3.3.7	Correlation with presence of ascites.....	47
3.3.8	Correlation with mutation status	48
3.4	Transcriptome Analysis	50
3.4.1	RNA Preparation	50
3.4.2	RNA-Seq and Functional Annotation	50
3.5	Immunofluorescence.....	62

4	Discussion.....	64
4.1	Sample preparation and spheroid digest	64
4.2	Flow cytometry	65
4.3	Presence of spheroids in ascites.....	67
4.4	Mode of peritoneal tumor spread.....	68
4.5	Presence of ascites	69
4.6	Mutation status.....	69
4.7	Molecular subclassification	70
4.8	Immunofluorescence.....	71
5	Conclusion.....	72
5.1	Limitations of the study/outlook.....	72
6	List of Abbreviations.....	74
7	References	76
8	Supplementary data	82
9	Acknowledgements	98
10	Abstract.....	99
11	Zusammenfassung	100
12	Curriculum vitae	101

1 Introduction

1.1 Overview

Ovarian cancer is the sixth leading cause of death among women with malignancies worldwide and the leading cause of death from gynecological cancers. (Jemal, Bray et al. 2011). Reasons for this bad outcome are the advanced stage of tumor progression at first diagnosis due to an asymptomatic course of the disease and the great extent of tumor implants within the peritoneal cavity, partly due to massive production of peritoneal fluid (ascites), providing a specific tumor microenvironment. Current treatment strategies involve primary cytoreductive surgery followed by platinum and taxane based chemotherapy (International Collaborative Ovarian Neoplasm 2002). Although there is an initial response to chemotherapy, patients with advanced stages will be most likely to relapse (25 % even within six month after initial treatment (Colombo, Van Gorp et al. 2006)) and finally develop platinum resistance. This and the late diagnosis account for a median survival rate of only 4.5 years over all stages. Optimal debulking surgery with minimal or no residual tumor is still the best prognostic factor.

For a better understanding of the disease, the main goal of this study is the characterization of tumor cell populations in the ascites, and linking it to the mode of tumor spread, mutation status, and molecular subclasses, allowing for prediction of the intraperitoneal situation, and examining the prognostic value of the ascites cell composition.

1.2 Ovarian cancer

Although there are other tumors comprising the ovaries like germ cell tumors or stromal sex chord tumor, 80 % of malignant neoplasms account for the epithelial subtype of ovarian cancer, named after the predominant epithelial cell type. According to histologic and cytological features, epithelial ovarian cancer can also be subdivided into serous, mucinous, endometrioid, clear cell, and mixed subtypes. Because of the glandular or papillary architecture the most common subtype is also referred to as serous papillary (Lengyel 2010).

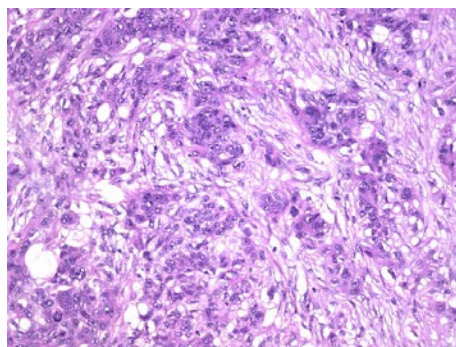


Figure 1. High grade adenocarcinoma with serous papillary histology invading the ovarian stroma. (Image taken from <http://www.webpathology.com/image.asp?case=525&n=21>; 1.8.2013)

The International Federation of Obstetricians and Gynaecologists (FIGO) defined an international staging system (FIGO stages), describing the size and spread of the tumor. It consists of four different major stages and substages (Odicino, Pecorelli et al. 2008). See Table 1.

Table 1. FIGO staging of ovarian carcinoma (Benedet, Bender et al. 2000)

<u>FIGO stage</u>	<u>Tumor characteristics</u>
I	Tumor confined to ovaries
IA	Tumor confined to one ovary, intact capsule, no tumor on surface of ovary, no malignant cells in ascites or peritoneal washing
IB	Tumor limited to both ovaries, rest as above
IC	Tumor limited to both ovaries, with any of the following: ruptured capsule, tumor on surface of ovary, malignant cells in ascites or peritoneal washing
II	Tumor on one or both ovaries and pelvic extension
IIA	Extensions/and or metastatic implants on uterus and/or fallopian tubes, no malignant cells in ascites or peritoneal washing
IIB	Extensions and/or implants in other pelvic organs, no malignant cells in ascites or peritoneal washing
IIC	one of the above (A or B) with malignant cells in ascites or peritoneal washing
III	Tumor on one or both ovaries with confirmed peritoneal metastasis outside the pelvis and/or metastasis in regional lymph nodes.
IIIA	Microscopic peritoneal metastasis outside the pelvis
IIIB	Macroscopic peritoneal metastasis outside the pelvis, up to 2cm in size
IIIC	Peritoneal metastasis outside the pelvis bigger than 2cm and/or regional lymph node metastasis
IV	Stage IV: Distant metastasis outside the peritoneal cavity

Furthermore, upon pathohistologic inspection of biopsied or debulked tumor tissue the degree of differentiation is assessed with a grading scheme consisting of G1 (low grade) for well differentiated tumor cells, G2 (intermediate grade) for intermediate differentiation of the tumor cells, and G3 (high grade) for low differentiated tumor cells.

1.3 Origin

The site of origin of epithelial ovarian carcinomas is still under debate. Although the ovarian surface epithelium was originally thought to give rise to serous carcinomas, new evidence accumulates that the epithelium of the fimbriae of the fallopian tube could be the site of origin of ovarian cancer. The surface of the ovary consists of a single layer of cells, the epithelium, that can get trapped in inclusion cysts due to frequent rounds of ovulation and surface repair which might contribute to malignant transformation (incessant ovulation theory) (Lengyel 2010). Widespread evidence suggests that the site of origin lies within the fallopian tube. Piek et al. (Piek, van Diest et al. 2001) and Kindelberger et al. (Kindelberger, Lee et al. 2007) observed, that BRCA mutated patients and patients with pelvic serous carcinomas often showed tubal intraepithelial carcinomas. Also a combination of these two sites is imaginable: epithelial cells of the tip of the fimbriae could implant on the naked surface of the ovary, leading to formation of inclusion cysts, which are transforming in the ovarian microenvironment (Kurman and Shih 2010). See figure 2.

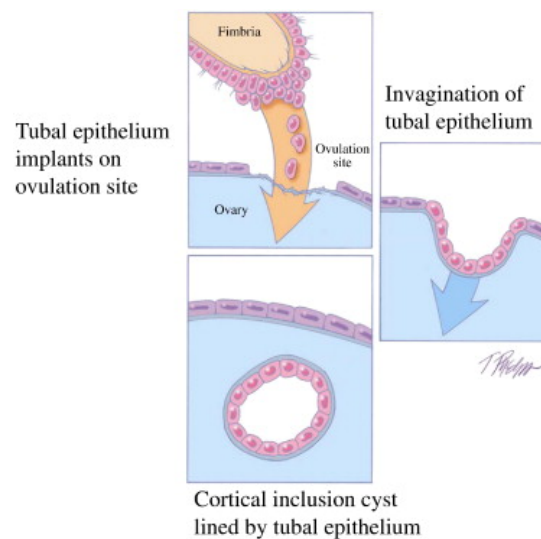


Figure 2. Theory of fimbriae and OSE involvement in origin of ovarian carcinoma
(Figure taken from <http://www.ncbi.nlm.nih.gov/pmc/articles/PMC2841791/>; 20.7.2013)

1.4 Metastatic process and EMT

In contrast to other tumors in the human body like breast cancers, ovarian tumor cells metastasize predominantly in the peritoneal cavity through the peritoneal fluid called ascites. Tumor cells shed off the primary tumor as single cells or aggregates and travel through the ascites in a rather passive way to the peritoneum that covers all organs within the peritoneal cavity. But it is still unclear if ascites is present, when the tumor cells first metastasize or if the peritoneal implants themselves are involved in ascites produc-

tion by blocking subperitoneal lymphatic channels, and elevated expression of VEGF, increasing the permeability of the peritoneum (Herr, Sallmann et al. 2012). Studies have shown that extraperitoneal metastases are rare and occur predominantly at very advanced time points of the disease (Tarin, Price et al. 1984), although involvement of local lymph nodes is common.

Once shed into the ascitic fluid, cells have to deal with an important hallmark of cancer, called anoikis, in order to metastasize. Anoikis is a specialized form of programmed cell death that anchorage dependent cells undergo upon losing cell-cell or cell-matrix contacts. Relating to epithelial ovarian cancer cells in the ascites, this could be a reason for aggregation of tumor cells as described by Allen et al. (Allen, Porter et al. 1987), although also single tumor cells can be found in the ascites and have been isolated in former studies (Allen, Porter et al. 1987). Resistance to anoikis can also be derived by epithelial to mesenchymal transition (EMT) (Taddei, Giannoni et al. 2012). So far it is unknown, whether single tumor cells, tumor cell aggregates or a combination of both adhere to the single layer of epithelial cells of the peritoneum, called mesothelium, to form metastases. Also the role of the immune system in preparing or preventing the mesothelial cells for or from tumor cell adherence, is still under debate (Melichar and Freedman 2002).

1.5 Cell surface markers

The characterization of cells in the ascites was done by multicolor flow cytometry using five different antibodies against known antigens on the surface of tumor and immune cells.

1.5.1 EpCAM

The epithelial cell adhesion molecule (EpCAM, CD326) is a glycoprotein encoded by the gene *GA-733-2* or *EPCAM* on chromosome 2. EpCAM is expressed on the surface of epithelial cells present in a variety of epithelia including epithelial carcinomas, such as epithelial ovarian cancer. An exception is the squamous epithelium covering the peritoneum and internal organs, the mesothelium. The cell adhesion marker is primarily expressed on the basolateral surface of epithelial cells and often overexpressed in carcinomas (van der Gun, Melchers et al. 2010), making it a good candidate as diagnostic or tumor cell marker. The major functions involve homophilic calcium-independent cell-cell adhesion and signal transduction (Rao, Chianese et al. 2005). The inner lining of the fallopian tubes, as well as the surface lining of the ovaries, is made from epithelium,

evolutionary originating from mesoderm (Piek, Kenemans et al. 2004) and thus prone to overexpress EpCAM after malignant transformation.

1.5.2 CD44

CD44 (Hermes) is a transmembrane glycoprotein encoded by the *CD44* gene on chromosome 11. It plays an important role in cell migration and cell adhesion because of its receptor function for hyaluronic acid (HA) and other components of the extracellular matrix (ECM) like collagen, fibronectin, laminin, etc. This cell surface adhesion protein is structured in an extracellular HA-binding domain, a cytoplasmic domain that is associated with the cytoskeleton via protein mediated actin binding (Fujita, Kitagawa et al. 2002), and a membrane-proximal region of variable length, accounting for multiple isoforms. These different isoforms are present on a variety of cells including leukocytes, mesothelial cells and to varying degrees also on tumor cells (Naor, Sionov et al. 1997). A specific non-sticky HA is expressed by the monolayer of mesothelial cells lining the peritoneum, and it remains questionable if specific isoforms of CD44 are capable of binding to this HA or if tumor initiation in the peritoneum starts with the adhesion to the underlying ECM. In breast cancers, CD44 together with other surface markers like CD24 was shown to characterize a side-population of tumor cells, resistant to chemotherapy and capable of reinitiation of tumors. Therefore CD44 is denoted as cancer stem cell (CSC) marker (Al-Hajj, Wicha et al. 2003).

1.5.3 CD133 (prominin-1)

CD133 or Prominin-1 is a 5-transmembrane domain molecule with a molecular weight of 120 kD and eight consensus sequences for glycosylation in the two extracellular loops (Miraglia, Godfrey et al. 1997). It is encoded by the gene *PROM1*.

CD133 is described as a putative marker for cancer stem cells (CSCs) in a variety of human tumors, including colon carcinoma (O'Brien, Pollett et al. 2007), hepatocellular carcinoma (Yin, Li et al. 2007), and renal tumors (Bruno, Bussolati et al. 2006). In ovarian cancer the subpopulation of CD133+ cells was found to have increased tumorigenic potential and recapitulated the original heterogeneous tumor when propagated in NOD/SCID mice. (Curley, Therrien et al. 2009). As the most important prognostic factor of epithelial ovarian cancer (EOC) is the residual tumor mass after primary debulking surgery (Bristow, Tomacruz et al. 2002), and upon recurrence many tumors have developed chemotherapy resistance, it might be speculated, that a distinct population of cells, capable of evading chemotherapy, is rebuilding the tumor mass.

1.5.4 L1CAM

L1-cell adhesion molecule (L1CAM) or neuronal cell adhesion molecule L1 is a 200-220 kD transmembrane protein, first described in neuronal cells where it is involved in axon growth and guidance (Schachner 1997). The corresponding gene *L1CAM* is located on chromosome X, elevated expression is described in various tumor entities and correlates with advanced-stage disease and metastasis (Raveh, Gavert et al. 2009). L1 has a variety of binding partners, including integrins, other immunoglobulin super family members, and itself (homophilic) (Brummendorf, Kenwrick et al. 1998). Previous studies have shown that the MAP kinase signaling pathway is associated with L1 expression (Poplawski, Tranziska et al. 2012) and L1CAM overexpression in tumor cells induces NF-kB activation by increasing the IL-1beta expression (Kiefel, Bondong et al. 2010). L1CAM expression is furthermore associated with epithelial to mesenchymal transition (EMT), shown in experiments proving the up-regulation of L1 expression upon treatment of cultured cancer cells with the EMT inducer TGF-beta (Kiefel, Bondong et al. 2012).

1.5.5 CD45 (PTPRC)

Cluster of differentiation 45 (CD45), formerly leukocyte common antigen (LCA) is encoded by the *PTPRC* gene on chromosome 1. The molecule belongs to the family of protein tyrosine phosphatases (PTP) and is required for the activation of T-cells (from http://www.ncbi.nlm.nih.gov/gene?cmd=Retrieve&dopt=full_report&list_uids=5788; 20.7.2013). Antibodies directed against CD45 are used as pan immune cell marker, due to its presence on all nucleated leukocytes and applications for flow cytometry involve discrimination of leukocytes from tumor cells in ascites and tumor tissue (Hristozova, Konschak et al. 2012).

1.6 Mutation status

Recent findings on genetic alterations associated with ovarian cancer suggest two different ways of carcinogenesis, rendering two types of cancers, Type I and Type II: Low grade serous, mucinous and endometrioid cancers exhibiting mutations in the genes for KRAS and BRAF often show slow tumor growth, mostly confined to the adnexa (type I) whereas high grade serous, mixed and undifferentiated carcinomas tend to be genetically unstable, show aggressive growth, and harbor mutations in the *TP53* gene (type II) (Lalwani, Prasad et al. 2011).

TP53 is a very prominent tumor suppressor gene; the 11 exons comprising sequence encodes a nuclear phosphoprotein involved in cell-cycle control, apoptosis, differentia-

tion, chromosome segregation, DNA recombination, and cellular senescence (Hofseth, Hussain et al. 2004). Mutations of the *TP53* gene often cluster between evolutionarily conserved exons 5 and 8 in human cancers and produce altered proteins (Hollstein, Sidransky et al. 1991). As the mutations are often missense and observed to affect the DNA binding domain (Berns, van Staveren et al. 1998), the oligomerization of altered proteins with the wildtype p53 accumulates inactive protein cluster (Silva, Rangel et al. 2013). In advanced stage ovarian cancer, mutations in *TP53* are frequent and associated with reduced overall survival (Smith-Sorensen, Kaern et al. 1998).

Furthermore, mutations in the *KRAS* gene are common in ovarian cancer (Nakayama, Nakayama et al. 2008). Ras proteins are small GTPases that lay downstream of the EGF receptor in the signaling cascade and function as signal transducers in pathways controlling cell proliferation and differentiation. Mutations of the *KRAS* gene are predominantly located at codons 12, 13 and 61 and lead to a state of permanent active ras protein, finally promoting cell proliferation and malignant transformation (Bos 1989). A study by us (Auner, Kriegshauser et al. 2009), screening 403 malignant and 394 benign ovarian tissue samples at the Medical University of Vienna found mutations at codon 12 and 13 in 15 % of the cases. Mutations were more frequent in borderline tumors than in carcinomas and furthermore overrepresented in the mucinous histotype in contrast to serous carcinomas.

1.7 Molecular subclassification

Similar to molecular subclassification approaches in breast cancer (Perou, Sorlie et al. 2000) (Nielsen, Parker et al. 2010) several attempts to classify epithelial ovarian cancer according to its molecular signature instead of or in addition to clinicopathological parameters like FIGO stage, grade, and residual tumor after primary debulking surgery, were made over the past years (De Cecco, Marchionni et al. 2004) (Tothill, Tinker et al. 2008). However, applicability to the clinical practice remained limited due to reduced statistical power of the analysis as a result of excluding missing data that could account for a selectable subgroup from small sample sizes or missing prognostic value (Clark, Stewart et al. 2001).

Yoshihara et al. established a new molecular subclassification of advanced stage ovarian carcinomas in 2009 using gene expression profiles. It distinguishes advanced stage EOC into two subclasses: subclass 1) consisting of patients with characteristics of less advanced EOC (all FIGO II tumors and FIGO III/IV carcinomas with better overall and progression free survival) and subclass 2) consisting of patients with different character-

istics and worse outcome (FIGOIII/IV carcinomas, association with peritoneal carcinomatosis, non-optimal debulking, and ultimately lower overall survival). The gene set used for this subclassification could be narrowed down to a molecular signature consisting of 112 genes, differentially expressed between the two groups and predicting prognostic factors (Yoshihara, Tajima et al. 2009). This study has been validated in our laboratory with a substantially higher number of patients, to test its applicability in the clinic, with regard to clinicopathological factors, gene expression profiles and outcome. (Pils, Hager et al. 2012).

During the course of my master thesis the 112 gene signature was also applied for analysis of patient samples in order to find differences and overlaps between evaluated patient groups.

1.8 Mode of tumor spread

As the cancer spreads from the ovaries or the fallopian tube to the peritoneum, different modes of re-implantation of tumor cells and therefore different tumor patterns on secondary sites can be observed. One type of metastatic spread is a miliary spread, whereby small, planar tumor cell implants are distributed all over a peritoneal area (e.g. the diaphragm or even the whole peritoneum). Those miliary tumor lesions are usually present in large numbers and were described as *miliary spread* in this study (Fig. 3B, see Material and Methods, Clinicopathological factors). A study conducted by Gosein et al. (Gosein, Narinesingh et al. 2013) found a similar pattern of miliary lesions in a number of female patients with ascites and elevated levels of CA-125, initially diagnosed with ovarian cancer but upon surgical inspection found to suffer from tuberculosis peritonitis. These results suggest a significant role of ascites in metastatic spread, irrespective of the origin. Furthermore, the importance of analyzing the peritoneal fluid for malignant cells becomes clear.

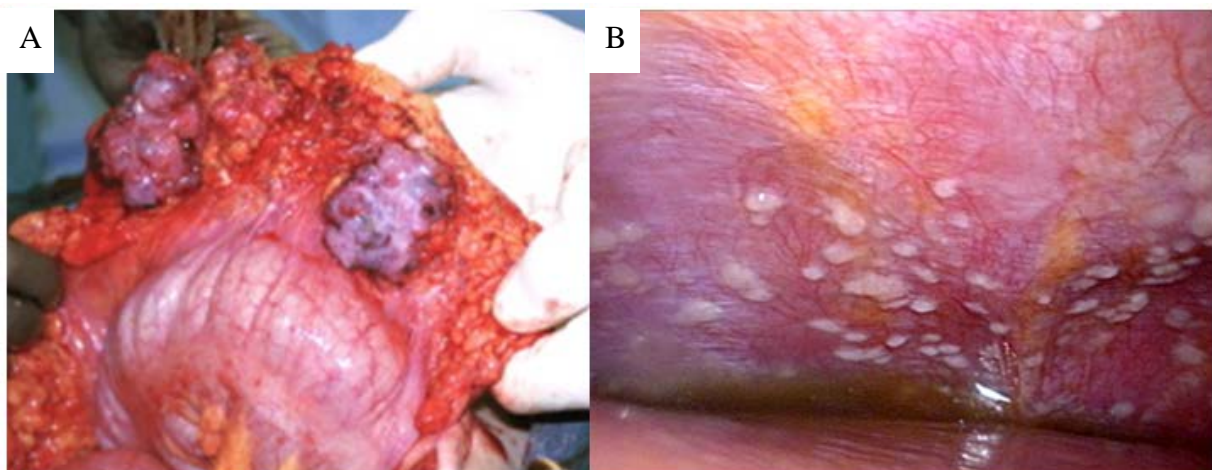


Figure 3. (A) Big nodular implants on the greater omentum, (B) miliary tumor spread on the diaphragm
(Image A taken from <http://img.medscape.com/pi/emed/ckb/oncology/276262-1340230-255771-1907403tn.jpg>, 20.7.2013)

The other type of EOC tumor spread observed in the peritoneal cavity is comprised of fewer and more exophytic growing tumor lesions. The aspect of these lesions is rather bulky, as distinct from the planar, miliary spread. Those large tumor masses are here referred to as *few, big implants* (Fig. 3A, see Material and Methods, Clinicopathological factors).

1.9 Working hypothesis

Observing differences in lymphatic involvement and peritoneal tumor spread in ovarian cancer patients, we saw a trend towards two distinct modes of tumor spread: a large peritoneal spread of miliary lesions and few, but bigger, exophytic growing tumor nodules. We hypothesized that differences in the clinically observable tumor spread are promoted by the immune status in the peritoneal cavity, triggered by the tumor and/or tumor microenvironmental factors. Figure 4 depicts a scheme of the working hypothesis: A) some patients show high inflammation in the peritoneum, resulting in an implan-tation-prone (“stressed”) mesothelium, B) some patients present with rather low or absent inflammation in the peritoneal cavity, whereby the mesothelium seems resistant to tumor implantation (due to secretion of anti-adhesive factors, etc.). In these patients, the tumor cells form no or only few implants in the peritoneal cavity.

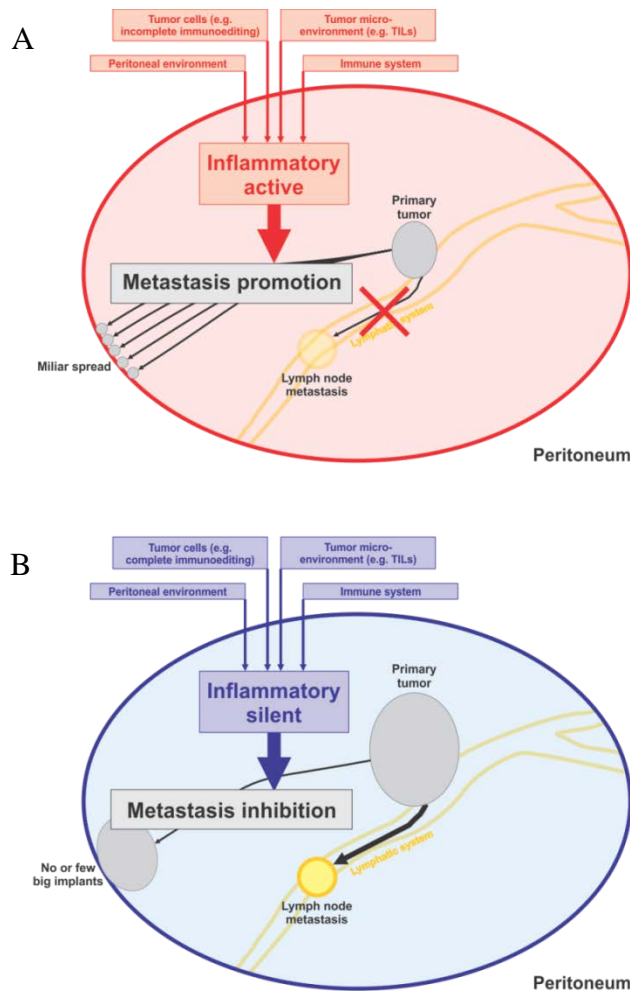


Figure 4. Working model showing distinct modes of peritoneal tumor spread: (A) miliary and (B) no or few big 9 implants as result of peritoneal inflammation (Figure provided by Pils, 2013).

1.10 Aim of the project

The aim of this project was the characterization of tumor cells in the ascitic fluid of EOC patients, based on surface markers allowing for quick analysis of cell populations in patients' biomaterials. Furthermore, validation of flow cytometric results was conducted using immunofluorescence and whole transcriptome analysis experiments were performed to contribute and support results about cell populations in the ascites of ovarian cancer patients. This study was part of a bigger project aiming to gain more comprehensive biological information about individual EOC patients allowing a more individualized approach in cancer treatment. Additionally to tumor and immune cells in the ascites, also tumor tissue of ovarian and/or peritoneal origin was analyzed. Figure 5 depicts the fractions collected and the methods used for the comprehensive analysis in the course of this project; all circled methods were conducted during my master thesis.

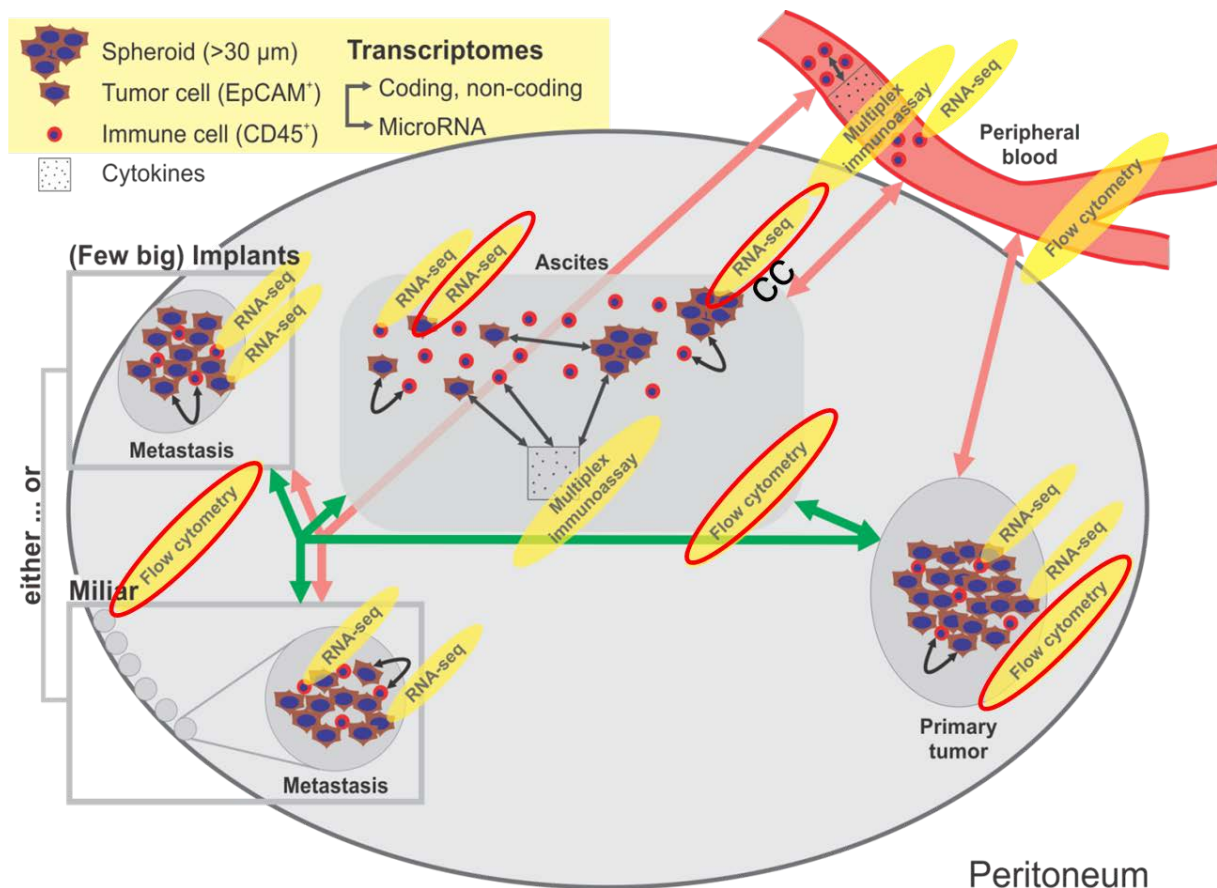


Figure 5. Scheme of the isolated fractions and compartments (tumor and immune cells from blood, ovarian tumor, peritoneal tumor, and ascites), the planned methods (yellow: long RNA and microRNA: RNA-seq, flow cytometry, and multiplex immunoassays), and the interactions to be analyzed (black, green, and pink arrows). All red circled methods were conducted during the course of this master thesis. (Figure provided by Pils, 2013)

2 Material and Methods

2.1 Clinicopathological factors

During primary surgery presence of ascites and the spread of the tumor in the peritoneum was described by an experienced surgeon. Peritoneal tumor spread was divided into the categories: i) no, ii) few, big lesions, or iii) miliary tumor spread. Clinicopathological factors including histology, FIGO, and grade were assessed by a skilled pathologist. Data about *KRAS* and functional *TP53* mutation status were determined by functional p53 assay (FASAY) and sequencing.

2.2 Patients' material

Preoperative blood, ascites (if present), and tumor tissues from patients with EOC were collected between March 2012 and May 2013 at the AKH Vienna/Department of Obstetrics and Gynecology at the Medical University of Vienna. All patients signed an informed consent for the use of blood/body fluids and tissue in the study. The study was approved by the local ethics committee.

2.2.1 Blood

A total of three milliliters whole blood, collected in EDTA tubes to prevent clumping, were obtained and two milliliters were immediately depleted of erythrocytes by ammonium chloride lysis (155 mM NH_4Cl , 10 mM KHCO_3 , 0.1 mM EDTA in ddH₂O) in a total volume of 30 mL for five minutes at room temperature (RT). Remaining peripheral blood mononuclear cells (PBMCs) were pelleted in a 10 minute centrifugation step at 400 g, followed by two washing steps with 50 mL PBS. Subsequently washed and pelleted cells were resuspended in 400 μL blood plasma from the same patient and slowly frozen with the addition of 5 % DMSO as cryoprotectant. After reaching -80 °C, aliquots were stored in liquid nitrogen.

One milliliter of whole blood was enriched for CD45+ cells. It was mixed with ice-cold Miltenyi buffer (2 mM EDTA, 0.5 % BSA in PBS) in a total volume of 10 mL, incubated with CD45 harboring beads for 20 minutes rotating at 4 °C and the CD45+ immune cells were collected by magnetic bead separation via the cell separation system Magnetat (as described below).

2.2.2 Tumor tissue

Tissue slices (sized between 0.5 cm and 3 cm in diameter and a width of few millimeters) from primary tumors and peritoneal implants were collected in buffered growth medium (DMEM + 10 mM HEPES, pH 8.0) during surgery and subsequently minced,

washed with DMEM and digested with 10,4 U Liberase DH research grade (Roche, Basel, Switzerland) stirring at 37 °C for one hour in an Erlenmeyer flask. The cell suspension was then filtered for single cells using a cell strainer with 40 µm mesh size; DMEM supplied with 4 mM EDTA was added to prevent clumping of the filtrate and used to wash it two more times. The cell pellet was resuspended in ice-cold Miltenyi buffer and CD45⁺ and EpCAM⁺ cells were enriched using the MagneStat system (see below).

Moreover the remaining cell solutions, depleted of the respective cell populations, were also collected for subsequent analysis.

2.2.3 Ascites

Fresh ascitic fluid was obtained immediately after paracentesis and first assessed under the light microscope for cell aggregates, followed by counting of the cellular content on the Countess® automated cell counter (Invitrogen). Decent volumes (20 to 150 mL depending of cell and cell aggregate count) of ascites were filtered consecutively for cell aggregates using *CellTrics*® filters with mesh sizes of 150 µm, 30 µm and 20 µm. The whole volume of ascites was first drawn through the 150-µm-filter to get rid of bulk, like pieces of tissue or fat. Afterwards the fluid was passed through a 30-µm-filter, that was rinsed with PBS after being clogged by cell aggregates, to wash away trapped single cells. The cell aggregates were found in the remaining retentate on the mesh and collected by flipping the filter over and washing it with five milliliters of DMEM into a new tube (spheroid fraction). The filtrate, in contrast, was again put on the smallest filter (20 µm mesh size) to ensure single cells in the last fraction. Both, cell aggregates and single cells were frozen and stored in liquid nitrogen until analysis via flow cytometry. An aliquot of the single cell fraction was also processed to isolate EpCAM positive cells using MagneStat whereas a 100 µL aliquot of cell aggregates was pelleted (400 g, 10 minutes) and lysed with 700 µL QIAzol (Qiagen, Venlo, Netherlands) for RNA preparation.

Furthermore, pellets of fixed ascites cells were washed in PBS and embedded into agarose and subsequently in paraffin (described below) for immunofluorescence.

2.3 Embedding of ascites

For embedding into paraffin, cells from 50 mL ascites were pelleted by centrifugation (10 minutes, 400 g) and subsequently fixed by addition of 2 mL 4.5 % formaldehyde and incubated at room temperature for 30 minutes. Washing with PBS and centrifugation at 400 g for 10 minutes removed the formaldehyde solution and the pellet was

transferred into 500 μ L molten agarose (90 °C, thermoblock). After mixing, the solution was centrifuged at 400 g for 5 minutes and cooled down at 4 °C for 2-4 hours. After cooling the solidified agarose cylinder was transferred into Shandon-tissue-sachets and incubated overnight in 70 % ethanol at 4 °C. The next day the samples in sachets were dehydrated at room temperature by incubation in 96 % ethanol for two hours, followed by one hour in 100 % ethanol, one hour in xylene, one hour in an 1:1 mix of xylene and paraffin at 58 °C, and finally one hour in paraffin also at 58 °C to prevent solidifying. Further processing of the cells into paraffin blocks and cutting of solid paraffin blocks on a microtome in order to get ascites slides was performed by skilled laboratory members.

2.4 Cryopreservation and thawing

For freezing of cells dimethylsulfoxide (DMSO) was added on ice to a final concentration of 5 % in medium (either ascites supernatant or fetal calf serum for ascites cells and tissues, plasma for blood cells) and the cell suspension is slowly cooled down to -80 °C, in an appropriate freezing container (Nalgene, cryo freezing container) cooling down at a rate of 1 °C per minute. Rapid freezing would result in intracellular solidification of water and damage cell organelles (Mazur 1984). DMSO acts as cryoprotectant, presumably by reducing the concentration of salts when water is converted to ice (Rasmussen and MacKenzie 1968). But DMSO also harms cells at room temperature, therefore thawing must not exceed 1-2 minutes at 37 °C. After thawing the cell solution was immediately diluted in a large volume (~10 mL) of growth medium and the cells were subsequently washed by centrifugation.

2.5 Enrichment of tumor/ immune cells (Magnestat)

Enrichment of EpCAM positive tumor cells and CD45 positive immune cells from blood, ascites and tumor tissue was performed with the Magnestat device (prototype, Clinical Genomics Pty Ltd, Sydney, Australia) according to the manufacturer's protocol. Single cell suspensions of around five million cells from tumor tissues, 1 mL whole blood or 7.5 mL 20- μ m-filtered ascites cells (about five million cells) were supplemented with Miltenyi buffer to a final volume of 10 mL in a 15 mL centrifuge tube. Miltenyi buffer contained PBS for pH stabilization, EDTA for complexation of bivalent ions, and BSA to mask the plastic walls of the tube and to provide a decent environment for cells. Magnetic beads (Dynabeads) coated with EpCAM or CD45 antibodies were washed in Dynabead wash buffer (1x PBS 0.1 % BSA, 0.6 % sodium citrate) before addition to the solution. After an incubation time of 20 minutes, rolling at 4 °C, the tube was attached to the device which draws the cell solution through a hose, passing by a magnet. The

cells, which are bound to magnetic beads via antibody-antigen binding, get immobilized at the magnet whereas unbound cells are drawn into a 20 mL syringe. After washing the immobilized cells with several milliliters of washing buffer (1x PBS/0.05 % Tween; PBS/T), cells were eluted by removing the tube from the magnet and applying a reverse stream of washing buffer (PBS/T), rinsing the cells into an Eppendorf tube. Subsequently an aliquot (50 μ L) of the bead/cell/elution buffer-mix was taken, the buffer was removed (by applying the tube to a magnet) and the cells still bound to beads were stored at -80 °C for later DNA analysis. The remaining solution was also depleted of elution buffer, mixed with QIAzol lysis reagent (Qiagen, Venlo, Netherlands) and also stored at -80 °C until preparation of RNAs.

2.6 Isolation of RNA

Total RNA was isolated from QIAzol lysed cell samples (up to 10^7 cells) collected via Magnestat or directly after filtration (only for spheroids) using the miRNeasy mini kit (Qiagen, Venlo, Netherlands) according to the manufacturer's protocol. QIAzol is a phenol containing solution for purification of RNA and intended to use with Qiagen cleanup kits. The use of RNeasy® Mini and RNeasy MinElute columns allowed for isolation of small RNAs up to a size of 200 nucleotides as well as large RNAs including mRNAs and tRNAs from the same sample. RNA concentration was quantified using NanoDrop ND-1000 spectrophotometer (Thermo Fisher Scientific, Waltham, USA). Agilent 2100 Bioanalyzer (Santa Clara, USA) was used to assess the quality of large RNAs (>200 nt) following the manufacturer's instructions.

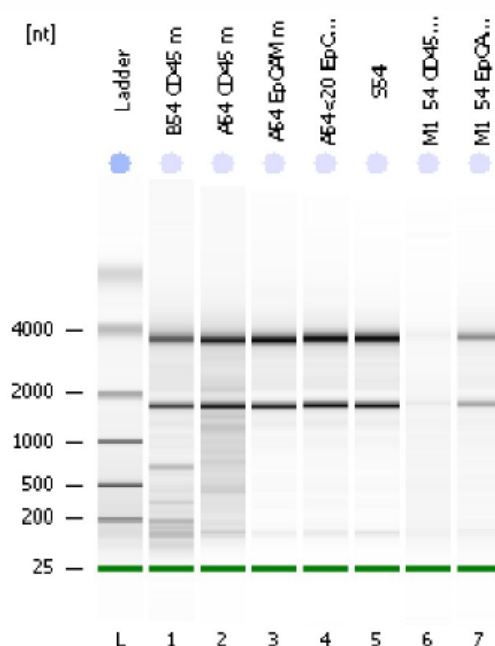


Figure 6. Bioanalyzer (Nanochip) electrophoresis of isolated RNA. 28S and 18S rRNA are visible as black bands and the left lane contains a ladder for size evaluation of fragments.

2.7 RNA-Seq

Whole transcriptome shotgun sequencing (RNA-Seq) of matched pairs of EpCAM+ ascites single cells and spheroid samples was performed at the next generation sequencing (NGS) core facility Campus Science Support Facilities GmbH (CSF). Preparations including library generation were carried out in our laboratory. Analysis and statistical evaluation of the raw data was performed by a bioinformatician (my supervisor).

2.7.1 Library preparation and sequencing

Large RNAs of eight matched pairs of ascites single cells and spheroid samples, confirmed to contain EpCAM+ tumor cells by flow cytometry, were prepared for RNA sequencing with the modified NEXTflex™ RNA-Seq Kit (Bioo Scientific, Austin, USA). Depletion of rRNA from samples of 200 ng was performed using the RiboZero™ kit (epicenter, Madison, USA). The introduction of barcodes allowed for pooling of eight samples in equimolar ratio in one lane each and sequencing was performed on the HiSeq 2000 (Illumina, San Diego, USA). Each library was sequenced 50 bp paired-end to a median depth of 20.4 million reads (10.6-33.1 million reads) and quality of sequencing was checked with FastQC and RSeQC and mapped with the RNA-Seq Unified Mapper (RUM). The median mapping percentage was 86.5 % (57.4 %-93.2 %). Circular RNAs were predicted with the scripts of Memczak et al. (<http://circrna.org/>) (Memczak, Jens et al. 2013) and mapped reads were filtered for all reads from putative circular RNAs which were discarded. Remaining reads were counted into the genemodel from Gencode v16 using htseq-count from the HTSeq Python framework (<http://www-huber.embl.de/users/anders/HTSeq/doc/overview.html>; 22.7.2013).

2.7.2 Statistical analysis and functional annotation

Genes with statistical significant differential expression were determined by limma v3.16.6 (R-package) using a False Discovery Rate (FDR) cut-off of 10 %. As search using limma revealed very few significantly deregulated genes between single cell samples and spheroid samples, a more sensitive method for analysis, especially developed for data from matched pairs, was employed, called pairedBayes (R-script) (Chung, Ferguson et al. 2013). Functional annotation with Database for Annotation, Visualization and Integrated Discovery (DAVID, v6.7) was performed online using the list of significantly deregulated genes, i.e. the list of ENSEMBL Gene IDs was uploaded, gene ontologies (GOTERM_BP_FAT, GOTERM_CC_FAT, GOTERM_MF_FAT) and pathways (KEGG_PATHWAY, PANTHER_PATHWAY, REACTOME_PATHWAY) for annotation were selected and functional annotation was executed. Subsequently, a functional annotation clustering as provided by the tool was performed. Additionally, a

Signaling Pathway Impact Analysis (SPIA) (Tarca, Draghici et al. 2009) was performed using the list of significantly deregulated genes with their corresponding log-2 fold changes using a 5 % FDR cut-off. For visualization of the significantly differentially expressed genes between patients with distinct modes of tumor spread, a heatmap was generated and the individual samples were clustered based on their expression profile.

To assign the 16 samples to one of the two molecular subclasses as defined by Yoshihara et al. (Yoshihara, Tajima et al. 2009) and validated by Pils et al. (Pils, Hager et al. 2012), the 112 genes used for classification were mapped to the ENSEMBL genes used for RNA-seq analysis and a non-negative matrix factorization (NMF) was performed on log2-transformed non-negative data ($\log_2(x+0.5) + |\min(\log_2(x+0.5))|$). To assess the optimal number of classes (ranks), NMF was performed with two to six factorization ranks and the cophenetic correlation coefficients were compared (Fig. 7). The “two rank” approach showed the highest cophenetic distance and was therefore applied. In addition, the same procedure was performed with all genes that were expressed reliably. In both cases, the same classification was achieved, indicating a robust subclassification.

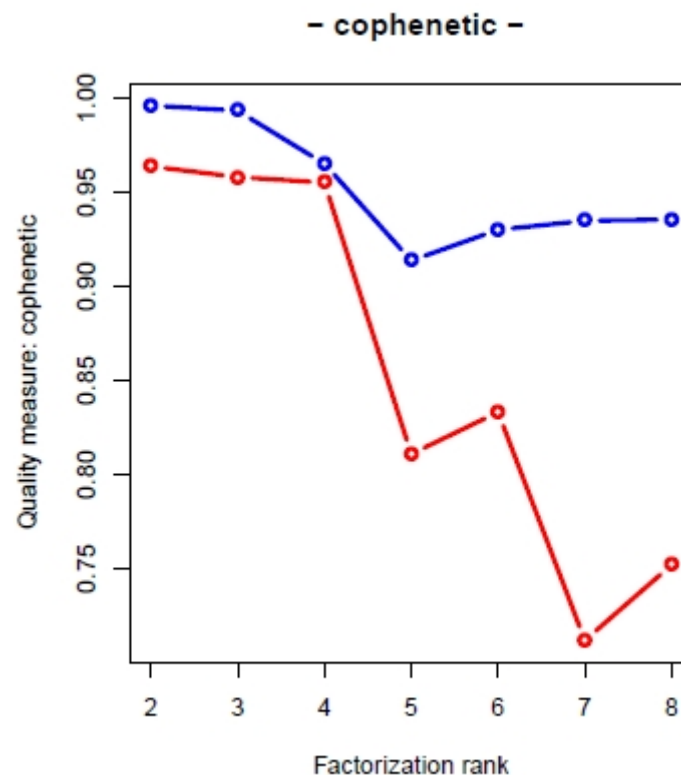


Figure 7. Rank estimation for NMF. Blue: 112 genes for classification; Red: randomly permuted data as control

2.8 Flow Cytometry (FC)

2.8.1 Antibodies

Conjugated monoclonal antibodies were used for flow cytometry. The FITC anti-human CD45 antibody (mouse IgG1) was obtained from BD Bioscience (New Jersey, USA), anti-human CD326 (mouse IgG1) conjugated to PerCP-eFluor 710 and anti-CD44 (rat IgG2b) PE-Cy7 were purchased from eBioscience (San Diego, USA), phycoerythrin (PE) anti-L1CAM antibody (mouse IgG2a) from abcam (Cambridge, UK), and anti-CD133 (mouse IgG1) conjugated to allophycocyanin (APC) from Miltenyi Biotec (Bergisch Gladbach, Germany). Dead cell staining was performed using the LIVE/DEAD® Fixable Dead Cell Stain Kit from Invitrogen™ (Carlsbad, USA).

2.8.2 Antibody titration and condition testing

Before starting to analyze patients' samples by flow cytometry a robust staining protocol was set up and all five fluorophor-coupled antibodies as well as the live/dead dye were titrated for best results. Therefore different cell lines known to express the desired antigens were grown in the respective medium at 37 °C and 5 % CO₂ until confluency, harvested, counted and 100 000 cells were stained in FACS-buffer (2 % BSA, 2 mM EDTA in PBS), testing different combinations of concentrations of antibody and formaldehyde for fixation. For the CD45 antibody, peripheral blood mononuclear cells (PBMCs) were used instead of established cell lines. HeLa was used for the establishment of the staining protocol for CD44, T84 for EpCAM, Panc1 for L1CAM, and HT29 for CD133. Acquisition was performed on a BD LSRFortessa, equipped with three lasers (405 nm, 488 nm, 640 nm), and subsequent analysis was performed using FACSDiVa software (BD). Conditions tested were non-fixed cells versus fixation of cells with 1 % formaldehyde for 15 minutes (prepared from solid para-formaldehyde in 1x PBS and stored at -20 °C), or 0.5 % formaldehyde over-night either before or after staining with the pure or a stepwise dilution of the antibody (1:2, 1:4; 1:8, 1:16). For titration of the fixable live/dead dye HeLa cells were treated with ethanol (add 96 % ethanol to cell pellet, vortex for 60 seconds, add wash buffer, centrifuge, remove supernatant, and stain with live/dead dye) and mixed with an untreated HeLa population to test if distinguishable. After proper titration of antibodies the single color stainings of all used cell lines as well as a multicolor staining of a cell mix (equal amounts of HeLa, HT29, T84, HT29, and ascites cells) was used to adjust PMT-voltage (so all data points appear in one plot) and compensate the emission of the different colors (to adjust for leaking of signals into other fluorescence channels.) Re-compensation was necessary

because of the aging of coupled fluorophores and accompanied changes of emission and was performed after data acquisition using FlowJo software (v7.6.2).

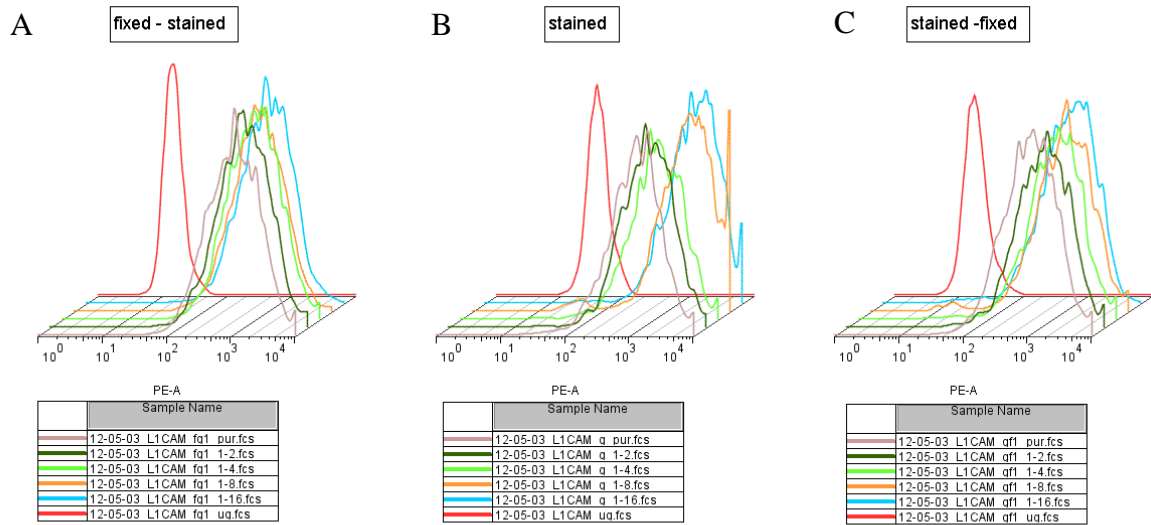


Figure 8. Condition testing and titration of the L1CAM- PE antibody (A) initial fixation of sample and subsequent staining using different antibody concentrations (staining volume = 100 μ L): pur= 20 μ L antibody solution, 1-2= 10 μ L, 1-4= 5 μ L, 1-8=2.5 μ L, 1-16= 1.25 μ L, ug= unstained control; (B) staining without fixation of the sample; (C) initial staining with different antibody concentration followed by fixation.

2.8.3 Disintegration of ascitic cell aggregates

Filtered cell aggregates from malignant ascites of ovarian cancer patients were thawed, washed in 10 mL DMEM to get rid of the DMSO and pelleted by centrifugation. Subsequently the pelleted cells were resuspended in 500 μ L either trypsin (0.05 % Trypsin-EDTA, Gibco/Life Technologies, Carlsbad, USA) or Accutase® Cell Dissociation Reagent (Life Technologies) in order to loosen and finally disrupt cell-cell contacts, responsible for the aggregation of cells into cell aggregates. A 10 μ L aliquot of each specimen was taken and examined under the microscope to evaluate the status of the cell aggregates at time point zero. The cell aggregates were incubated for ten minutes at 37 °C and then dispersed mechanically by pipetting up and down 50 times using a pipette equipped with a 1000- μ L-tip. Ten microliter of the solution were examined again and depending on the grade of dispersion of the multicellular aggregates into single cells the enzymatic process was either stopped by addition of 1 mL DMEM containing 10 % FCS or the incubation with following mechanically disruption was repeated until the majority of cells was singulated. Usually two to three rounds of this process were necessary to get adequate numbers of single cells without killing too many. Subsequently the cells were incubated in growth medium for 30 minutes at 37 °C to relax and reestablish enzymatically digested surface markers. The cells were pelleted again, resuspended in 200 μ L of ice-cold PBS, counted, and split up in two Eppendorf centrifuge

tubes for staining (usually around 200 000 cells were stained in one tube for flow cytometric analysis, but since in some samples many cells got lost in the disruption process, all remaining cells were used).

2.8.4 Staining

The staining panel included a live/dead stain to distinguish living from dead cells, anti-CD45, anti-EpCAM, anti-L1CAM, and anti-CD133 antibodies. All steps were performed on ice or at 4 °C. First 0.5 µL of live/dead staining solution was added to approximately 200 000 cells in a volume of 100 µL and incubated for 30 minutes at 4 °C, protected from light to preserve the dye from bleaching. Cells were then washed in 1x PBS, to get rid of excess unbound reagent, and fixed in 1 % formaldehyde. After two washing steps to remove all formaldehyde from the solution, since it impairs the tandem dye PE-Cy7, FACS-buffer was added and staining with the 5-color antibody mix was performed in a total volume of 100 µL for 30 minutes at 4 °C in the dark. After a final washing step, the cell pellets were resuspended in 400 µL FACS-Buffer and the vials were stored overnight at 4 °C protected from light until analysis.

The next day the tubes were vortexed and cells were acquired on a BD LSRFortessa flow cytometer, equipped with three lasers (405 nm, 488 nm, 640 nm). For every tube 20 000 events were recorded (if possible, minimum 2 000) and assessed using FACSDiVa software. Each event results from a light signal converted into an electronic pulse, stored as data point. The digital files were exported in fcs3.0 format and gating was performed using FlowJo software (v7.6.2), and prepared templates for gating.

2.8.5 Gating

The flow cytometry data set of each individual patient (comprising data from ascites single cells, spheroids, primary and peritoneal tumor tissue) was first visually assessed in the forward scatter (FSC) – side scatter (SSC) plot (exemplified in the results section: Fig. 12, 1) and then cell doublets and triplets were discriminated in the SSC-area (SSC-A) and FSC-width blot (FSC-W) (Fig 12, 2). To ensure the counting of whole cells a cut-off at 400 in the FSC channel was employed to gate out cell debris (during acquisition a threshold of 200 was applied but this was not enough to discriminate the majority of cellular debris). Events from the single cell gate without debris were then checked for viability in the SSC-A and Alexa-405-A fluorescence channel (emission of live/dead stain Fig. 12, 4). Furthermore, immune cells were discriminated by out-gating CD45 positive events, visible in the FITC channel (Fig. 12, 5). In the PerCP-eFluor710 channel (Fig. 12, 6) cells were sorted in EpCAM positive and negative events, for CD44

positivity in the PE-Cy7 channel (Fig. 12, 9), for CD133 positivity in the APC channel (Fig. 12, 8) and for L1CAM positivity in the PE channel (Fig. 12, 7). This was done to fine-tune the gating borders for each dye since samples varied in fluorescence intensity and autofluorescence of the cells. Furthermore, EpCAM⁺ and EpCAM⁻ events were gated for combined L1CAM/CD44, L1CAM/CD133 and CD44/CD133 double positive analysis. The resulting populations were collected in a table (see Tab. 3 as example).

2.8.6 Statistics

Data from flow cytometry were analyzed using IBM SPSS statistics software (v21) and R (v2.15.2). Associations between markers were assessed using Spearman's rank order correlations. Continuous non-normally distributed variables were compared between groups of two categories using Mann-Whitney-U test and Kruskal-Wallis test for more than two categories. In all tests a p-value below 0.05 was considered significant. Similar to isomap as dimension reduction tool for non-linear associations between data points from RNA-seq data, for FC data, the linear Principal Component Analysis (PCA) approach was used. Big amounts of data, as produced by FC gating for surface marker combinations, and their associations were either visualized as boxplots and beanplots, or summarized in star-blots.

2.9 Immunofluorescence

2.9.1 Antibodies

A set of four different antibodies was tested for multicolor immunofluorescence staining of embedded ascites cells. Primary antibodies from different species or isotypes were used to allow for multiple staining of single slides. The anti-human CD45 antibody (rabbit, clone E19-G) was obtained from DB Biotech (Kosice, Slovakia), the monoclonal mouse anti-human EpCAM antibody (clone VU1D9, isotype IgG1) was purchased from Cell Signaling Technology (Danvers, USA), the rat anti-human CD44 antibody (IM7, isotype IgG2b) from BioLegend (San Diego, USA), and the monoclonal mouse anti-Vimentin (clone 2D1, isotype IgG2a) from abcam (Cambridge, UK). The secondary antibodies (all from Invitrogen, Carlsbad, USA) were directed against the species (and isotype) of the primary ones and were purified from the serum of goats. Furthermore, they were labeled with different Alexa Fluor dyes. The Alexa Fluor 488 anti-mouse IgG2a and the IgG Alexa Fluor 647 anti-rabbit antibody consist of F(ab')₂ fragments, whereas the Alexa-Fluor 555 anti-rat and the Alexa Fluor 594 anti-mouse IgG1 were whole antibodies. Secondary antibodies were chosen according to their dye, for minimal overlay of the emission spectra (Fig. 9).

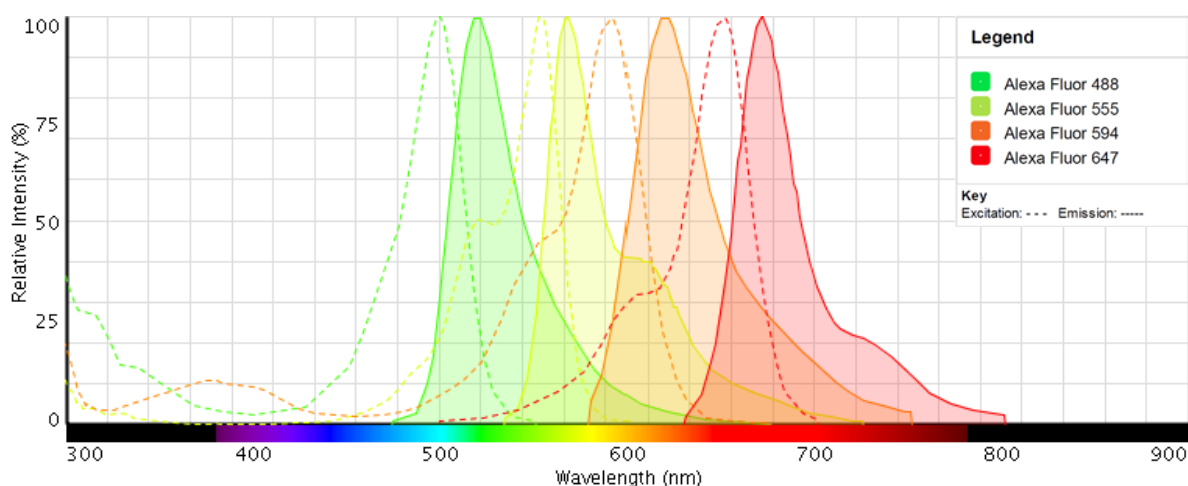


Figure 9. Excitation (dotted line) and emission spectra (filled curve) of fluorophores used for immunofluorescent stainings of ascites cells. (Taken from <http://www.lifetechnologies.com/europe-other/en/home/life-science/cell-analysis/labeling-chemistry/fluorescence-spectraviewer.html>, 3.7. 2013)

2.9.2 Staining Procedure

Paraffin blocks of ascites cell pellets were cut into sections of four micrometers and applied to ultra-adhesive slides. Prior to staining, the slides were baked for one hour at 58 °C and subsequently deparaffinized in xylene (2x 5 min), followed by a rehydration step with a descending alcohol gradient (2x 3 min 100 % ethanol, 1x 1 min 96 % ethanol, 1x 1 min 80 % ethanol, 1x1 min 70 % ethanol, 5 min rinsing in distilled water). For antigen retrieval (to unmask fixed epitopes) the slides were cooked in 1 mM EDTA buffer in the microwave (2.5 min at 850 W followed by 13 min at 160 W) and slowly cooled to room temperature. For blocking of unspecific antibody binding sites Ultra V block (Thermo Scientific, USA) was applied to the sections for seven minutes. The staining was done with a mixture of three or four primary antibodies, diluted in DAKO AB diluent in optimized concentrations and incubated overnight at 4 °C. The next day the antibody solution was removed via two washing steps in PBS and the fluorescence labeled secondary antibodies (1:1000 in PBS, 6 % BSA) were applied as a mixture and incubated for one hour at room temperature. Followed by another washing step with 1x PBS, the nuclei were counterstained with DAPI (0.5 µg/mL) for exactly five minutes, washed in distilled water and mounted with the fluorescence protective Fluoromount-GTM (Southern Biotech, USA).

Cells were visualized on a confocal laser scanning microscope LSM780.

3 Results

3.1 Overview

Blood samples from 43 ovarian cancer patients with suspicion for primary ovarian cancer were collected between May 2012 and April 2013. Twenty patients were finally diagnosed with epithelial ovarian cancer and fifteen of these presented with ascites. The analysis was restricted to samples from patients with ovarian carcinomas of the serous histological subtype in order to analyze a homogenous group of patients. Hence, bio-materials (ascites, peritoneal and ovarian tumor tissues) could be obtained from seventeen patients prior to or during surgery. The characteristics of the patients, tumors and ascitic fluids are shown in table 2. From the whole patient cohort, twelve ascitic fluid samples, ten samples from ovarian tumors, and thirteen samples from peritoneal tumors were included in the study. Ascites samples were filtered, tissue samples digested, and the abundance and frequency of surface markers was analyzed by flow cytometry. Additionally, the location of different cell subpopulations within ascites spheroids or single cells was investigated using immunofluorescence.

Table 2. Patient and tumor characteristics

Characteristic	Number of Patients (%) n=17
Histology	
Serous	17 (100)
FIGO	
IIC	1 (5.9)
IIIA/B	6 (35.3)
IIIC	9 (52.9)
IV	1 (5.9)
Grade	
1	1 (5.9)
2	1 (5.9)
3	14 (82.3)
not specified	1 (5.9)
Mode of tumor spread	
none	2 (11.8)
few big	5 (29.4)
miliary	9 (52.9)
unknown	1 (5.9)
Ascites volume	
0	3 (17.6)
<500	5 (29.4)
>1000	9 (52.9)

Mutation	
p53/KRAS WT	2 (11.8)
KRAS*	1 (5.9)
p53**	12 (70.6)
unknown	2 (11.8)
Cell aggregates in Ascites	
yes	10 (58.5)
no	2 (11.8)
unknown	2 (11.8)

* mutation in KRAS gene, ** functional mutation

3.2 Processing of Ascites

The filtration of freshly obtained ascites (Fig. 10 A) through filters with 150 μm , 30 μm , and 20 μm mesh size resulted in separation of i) spheroids with a size bigger than 30 μm (Fig. 10 B) from ii) single cells (smaller than 20 μm) in the sample.

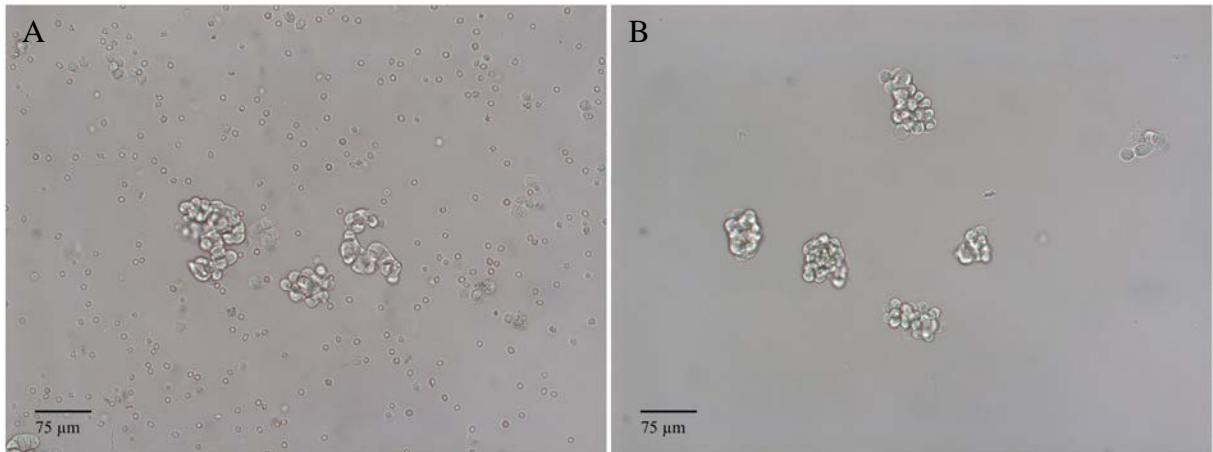


Figure 10. Malignant ascites from the same patient (A) before and (B) after filtration.

The enzymatic digest of cell surface proteins, responsible for cell-cell adhesion, and mechanical disruption of spheroids, followed by 30 minutes incubation at 37 °C for cell recovery, resulted in mostly viable, detached cells ready to be stained for flow cytometry (Fig. 11).

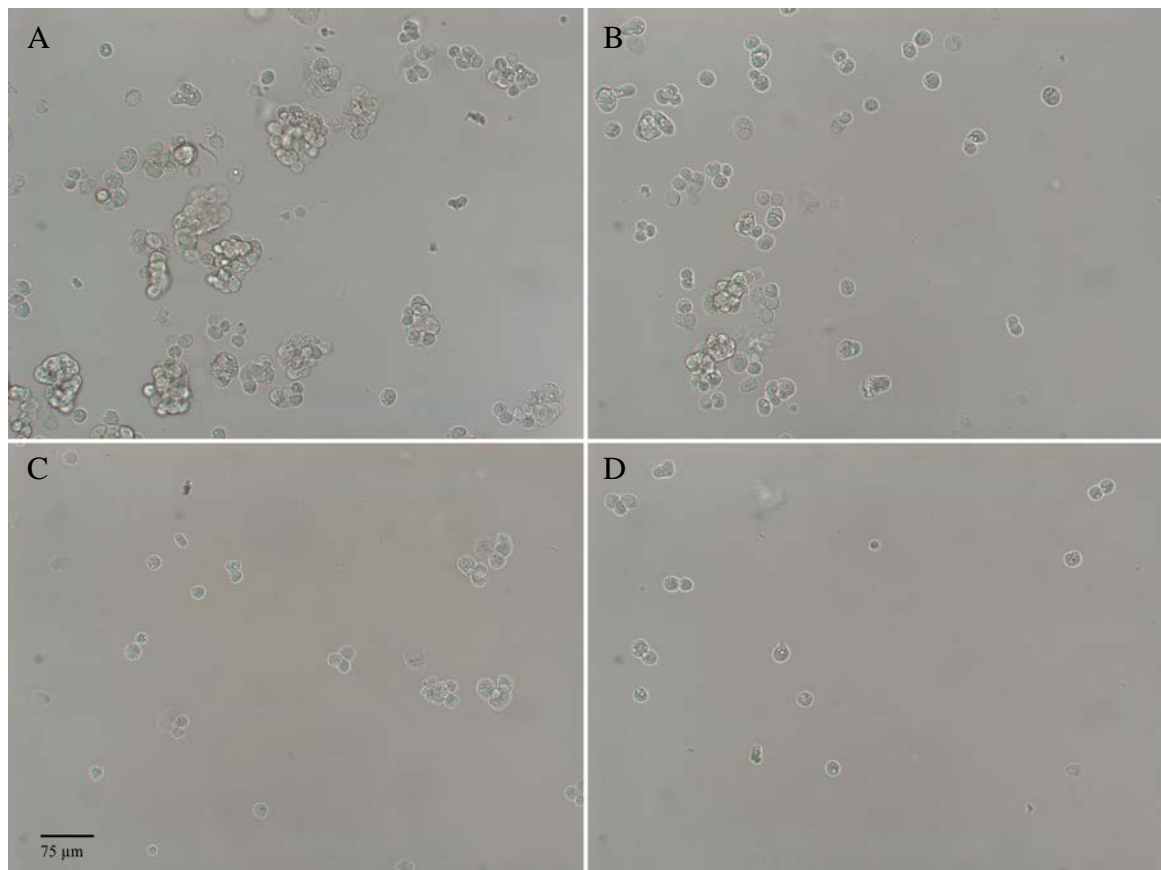


Figure 11. Disintegration of ascitic cell aggregates. (A) start: time point 0 (B) after 10 min (C) after 20 min (D) after 25 min incubation with Accutase followed by mechanical disruption.

3.3 Flow Cytometry

Thawed samples of filtered ascites single cells and supernatants from magnetic bead separation of dissociated tumor tissues were counted, around 200 000 cells or all disintegrated cell aggregates were fixed, and subsequently stained employing the 6-color flow cytometry antibody panel (or treated as unstained control) for flow cytometric analysis the next day.

3.3.1 Gating

Using the predefined gating template (Fig. 12), 33 populations and subpopulations of cells in ascites and tumor tissues were examined. Frequencies (in percent) of cells positive or negative for the analyzed markers were collected in a table (see Tab. 3 as example). Doublets and cell aggregates with more cells were usually more abundant in samples from disintegrated spheroids, but never exceeded 10 % of the whole count including debris. Individual samples varied in the amount of dead cells but 85 % of cells gated as alive were the minimum. In filtered ascites single cell samples, CD45 positive cells accounted for up to 75.9 % (median 60.9 %) of all living cells, whereas cells from tumor tissues showed a significantly lower abundance of CD45 positive immune cells.

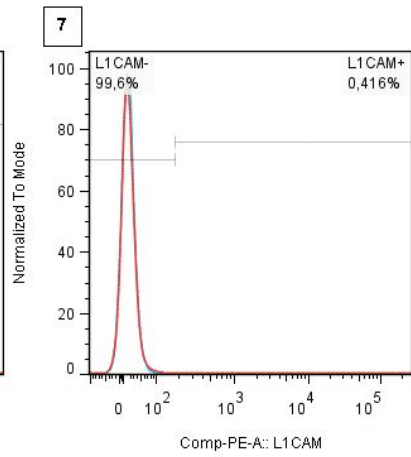
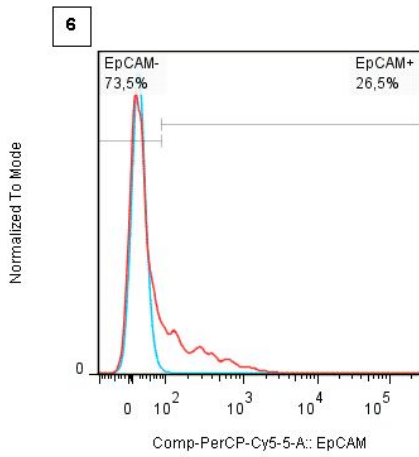
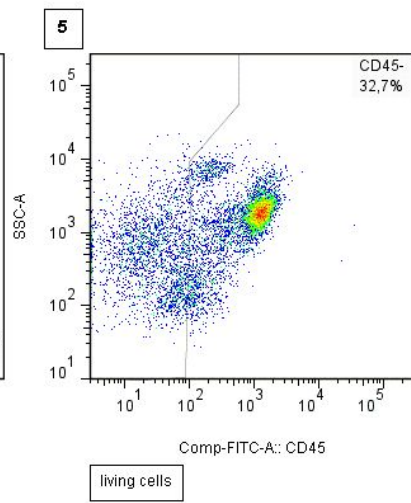
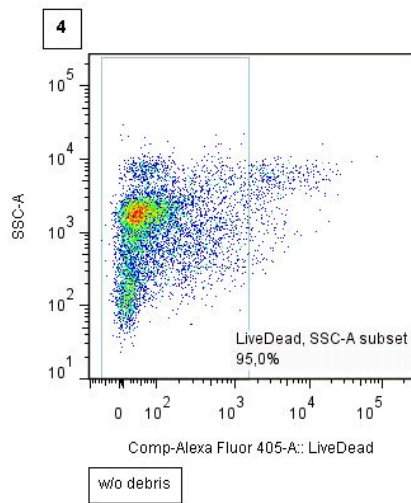
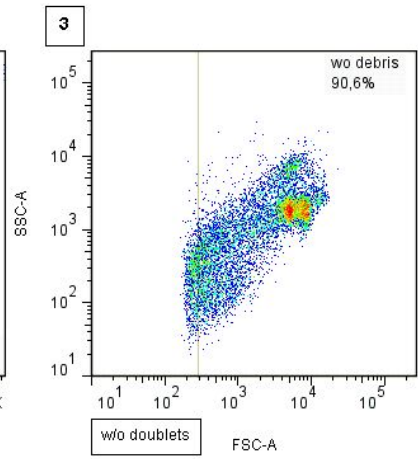
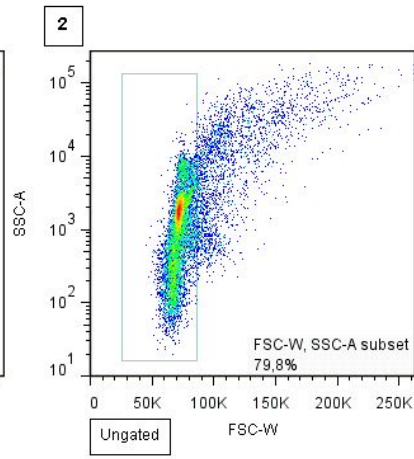
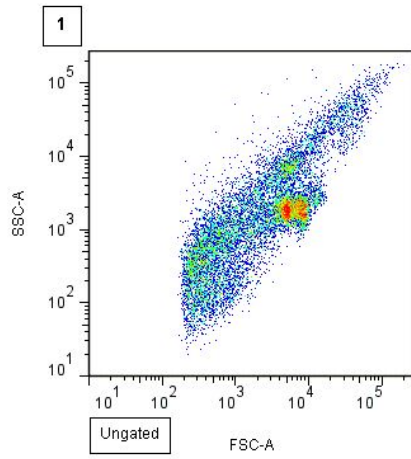
Spheroids varied in their number of CD45 positive events. The anti-CD133 antibody almost exclusively stained EpCAM positive cells, and could also be observed in combination with CD44, but in almost negligible numbers together with L1CAM+ cells. (See Supp. Table S2 for whole list.)

Table 3. Gated cell populations and frequencies

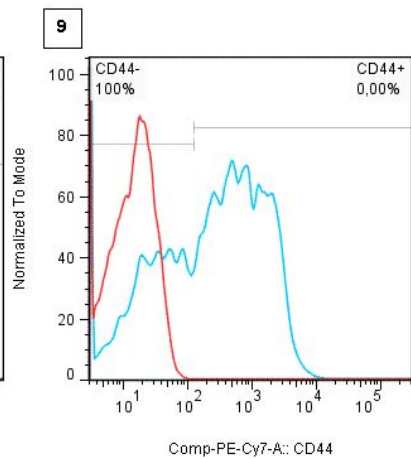
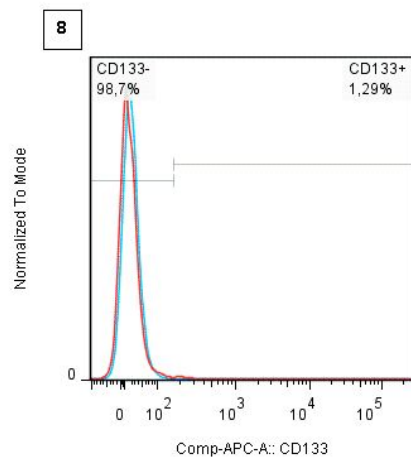
Population	Name in Graphs	Statistics		
CD45+	C45p	Freq. of alive		
CD45-	C45n	Freq. of alive	100%	
CD45-	CD44+	C44pC45n	Freq. of alive*	
	CD133+	C133pC45n	Freq. of alive*	
	L1CAM+	L1pC45n	Freq. of alive*	
	EpCAM+	EpC45n	Freq. of alive*	
	EpCAM+	CD44-CD133+	EpC133pC44n	Freq. of CD45-
		CD44+CD133+	EpC133pC44p	Freq. of CD45-
		CD44+CD133-	EpC133nC44p	Freq. of CD45-
		CD44-CD133-	EpC133nC44n	Freq. of CD45-
		CD44-L1CAM+	EpL1pC44n	Freq. of CD45-
		CD44+L1CAM+	EpL1pC44p	Freq. of CD45-
		CD44+L1CAM-	EpL1nC44p	Freq. of CD45-
		CD44-L1CAM-	EpL1nC44n	Freq. of CD45-
		CD133-L1CAM+	EpC133nL1p	Freq. of CD45-
		CD133+L1CAM+	EpC133pL1p	Freq. of CD45-
		CD133+L1CAM-	EpC133pL1n	Freq. of CD45-
		CD133-L1CAM-	EpC133nL1n	Freq. of CD45-
		CD44+	CD44pEp	Freq. of CD45-
CD45-	EpCAM-	EnC45n	Freq. of alive	
	EpCAM-	CD44-CD133+	EnC133pC44n	Freq. of CD45-
		CD44+CD133+	EnC133pC44p	Freq. of CD45-
		CD44+CD133-	EnC133nC44p	Freq. of CD45-
		CD44-CD133-	EnC133nC44n	Freq. of CD45-
		CD44-L1CAM+	EnL1pC44n	Freq. of CD45-
		CD44+L1CAM+	EnL1pC44p	Freq. of CD45-
		CD44+L1CAM-	EnL1nC44p	Freq. of CD45-
		CD44-L1CAM-	EnL1nC44n	Freq. of CD45-
		CD133-L1CAM+	EnC133nL1p	Freq. of CD45-
		CD133+L1CAM+	EnC133pL1p	Freq. of CD45-
		CD133+L1CAM-	EnC133pL1n	Freq. of CD45-
		CD133-L1CAM-	EnC133nL1n	Freq. of CD45-
		CD44+	CD44pEn	Freq. of CD45-

Color gradation stands for hierarchically gating of populations, all populations with the same color origin from the same parent generation which is located above and left. Freq. = frequency, * in tissues: frequency of CD45-

Figure 12 depicts a typical gating hierarchy represented as pseudo-color plots.



	staining
red	stained
blue	unstained



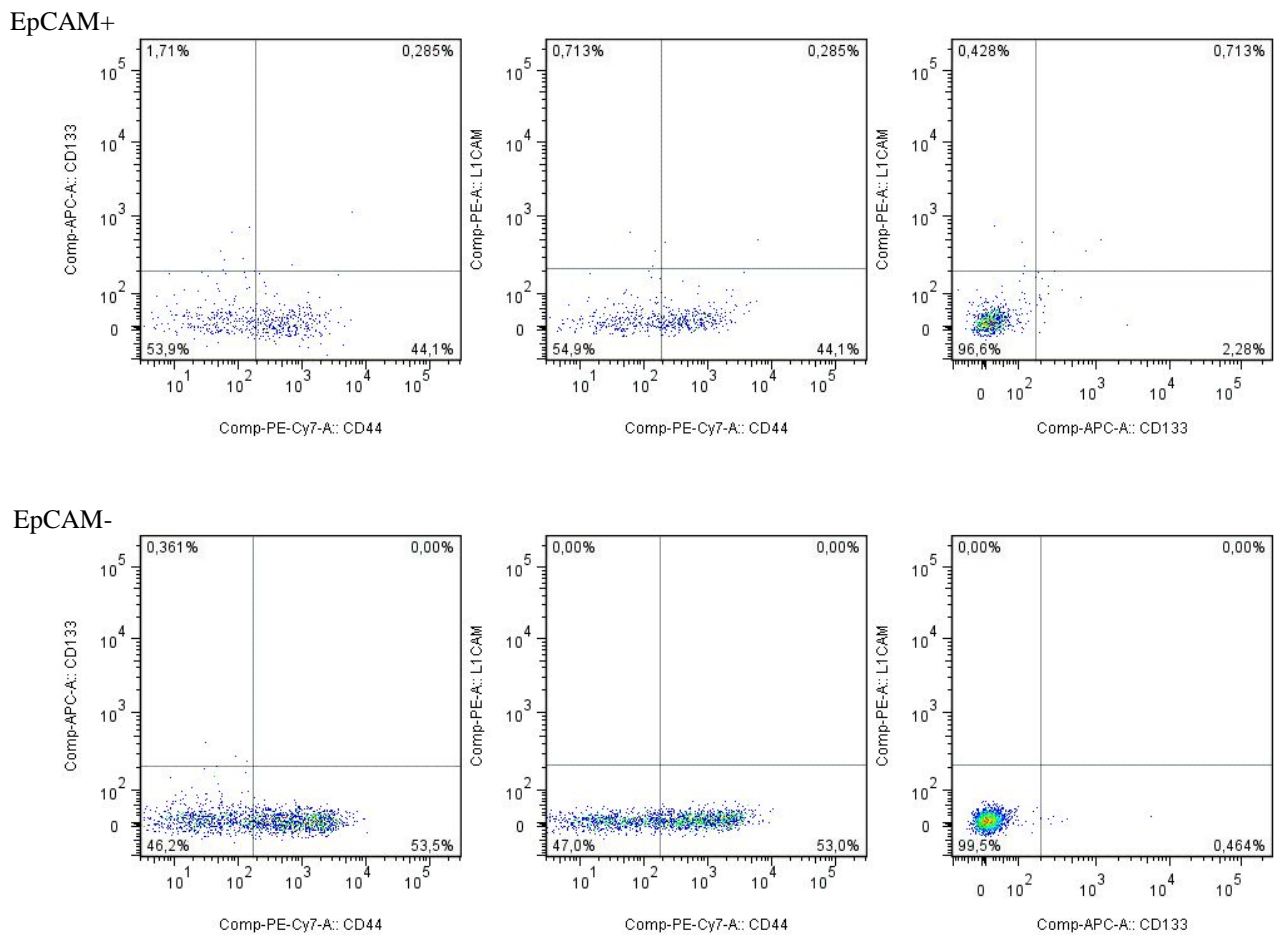


Figure 12. Gating strategy for flow cytometry data. The numbers depict the chronological sequential of gates, each following plot is constructed using the gated population of the previous plot (marked in boxes). The last two rows of plots stem from EpCAM positive (upper) and EpCAM negative (lower) events, gated for CD44/CD133, CD44/L1CAM, and CD133/L1CAM. CAVE: in box 9 the colors of stained and unstained populations are reversed: blue is stained and red is unstained.

3.3.2 Correlations

Obtained frequencies of cells with analyzed marker combinations (Tab. 3) were tested for associations between each other with Spearman rank order correlation tests. Significant results are shown in table 4.

Table 4. Significant correlations of all marker combinations

Variables		Spearman's rho	Significance (2-tailed)	
CD45	CD44	0.511	0.015	*
CD45	EpCAM	-0.598	0.003	**
CD45	CD133	-0.595	0.004	**
EpCAM	CD133	0.644	0.001	**
EPCAM	L1CAM	0.491	0.020	*
CD133	L1CAM	0.750	<0.001	**

* significance at the 0.05 level, ** significance at the 0.01 level

3.3.3 Specimen and cell populations

3.3.3.1 Ascites

Gating of data from flow cytometry was performed as described above, resulting frequencies of cell populations are summarized in tables (Tab. 5 ff) and displayed in bean- and boxplots for ascites samples (single cells or spheroids) as depicted in Fig. 13 ff. (*Cave*: the y-axis is sometimes in log space, as stated in the figure legends):

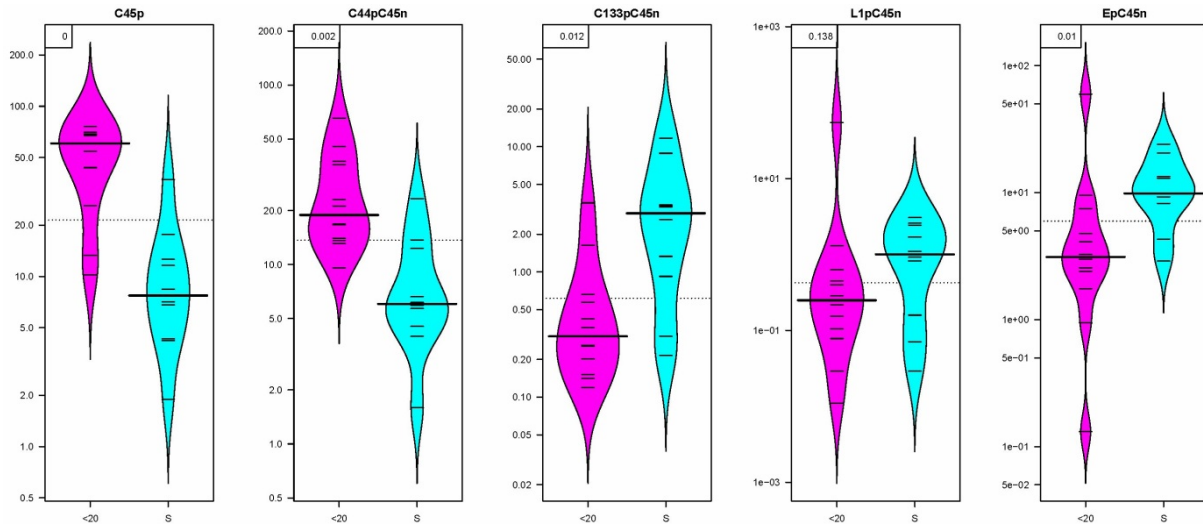


Figure 13. Beanplots from frequencies of cell populations as obtained by gating of flow cytometry data. The whole cell count (after discrimination of doublets and dead cells) was gated for CD45 negativity (A, whole cell count minus CD45-) and positivity of the cells for (B) CD44, (C) CD133, (D) L1CAM, and (E) EpCAM. The term <20 denotes single cells and S cell aggregates, p denotes positively gated cells, n denotes negatively gated cell. p-values from the Mann-Whitney-U test are shown in the upper left corner. Y-axis in log space. Individual data points are shown as black lines, whereas the black bar represents the median, the colored parts show the distribution: a bulky shape stands for a lot of data points whereas a slim part only consists of a few. The pointed line shows the overall median.

Figure 13 demonstrates an overview of the cumulative frequencies of counts for distinct cell surface markers in filtered ascites single cells (<20) and cell aggregates (S) as determined by flow cytometry. In the beanplots CD45+ immune cells and CD44+ cells were significantly enriched in the single cell fraction, ($p < 0.001$ for CD45, Fig. 13A; and $p = 0.002$ for CD44, Fig. 13B, respectively) whereas EpCAM positive tumor cells were enriched in the aggregated cell fraction ($p = 0.01$, Fig. 13E)

CD133+ and L1CAM+ cell populations were both enriched in cell aggregates but only the abundance of CD133+ cells reached statistical significance ($p = 0.012$, Fig. 13C).

Single Cells:

Table 5. Cell populations in ascites single cell fractions

Single Cells in Ascites (%)				
n=12	Median	Standard Deviation	Minimum	Maximum
CD45+	60.90	23.29	10.20	75.90
CD44+	19.00	16.81	9.58	65.50
CD133+	0.31	0.99	0.12	3.56
L1CAM+	0.25	15.67	0.01	54.60
EpCAM+	3.12	16.37	0.13	59.60
CD44+EpCAM+	2.98	18.39	0.09	65.64
CD44+EpCAM-	46.64	21.71	1.44	69.90

As expected, CD45+ immune cells were abundant in the single cell fraction of malignant ascites samples (median 60.9 %), whereas the frequency of EpCAM+ cells was much lower (median 3.12 %). The maximum frequency of 59.6 % EpCAM+ cells in this fraction was measured in samples from the KRAS mutated patient.

Also a high frequency of CD44+ cells was measured (median 19 %), in contrast to the low frequency of CD133+ (median 0.31 %) and L1CAM+ (median 0.25 %) cells in this fraction.

Spheroids:

Table 6. Cell populations in ascites spheroid fraction

Spheroids in Ascites (%)				
n=10	Median	Standard Deviation	Minimum	Maximum
CD45+	7.75	10.23	1.90	37.10
CD44+	6.04	6.40	1.59	23.30
CD133+	2.96	3.79	0.22	11.70
L1CAM+	1.01	1.11	0.03	3.06
EpCAM+	9.86	6.58	2.89	24.00
CD44+EpCAM+	2.43	6.76	0.41	23.32
CD44+EpCAM-	5.03	5.36	0.40	14.90

In spheroids, CD45+ cells were less frequent (median 7.75 % of living cells), whereas EpCAM+ cells were more abundant in this fraction (median 9.86 %). The population of CD133 positive cells was generally relatively small but in cell aggregates a median of 2.96 % was measured.

In the examined ascites spheroid samples only very low numbers of L1CAM positive cells could be detected. An exception was the ascites sample from the only patient with a confirmed KRAS mutation in the tumor, which showed a L1CAM abundance of 54.6 % in single cells and 3.06 % in the aggregated ascites cell fraction. Contrary to these results, the median frequency of L1CAM in cell aggregates was 0.87 %.

To sum this up: CD45+ cells were the most frequent population in the single cell fraction of ascites cells, in cell aggregates EpCAM+ cells were most abundant and CD44+ cells were frequent in both but with a clear tendency to reside as single cells. CD45+ cells can clearly be defined as immune cells and EpCAM+ cells as epithelial tumor cells (Latifi, Luwor et al. 2012), but as CD44 is a very abundant cell marker, the type of ascites cells expressing it remains to be elucidated. Therefore this CD44+ cell population was subdivided into cells positive or negative for EpCAM: (Fig. 14).

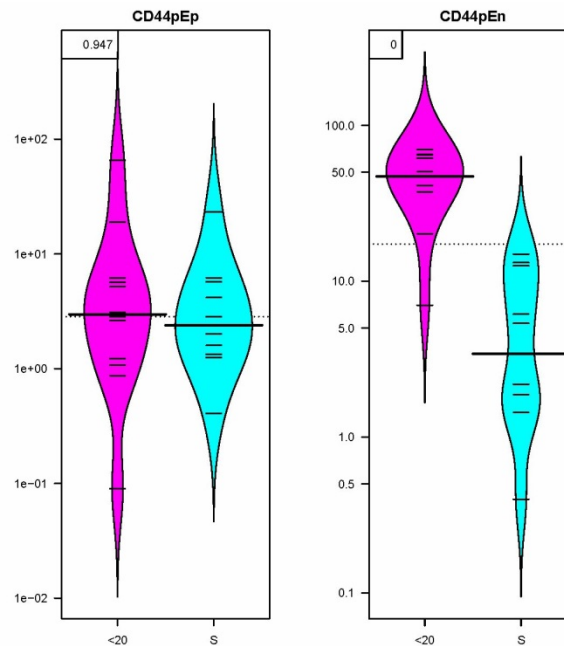


Figure 14. (left) CD44+EpCAM+; (right) CD44+EpCAM- distribution in single cell (<20) and spheroid (S) fraction of malignant ascites

Cells expressing CD44 and EpCAM simultaneously were similarly distributed between single cells and spheroids, but CD44+ cells that do not express EpCAM were significantly enriched in the single cell fraction ($p < 0.001$).

Furthermore, all possible combinations of the surface markers CD44, CD133, and L1CAM were tested on EpCAM positive and EpCAM negative subpopulations (Tab. 7 f). The results are presented below, and populations with statistically significant difference between single cells and spheroids are marked as bold:

Table 7. Cell populations in ascites single cell fraction: EpCAM+ and EpCAM- subpopulations

Single Cells (%)							
EpCAM+	Median	Min.	Max.	EpCAM-	Median	Min.	Max.
CD133+CD44-	0.24	0.00	1.17	CD133+CD44-	0.12	0.04	0.42
CD133+CD44-	0.30	0.00	2.19	CD133+CD44-	0.01	0.00	0.23
CD133-CD44+	2.87	0.09	64.10	CD133-CD44+	46.60	6.99	69.90
CD133-CD44-	2.33	0.14	17.70	CD133-CD44-	38.80	22.60	75.80
L1CAM+CD44-	0.16	0.00	0.71	L1CAM+CD44-	0.11	0.00	0.72
L1CAM+C44+	0.16	0.00	57.20	L1CAM+C44+	0.03	0.00	2.20
L1CAM-C44+	2.85	0.09	18.50	L1CAM-C44+	46.65	4.82	69.70
L1CAM-C44-	2.36	0.27	17.30	L1CAM-C44-	38.90	22.50	75.80
CD133+L1CAM-	0.33	0.00	56.00	CD133+L1CAM-	0.15	0.00	2.36
CD133+L1CAM+	0.05	0.00	1.50	CD133+L1CAM+	0.00	0.00	0.14
CD133-L1CAM+	0.37	0.00	1.51	CD133-L1CAM+	0.12	0.06	0.36
CD133-L1CAM-	5.30	0.14	28.20	CD133-L1CAM-	91.75	31.20	98.60

Table 8. Cell populations in ascites spheroid fraction: EpCAM+ and EpCAM- subpopulations

Spheroids (%)							
EpCAM+	Median	Min.	Max.	EpCAM-	Median	Min.	Max.
CD133+CD44-	1.09	0.00	2.82	CD133+CD44-	0.24	0.05	1.82
CD133+CD44-	0.33	0.02	14.70	CD133+CD44-	0.01	0.00	0.19
CD133-CD44+	1.42	0.14	8.62	CD133-CD44+	3.74	0.07	14.90
CD133-CD44-	8.42	0.73	17.50	CD133-CD44-	83.65	48.40	92.10
L1CAM+CD44-	0.34	0.00	2.20	L1CAM+CD44-	0.18	0.00	0.96
L1CAM+C44+	0.15	0.00	1.51	L1CAM+C44+	0.00	0.00	0.10
L1CAM-C44+	2.38	0.19	22.90	L1CAM-C44+	2.03	0.14	14.70
L1CAM-C44-	8.85	1.72	19.30	L1CAM-C44-	83.65	47.80	93.80
CD133+L1CAM-	0.41	0.00	7.93	CD133+L1CAM-	0.16	0.00	1.22
CD133+L1CAM+	0.28	0.00	0.63	CD133+L1CAM+	0.00	0.00	0.04
CD133-L1CAM+	0.79	0.02	17.50	CD133-L1CAM+	0.31	0.10	2.01
CD133-L1CAM-	10.34	0.82	18.10	CD133-L1CAM-	86.35	60.50	96.30

Frequencies (in percent) of CD45-EpCAM+ and CD45-EpCAM- events resulting from combination of the markers CD133, CD44 and L1CAM in single cells (upper table) and spheroid samples (lower table) of malignant ascites. Statistical significance in differential frequencies between spheroids and single cells is marked as bold.

In the EpCAM+ spheroid fraction of ascites, more CD133+CD44- cells were abundant than in the single cell fraction (p=0.01), whereas the abundance of CD133+CD44+ cell was similar in both fractions (Fig. 15).

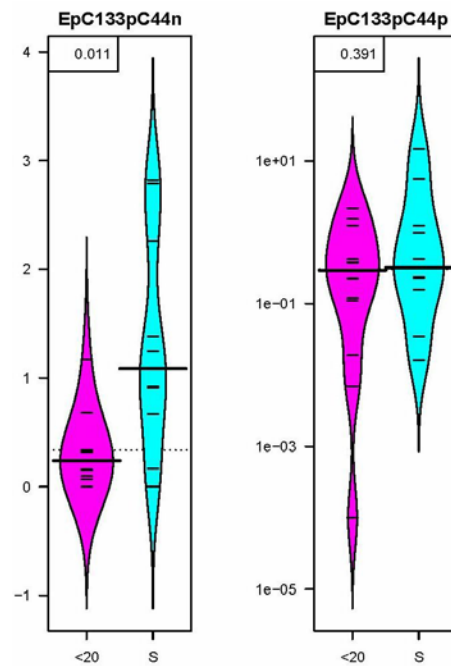


Figure 15. EpCAM+ (left) CD133+CD44- cell population, (right) CD133+CD44+ cell population in single cell (<20) and spheroid (S) fraction. Y-axis: scale for frequency of populations among all CD45 negative events

The L1CAM-CD44- cell population was also more abundant in spheroids from ascites samples than in single cells ($p=0.048$), whereas the abundance of L1CAM+CD44- cells was similar in both fractions (Fig. 16).

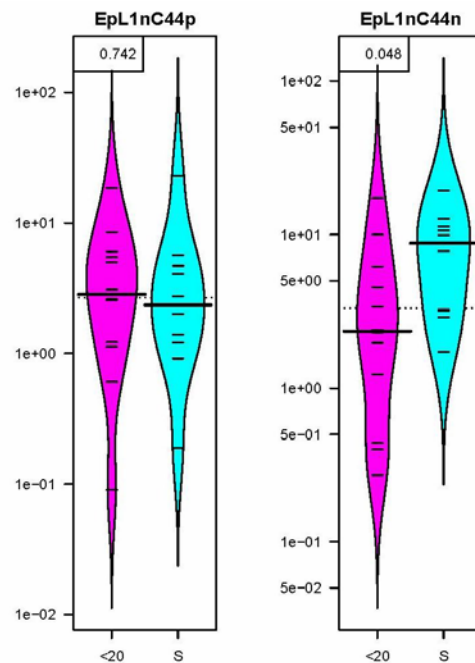
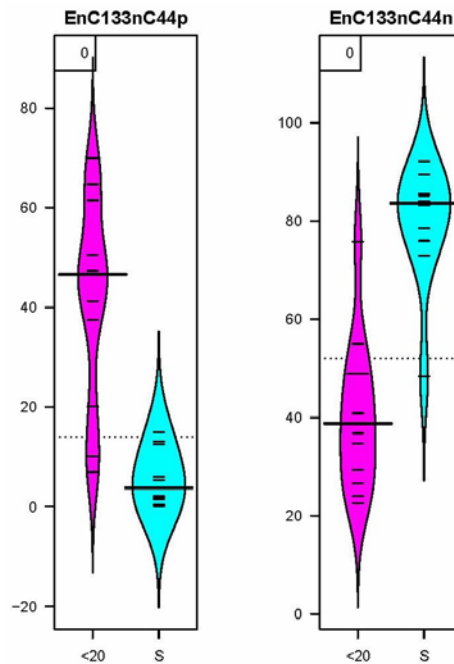


Figure 16. CD45-EpCAM+ (left) L1CAM+CD44+ cell population, (right) L1CAM-CD44- cell population in single cell (<20) and spheroid (S) fraction

Among the EpCAM⁻ events, the CD133-CD44⁺ cell population was enriched in the single cell fraction ($p<0.001$), whereas the CD133-CD44⁻ population was enriched in spheroids ($p<0.001$) (Fig. 17).



3.3.3.2 Tumor Tissue

The abundance of cell populations in tumor tissue of ovarian (“primary tumor”) or peritoneal origin (“metastasis”) –both depleted of CD45⁺ cells– was assessed by flow cytometry as well. Thereof, frequencies of CD44⁺, CD133⁺, L1CAM⁺, EpCAM⁺, and EpCAM⁻ population were compared. Because of the sampling process, populations were calculated as frequency of CD45⁻ events, to compensate for previous depletion of CD45⁺ cells by magnetic bead separation.

Table 9. Frequency (%) of cell populations in ovarian tumor tissue

Ovarian Tumor (%)				
n=10	Median	Standard Deviation	Minimum	Maximum
CD44 ⁺	14.41	14.34	4.61	52.69
CD133 ⁺	0.54	1.12	0.00	3.20
L1CAM ⁺	0.55	1.62	0.04	5.46
EPCAM ⁺	30.44	17.93	2.89	65.72
CD44 ⁺ EPCAM ⁺	3.74	5.57	1.61	18.11
CD44 ⁺ EpCAM ⁻	11.15	11.98	2.89	43.51

Table 10. Frequency (%) of cell populations in peritoneal tumor tissue

Peritoneal Tumor (%)				
n=13	Median	Standard Deviation	Minimum	Maximum
CD44+	21.05	23.31	1.95	84.51
CD133+	0.41	1.34	0.00	4.15
L1CAM+	0.54	0.69	0.14	2.02
EPCAM+	12.46	15.56	2.56	49.50
CD44+EPCAM+	3.30	3.64	0.65	13.10
CD44+EpCAM-	17.70	29.09	1.22	94.90

In tumor tissues of peritoneal or ovarian location, similar frequencies of cell populations analyzed by flow cytometry were observed. Cells expressing either EpCAM or CD44 were most abundant in tumor tissues, whereas CD133+ and L1CAM+ cells only accounted for a small number of gated events. Furthermore, gating of EpCAM+ and EpCAM- cells allowed for analysis of cell subpopulations (Tab. 11 f.).

Table 11. Frequency (%) of cell populations in ovarian tumors: EpCAM+ and EpCAM- subpopulations

Ovarian Tumor (%)							
EpCAM+	Median	Min.	Max.	EpCAM-	Median	Min.	Max.
CD133+CD44-	0.50	0.04	4.48	CD133+CD44-	0.06	0.00	0.83
CD133+CD44-	0.21	0.04	3.41	CD133+CD44-	0.00	0.00	0.11
CD133-CD44+	3.63	1.50	14.70	CD133-CD44+	11.10	2.89	43.50
CD133-CD44-	34.60	1.77	65.90	CD133-CD44-	44.80	26.60	85.30
L1CAM+CD44-	0.22	0.00	3.36	L1CAM+CD44-	0.02	0.00	0.53
L1CAM+C44+	0.23	0.00	2.35	L1CAM+C44+	0.00	0.00	0.08
L1CAM-C44+	3.73	1.35	16.30	L1CAM-C44+	11.14	2.89	43.00
L1CAM-C44-	33.55	1.99	66.40	L1CAM-C44-	44.75	27.10	85.60
CD133+L1CAM-	0.32	0.03	4.81	CD133+L1CAM-	0.04	0.00	0.53
CD133+L1CAM+	0.13	0.00	1.53	CD133+L1CAM+	0.00	0.00	0.04
CD133-L1CAM+	0.73	0.17	6.97	CD133-L1CAM+	0.09	0.02	1.11
CD133-L1CAM-	40.15	2.75	68.00	CD133-L1CAM-	59.20	31.30	94.70

Comparison of EpCAM+ and EpCAM- subpopulations in tumor tissues revealed no statistically significant difference between cell populations from peritoneal and ovarian tumors, proposing a consistency in tumor composition between primary and secondary lesions prior to clinical treatment.

Table 12. Frequency (%) of cell populations in peritoneal tumors: EpCAM+ and EpCAM- subpopulations

Peritoneal Tumor							
EpCAM+	Median	Min.	Max.	EpCAM-	Median	Min.	Max.
CD133+CD44-	0.51	0.01	2.28	CD133+CD44-	0.19	0.00	0.61
CD133+CD44-	0.32	0.01	1.70	CD133+CD44-	0.00	0.00	0.05
CD133-CD44+	2.90	0.46	11.40	CD133-CD44+	17.70	1.22	94.90
CD133-CD44-	14.20	2.25	51.40	CD133-CD44-	46.30	2.16	68.20
L1CAM+CD44-	0.21	0.06	1.69	L1CAM+CD44-	0.04	0.00	0.47
L1CAM+C44+	0.11	0.03	0.96	L1CAM+C44+	0.00	0.00	0.06
L1CAM-C44+	3.21	0.58	13.00	L1CAM-C44+	17.70	1.22	95.00
L1CAM-C44-	14.30	2.19	51.80	L1CAM-C44-	46.90	2.06	69.00
CD133+L1CAM-	0.18	0.06	2.01	CD133+L1CAM-	0.06	0.00	0.47
CD133+L1CAM+	0.07	0.00	0.92	CD133+L1CAM+	0.00	0.00	0.00
CD133-L1CAM+	1.11	0.01	3.95	CD133-L1CAM+	0.21	0.01	0.73
CD133-L1CAM-	17.80	2.76	55.80	CD133-L1CAM-	79.60	40.80	97.10

3.3.4 Principal Component Analysis

Combining frequencies of all evaluated markers and marker combinations from cell fractions (single ascites cells, ascites cell aggregates, primary tumor, and metastasis) and reducing the dimensionality of these variables to linearly uncorrelated components by Principal Component Analysis (PCA) a plot was generated (Fig. 18). Principal Components (PC) 1, 2, and 3 depict variables (linearly uncorrelated) that together account for 55.1 % of the variability in the dataset. PC1 accounts for 22.5 %, PC2 for 18.1 %, and PC3 for 14.6 % of data variability. As shown in figure 18, patients can be divided according to their mode of tumor spread (red versus black) in the first and second PC. The only exception is patient 16, which had an unusual high amount of CD133+ cells in the ascites (see Supp. Table S2). PC3 separates patient 29 (no known mutation) from patient 22 (*KRAS* mutated), while patient 24 (the second patient without any observable mutation) clusters within the group of *TP53* mutated samples.

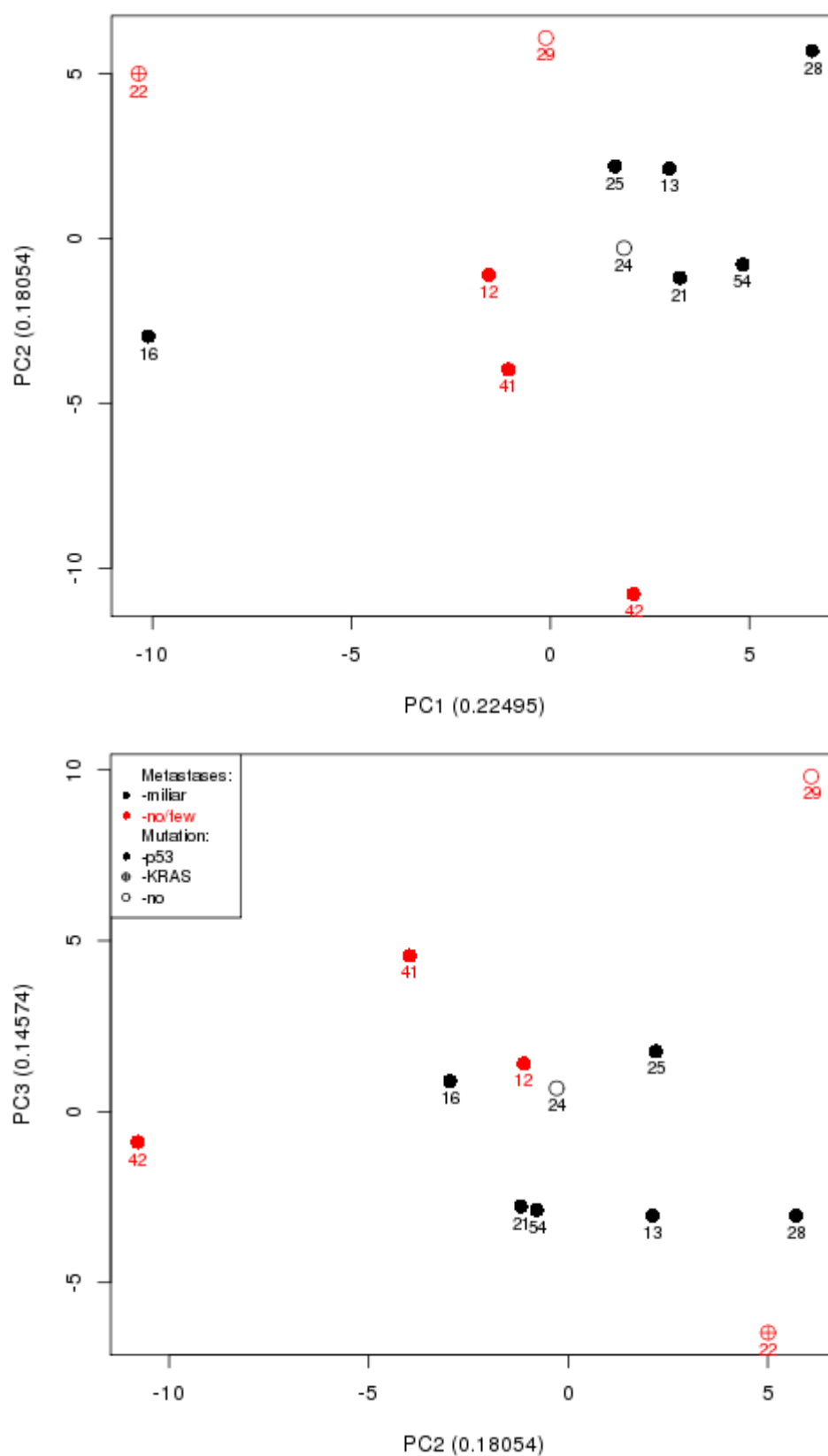


Figure 18. PCA of FC data. Numbers depict patients (n=12); filled circles stand for patients with functional p53 mutations, open circles for patients without mutated *KRAS* or p53 (according to our tests), and the circle with the cross depicts the only patient with *KRAS* mutation.

3.3.5 Correlation of cell frequencies with presence of spheroids

The presence of spheroids in malignant ascites of EOC patients was not significantly correlated to the abundance of any of the surface markers examined in the tumor tissues (ovarian or peritoneal) or in the filtered ascites single cells as tested with Mann Whitney-U tests. Yet, the co-expression of CD44 and EpCAM in ovarian tumor tissues, as well as in ascites single cells, revealed a trend towards presence of cell aggregates in the ascites if abundant (Fig. 19 and 20). In tumor tissues of peritoneal origin (metastases) from nine patients with ascites, seven ascites samples contained filterable cell spheroids, whereas two samples had none. The proportion of EpCAM+ cells was higher in peritoneal tissues from patients with spheroids compared to those without ($p=0.117$, Fig. 21), whereas the frequency of CD45+ cells was slightly higher in the latter ($p=0.143$), but the differences were not statistically significant.

Ascites Single Cells	Spheroids (%)				p-value
	yes		no		
	Median	Standard Deviation	Median	Standard Deviation	
CD45+	60.90	22.92	51.00	35.21	0.667
CD44+	18.90	17.93	27.15	14.64	0.519
CD133+	0.31	1.08	0.29	0.19	0.667
L1CAM+	0.34	17.15	0.16	0.08	0.519
EpCAM+	3.54	17.76	1.69	2.21	0.283
CD44+EpCAM+	4.01	19.91	1.60	2.14	0.283
CD44+ EpCAM-	43.95	21.64	58.25	16.48	0.390

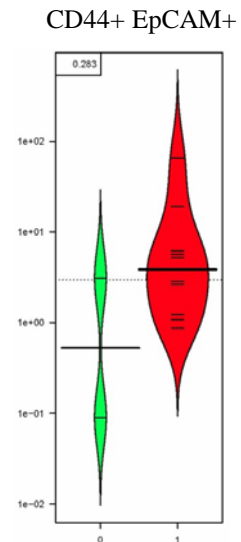


Figure 19. Correlation of the frequency (%) of cell populations in ascites single cell fractions with the presence of spheroids

Ovarian Tumor	Spheroids (%)				p-value
	yes		no		
	Median	Standard Deviation	Median	Standard Deviation	
CD45+	4.90	4.48	7.90	9.19	1.000
CD44+	14.78	18.46	11.78	3.80	0.699
CD133+	0.64	1.33	0.57	0.80	0.688
L1CAM+	0.24	2.33	0.75	1.00	0.699
EpCAM+	38.38	15.11	20.97	25.56	0.245
CD44+EpCAM+	5.16	4.41	1.67	0.09	0.053
CD44+ EpCAM-	13.00	16.24	12.54	7.58	0.699

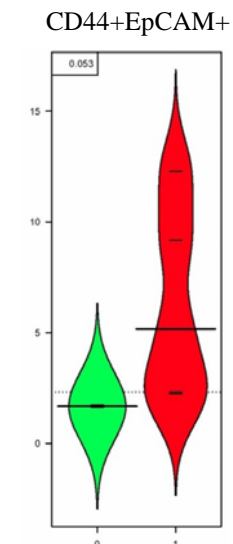


Figure 20. Correlation of the frequency (%) of cell populations in ovarian tumor tissues with the presence of spheroids

Peritoneal Tumor	Spheroids (%)				p-value
	yes		no		
	Median	Standard Deviation	Median	Standard Deviation	
CD45+	6.70	5.81	23.65	14.78	0.143
CD44+	18.30	29.14	31.22	32.69	0.558
CD133+	1.43	1.58	0.20	0.29	0.242
L1CAM+	0.54	0.64	0.24	0.15	0.143
EpCAM+	22.58	13.85	8.40	1.26	0.143
CD44+EpCAM+	3.30	4.77	4.37	2.37	0.770
CD44+ EpCAM-	13.65	33.25	40.27	34.83	0.380

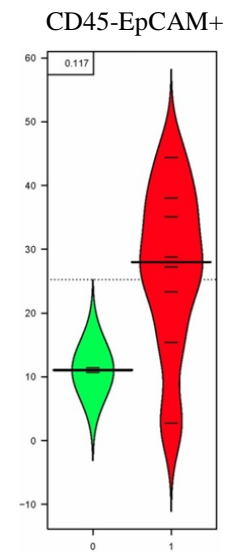


Figure 21. Correlation of the frequency (%) of cell populations in peritoneal tumor tissues with the presence of spheroids

The presence of spheroids was furthermore compared to subpopulations of epithelial tumor cells (EpCAM+) and non-epithelial cells (EpCAM-), assessed by combination of the markers CD44, CD133, and L1CAM, and shown in starplots below (Fig. 22). Although the amount of double negative-populations (e.g. CD133-CD44-) shows a statistically significant difference between patients bearing spheroids and patients without spheroids in the ascites, interpretation of this fact is difficult, because of cell debris in FC plots. More information is gained through analysis of single and double positive subpopulations. In primary tumors the CD44+CD133- cells in the EpCAM+ tumor cell populations were more frequent when spheroids were present in the corresponding ascites samples

The correlation of subpopulations of EpCAM positive and negative cells (assessed with combination of the markers CD44, CD133, and L1CAM) and spheroid abundance was tested for statistical significance with Mann-Whitney-U tests and depicted as starplots in Fig. 22. No difference in the frequency of the depicted cell populations between spheroid bearing and missing ascites showed statistical significance (see Tab. 13).

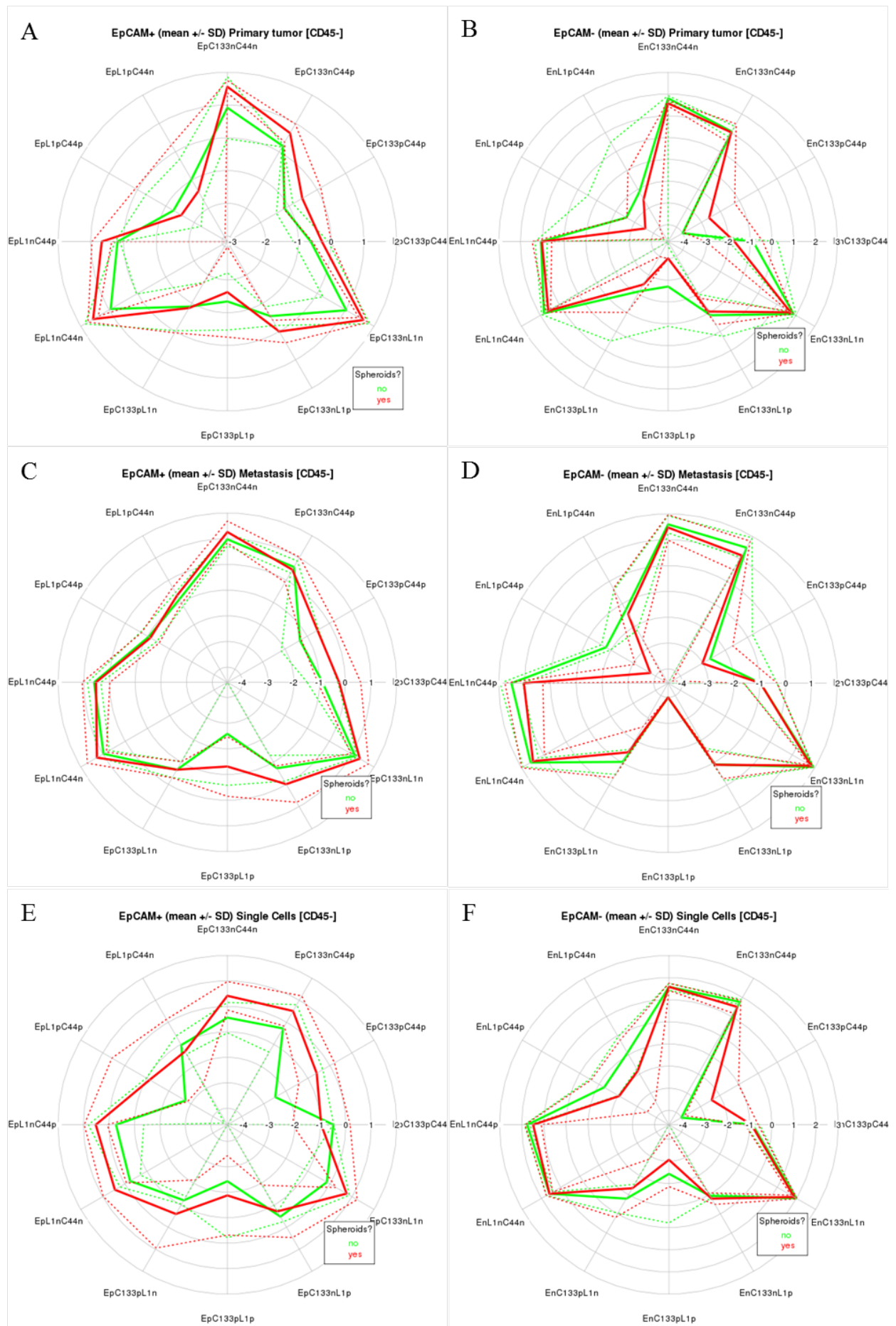


Figure 22. No ascites subpopulation is significantly enriched in patients with spheroidal cell aggregates. Starplots describe the frequency of the cell populations (clockwise, from the top) EpCAM+ (left column) or EpCAM- (right column) and CD133-CD44-, CD133-CD44+, CD133+CD44-, CD133+CD44+, CD133-L1CAM-, CD133-L1CAM+, CD133+L1CAM-, CD133+L1CAM+, L1CAM-CD44-, L1CAM-CD44+, L1CAM+CD44-, and L1CAM+CD44-. Bold lines stand for means, spotted lines for standard deviation, green: samples without spheroids in ascites, red: samples from ascites with spheroids.

Table 13. Median frequencies (%) of cell populations from patients with and without spheroids in the ascites

A and B

Ovarian Tumor	Spheroids				Spheroids		
	Median		P-value		Median		P-value
EpCAM+	no (2)	yes (5)		EpCAM-	no (2)	yes (5)	
CD133+CD44-	0.33	0.51	0.439	CD133+CD44-	0.42	0.05	0.699
CD133+CD44+	0.08	0.17	0.245	CD133+CD44-	0.00	0.01	0.200
CD133-CD44+	1.60	5.10	0.053	CD133-CD44+	12.54	13.00	0.699
CD133-CD44-	20.04	34.60	0.439	CD133-CD44-	64.95	42.20	0.053
L1CAM+CD44-	0.19	0.06	1.000	L1CAM+CD44-	0.26	0.00	0.688
L1CAM+C44+	0.14	0.03	1.000	L1CAM+C44+	0.04	0.00	0.334
<i>L1CAM-C44+</i>	<i>1.54</i>	<i>5.14</i>	<i>0.053</i>	L1CAM-C44+	12.60	13.00	0.699
L1CAM-C44-	20.20	32.90	0.439	L1CAM-C44-	65.05	42.30	0.053
CD133+L1CAM-	0.28	0.08	1.000	CD133+L1CAM-	0.26	0.00	0.688
CD133+L1CAM+	0.10	0.05	1.000	CD133+L1CAM+	0.02	0.00	0.334
CD133-L1CAM+	0.33	1.15	0.121	CD133-L1CAM+	0.42	0.06	0.845
CD133-L1CAM-	21.38	41.00	0.245	CD133-L1CAM-	77.25	55.20	0.245

C and D

Peritoneal Tumor	Spheroids				Spheroids		
	Median		P- value		Median		P- value
EpCAM+	no (2)	yes (7)		EpCAM-	no (2)	yes (7)	
CD133+CD44-	0.20	0.80	0.143	CD133+CD44-	0.17	0.23	0.770
CD133+CD44+	0.10	0.33	0.143	CD133+CD44-	0.02	0.00	0.872
CD133-CD44+	4.27	2.90	0.770	CD133-CD44+	40.25	13.60	0.380
CD133-CD44-	10.21	23.00	0.380	CD133-CD44-	44.75	48.50	0.770
L1CAM+CD44-	0.16	0.21	0.770	L1CAM+CD44-	0.12	0.05	0.770
L1CAM+C44+	0.10	0.06	0.769	<i>L1CAM+C44+</i>	<i>0.02</i>	<i>0.00</i>	<i>0.015</i>
L1CAM-C44+	4.29	3.21	0.770	L1CAM-C44+	40.55	10.70	0.380
L1CAM-C44-	10.24	23.50	0.380	L1CAM-C44-	44.55	50.70	0.770
CD133+L1CAM-	0.26	0.18	1.000	CD133+L1CAM-	0.13	0.05	1.000
CD133+L1CAM+	0.03	0.07	0.303	CD133+L1CAM+	0.00	0.00	1.000
CD133-L1CAM+	0.28	1.22	0.143	CD133-L1CAM+	0.21	0.23	1.000
CD133-L1CAM-	14.20	31.60	0.143	CD133-L1CAM-	84.85	67.00	0.143

E and F

Single Cells	Spheroids				Spheroids		
	Median		P-value		Median		P-value
EpCAM+	no (2)	yes (10)			EpCAM-	no (2)	
CD133+CD44-	0.32	0.16	0.519	CD133+CD44-	0.15	0.12	0.830
<i>CD133+CD44+</i>	<i>0.06</i>	<i>0.38</i>	<i>0.086</i>	CD133+CD44-	0.00	0.02	0.169
CD133-CD44+	1.55	3.57	0.283	CD133-CD44+	58.25	43.90	0.237
CD133-CD44-	0.54	2.73	0.133	CD133-CD44-	39.10	38.80	0.914
L1CAM+CD44-	0.11	0.16	0.830	L1CAM+CD44-	0.27	0.11	0.516
L1CAM+C44+	0.02	0.20	0.130	L1CAM+C44+	0.10	0.03	0.665
L1CAM-C44+	1.59	3.80	0.283	L1CAM-C44+	58.15	42.40	0.283
L1CAM-C44-	0.75	2.90	0.086	L1CAM-C44-	38.95	38.90	1.000
CD133+L1CAM-	0.06	0.43	0.197	CD133+L1CAM-	0.30	0.15	0.667
CD133+L1CAM+	0.07	0.05	0.913	CD133+L1CAM+	0.07	0.00	0.472
CD133-L1CAM+	0.35	0.37	0.830	CD133-L1CAM+	0.12	0.17	0.667
CD133-L1CAM-	1.98	7.33	0.197	CD133-L1CAM-	97.05	89.15	0.133

Italic: population mentioned in text

No cell population was found to differ statistically significantly between patients with and without spheroids, only the abundance of EpCAM+CD44+CD133+ cells in the ascites single cell fraction correlated with cell aggregates, but statistical significance was not reached ($p=0.086$, Tab. 13E). Furthermore, levels of L1CAM-C44+ cells in ovarian tumors of patients with spheroids were higher than those from patients without spheroids ($p=0.053$, Tab. 13A), but again not reaching statistical significance. The p-value of 0.015 for EpCAM-L1CAM+C44+ cells in the peritoneal tumor fraction (Fig. 13D) may be due to a statistical misinterpretation of the data, as in the seven samples from ascites with spheroids all cells were negative for this population and one of the two samples from patients without spheroids showed a negligibly population of these cell types, most likely to represent a spill-over from another more prominent population (EpCAM-CD44+) in the L1CAM gate.

3.3.6 Correlation with peritoneal tumor spread

Staining with antibodies against surface antigens and subsequent flow cytometric analysis of ascites and tissue cells together with data about the peritoneal tumor spread allowed for comparison of the abundance of cell types with the patterns of peritoneal tumor spread in these patients. For statistical analyses patterns 0 (no peritoneal implants, $n=2$) and 1 (few big implants, $n=5$) were combined as type 0 and a miliary tumor spread was denoted type 1 ($n=9$). Again, both fractions of ascites cells, single cells, and spheroids were analyzed and differences between samples from patients with type 0 or 1 tumor spread were statistically assessed with the Mann-Whitney-U test (Fig. 23 ff.).

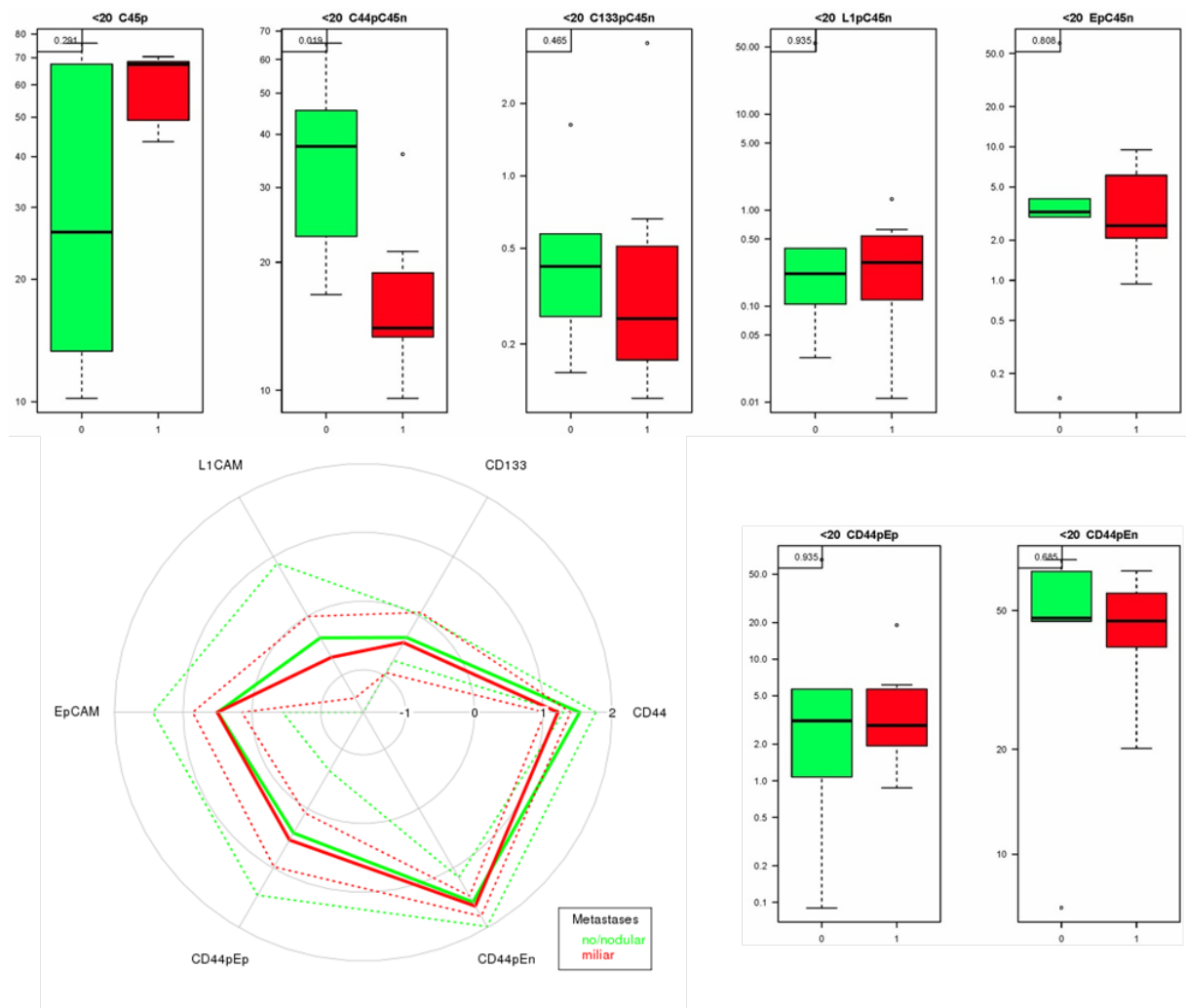


Figure 23. Starplot and boxplots of ascites single cell populations in patients with different modes of peritoneal tumor spread. 0: no/ few big lesions, 1: miliary tumor spread.

In the single cell fraction of ascites frequencies of leukocyte populations (CD45+) were very heterogeneous in patients without or with few big implants, but higher in patients presenting with a miliary tumor spread in the peritoneum (but not statistically significant). The situation was reversed for cells expressing CD44; here the frequency of this subtype was significantly lower in samples from the miliary type. The distribution of the other single markers CD133, L1CAM, and EpCAM were similar in both subtypes.

Looking at EpCAM positive and negative subtypes of cells expressing CD44, the abundance of the EpCAM negative cells was much higher in both subtypes of tumor spread compared to EpCAM positive cells, but there were no differences between the two subtypes.

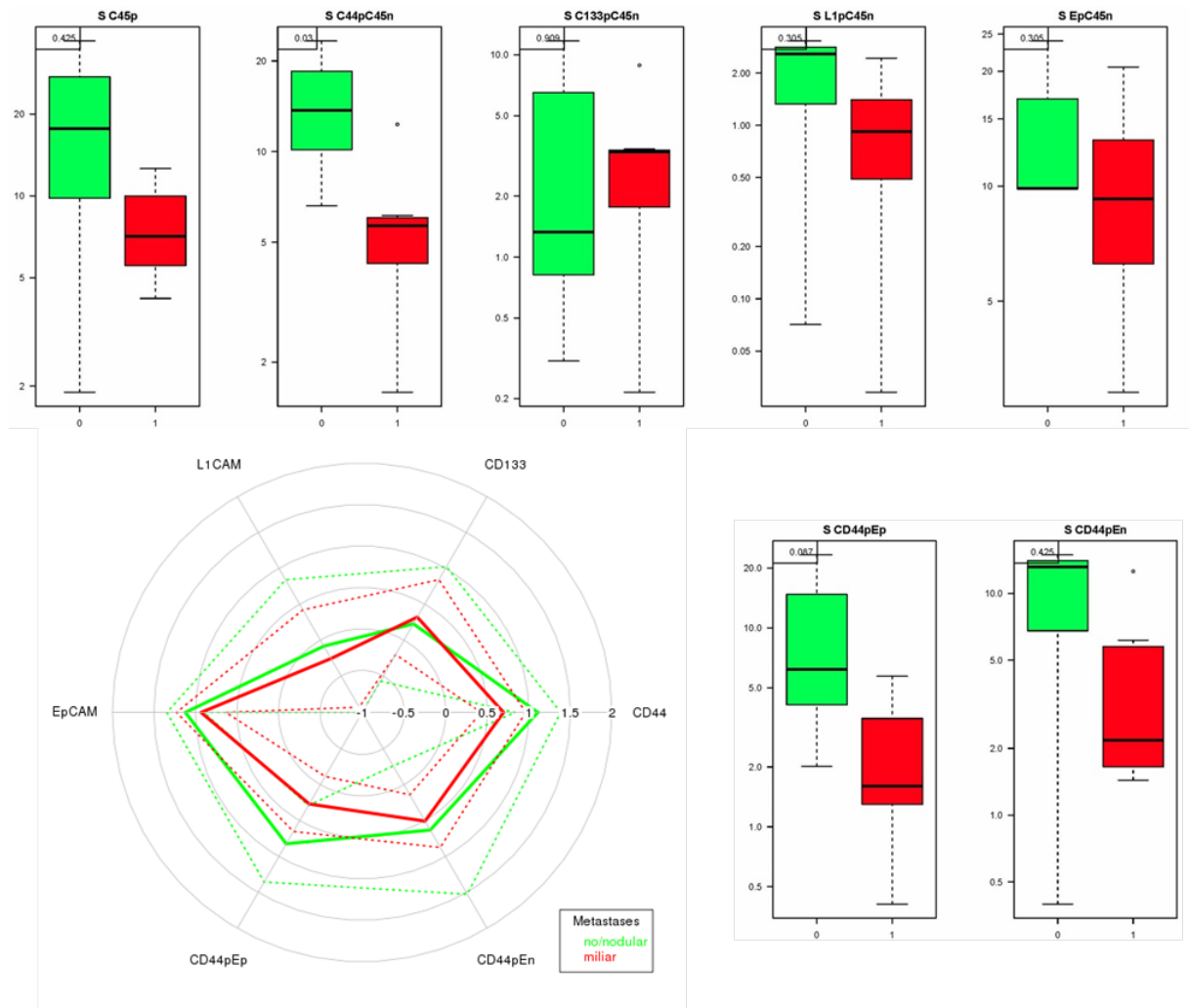
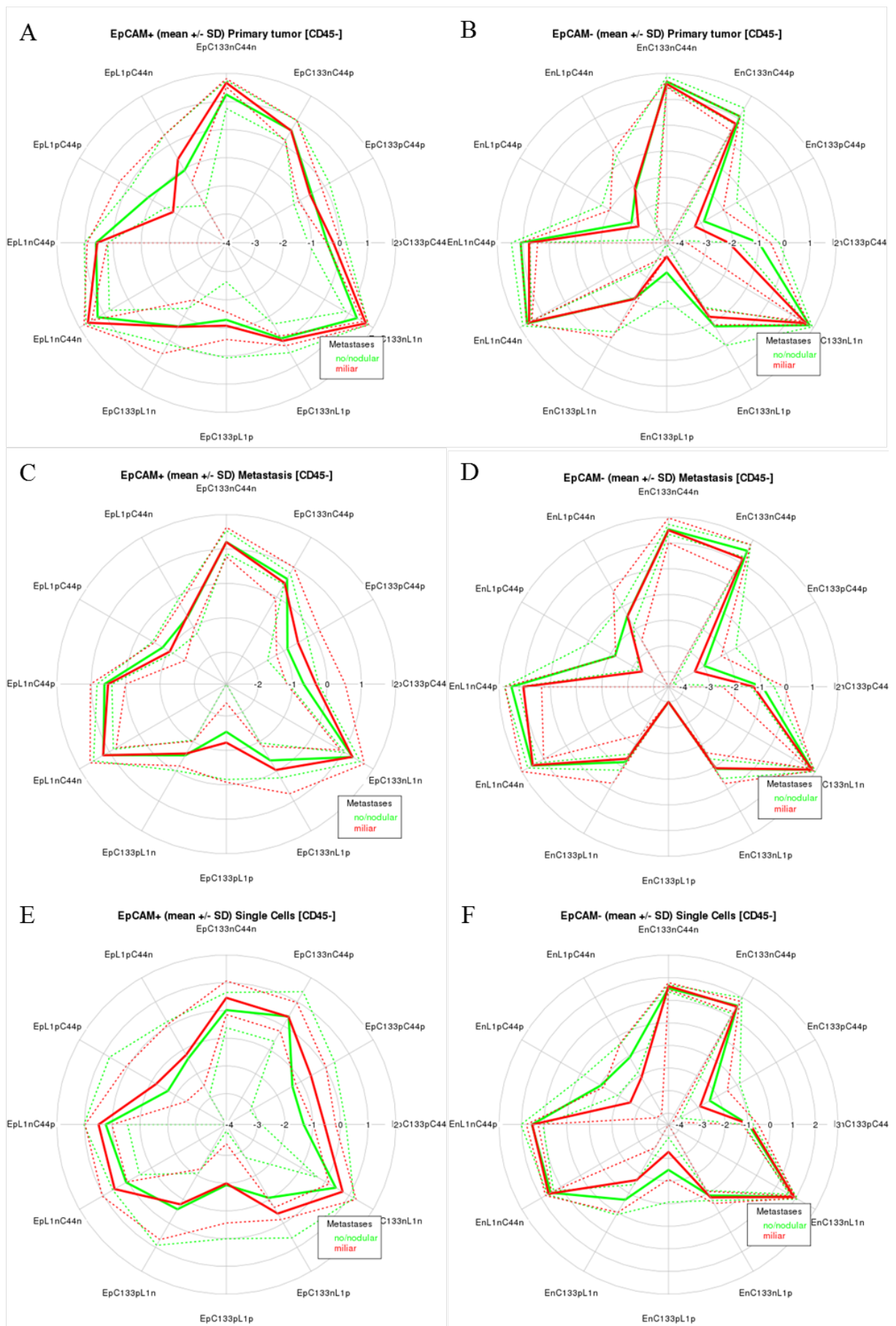


Figure 24. Starplot and boxplots of ascites spheroid populations in patients with different modes of peritoneal tumor spread. 0: no/ few big lesions, 1: miliary tumor spread.

In spheroids similar results were obtained. Multicellular aggregates from patients with miliary peritoneal tumor spread showed a lower frequency of leukocytes. CD44 positive cells were significantly reduced in spheroids from ascites of the miliary type ($p=0.03$), but examining this population for EpCAM expression, both EpCAM+ and EpCAM- cells were found to be enriched in type 0, but statistical significance is gone (CD44+EpCAM+, $p=0.087$; CD44+EpCAM-, $p=0.425$).

When looking at the markers CD44, L1CAM, and CD133 in cells positively or negatively gated for EpCAM, no statistical significant correlation between the abundance of these markers and the peritoneal tumor spread can be observed. However, in spheroids the population of CD44+EpCAM+ cells described above, was shown to mostly consist of cells negative for CD133 and L1CAM (see table 14G, row “CD133-CD44+”, and “L1CAM-CD44+”).



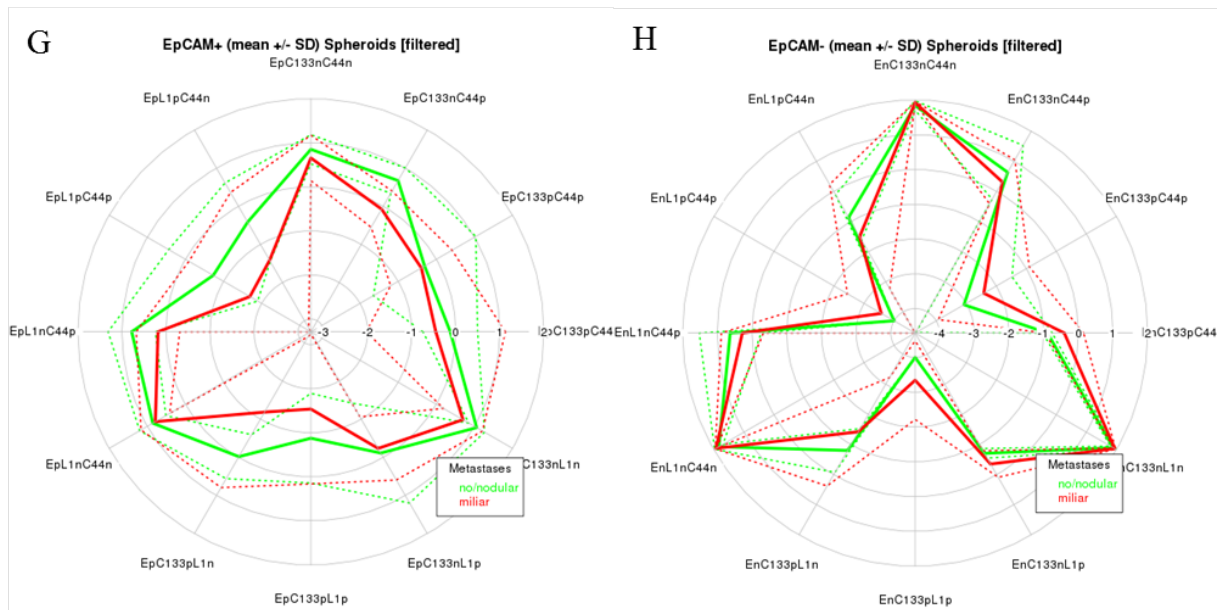


Figure 25. Starplots of FC data for combinations of the markers CD44, L1CAM, and CD133 in EpCAM+ (left column) and EpCAM- (right) gated events. A and B ovarian tumor, C and D peritoneal tumor, E and F single cells, G and H spheroids

Table 14. Median frequencies (%) of cell populations of patients with different modes of tumor spread

A and B

Ovarian Tumor	Tumor spread median				Tumor spread median			
EpCAM+	no/few	miliary	p-value		EpCAM-	no/few	miliary	p-value
CD133+CD44-	0.53	0.51	0.569		CD133+CD44-	0.26	0.05	0.305
CD133+CD44+	0.24	0.17	0.909		CD133+CD44+	0.00	0.00	0.700
CD133-CD44+	3.40	2.16	0.732		CD133-CD44+	11.60	5.29	0.138
CD133-CD44-	26.25	41.20	0.067		CD133-CD44-	50.15	42.20	0.425
L1CAM+CD44-	0.20	0.10	0.732		L1CAM+CD44-	0.02	0.06	0.908
L1CAM+C44+	0.23	0.01	0.569		L1CAM+C44+	0.00	0.00	0.606
L1CAM-C44+	3.43	2.31	0.732		L1CAM-C44+	11.69	5.38	0.138
L1CAM-C44-	27.05	42.20	0.137		L1CAM-C44-	50.15	42.30	0.425
CD133+L1CAM-	0.32	0.08	0.909		CD133+L1CAM-	0.03	0.08	0.908
CD133+L1CAM+	0.15	0.05	0.909		CD133+L1CAM+	0.00	0.00	0.329
CD133-L1CAM+	0.67	1.15	0.425		CD133-L1CAM+	0.54	0.06	0.732
CD133-L1CAM-	32.00	43.10	0.053		CD133-L1CAM-	65.50	52.50	0.053

C and D

Peritoneal Tumor	Tumor spread median				Tumor spread median			
EpCAM+	no/few	miliary	p-value		EpCAM-	no/few	miliary	p-value
CD133+CD44-	0.38	0.81	0.072		CD133+CD44-	0.17	0.21	0.841
CD133+CD44+	0.28	0.33	0.317		CD133+CD44+	0.02	0.00	0.676
CD133-CD44+	5.17	2.58	0.947		CD133-CD44+	30.60	12.80	0.257
CD133-CD44-	13.40	17.20	0.947		CD133-CD44-	30.10	49.55	0.549
L1CAM+CD44-	0.15	0.20	0.739		L1CAM+CD44-	0.03	0.08	0.549

L1CAM+C44+	0.17	0.08	0.205	L1CAM+C44+	0.01	0.00	0.140
L1CAM-C44+	5.76	2.75	0.947	L1CAM-C44+	30.15	11.20	0.257
L1CAM-C44-	13.75	17.80	0.947	L1CAM-C44-	30.70	54.55	0.549
CD133+L1CAM-	0.15	0.21	0.947	CD133+L1CAM-	0.04	0.09	0.841
CD133+L1CAM+	0.09	0.07	0.789	CD133+L1CAM+	0.00	0.00	
CD133-L1CAM+	0.79	1.42	0.162	CD133-L1CAM+	0.13	0.24	0.641
CD133-L1CAM-	16.95	26.20	0.739	CD133-L1CAM-	81.40	69.85	0.549

E and F

Single Cells	Tumor spread				Tumor spread		
	median				median		
EpCAM+	no/few	miliary	p-value	EpCAM-	no/few	miliary	p-value
CD133+CD44-	0.32	0.16	0.372	CD133+CD44-	0.10	0.15	0.570
CD133+CD44+	0.11	0.38	0.465	CD133+CD44+	0.02	0.00	0.665
CD133-CD44+	3.00	2.73	0.935	CD133-CD44+	47.30	41.20	0.329
CD133-CD44-	0.95	3.10	0.291	CD133-CD44-	29.30	40.80	0.371
L1CAM+CD44-	0.18	0.15	0.745	L1CAM+CD44-	0.18	0.04	0.683
L1CAM+C44+	0.03	0.19	0.567	L1CAM+C44+	0.04	0.02	0.219
L1CAM-C44+	3.08	2.61	0.808	L1CAM-C44+	47.50	38.10	0.372
L1CAM-C44-	1.23	3.40	0.123	L1CAM-C44-	29.00	39.90	0.372
CD133+L1CAM-	0.08	0.36	0.685	CD133+L1CAM-	0.24	0.08	0.371
CD133+L1CAM+	0.10	0.04	0.679	CD133+L1CAM+	0.01	0.00	0.415
CD133-L1CAM+	0.29	0.38	0.685	CD133-L1CAM+	0.10	0.23	0.685
CD133-L1CAM-	3.82	6.78	0.808	CD133-L1CAM-	95.50	91.20	0.570

G and H

Spheroids	Tumor spread				Tumor spread		
	median				median		
EpCAM+	no/few	miliary	p-value	EpCAM-	no/few	miliary	p-value
CD133+CD44-	0.92	1.25	0.909	CD133+CD44-	0.13	0.39	0.138
CD133+CD44+	0.23	0.43	0.909	CD133+CD44+	0.00	0.02	0.543
CD133-CD44+	5.97	1.17	0.003	CD133-CD44+	13.10	2.18	0.305
CD133-CD44-	9.78	7.73	0.569	CD133-CD44-	73.00	84.10	0.305
L1CAM+CD44-	0.98	0.30	0.209	L1CAM+CD44-	0.12	0.24	0.909
L1CAM+C44+	0.48	0.10	0.209	L1CAM+C44+	0.00	0.00	0.513
<i>L1CAM-C44+</i>	<i>4.68</i>	<i>1.40</i>	<i>0.138</i>	L1CAM-C44+	13.20	1.87	0.305
L1CAM-C44-	9.91	7.78	0.909	L1CAM-C44-	73.30	83.90	0.305
CD133+L1CAM-	1.86	0.39	0.424	CD133+L1CAM-	0.12	0.21	0.909
CD133+L1CAM+	0.42	0.27	0.304	CD133+L1CAM+	0.00	0.00	0.329
CD133-L1CAM+	0.60	0.92	0.909	CD133-L1CAM+	0.16	0.43	0.138
CD133-L1CAM-	11.70	8.97	0.360	CD133-L1CAM-	87.80	84.90	0.569

Bold= Statistical significant differences in abundance of cell population between the modes of tumor spread, italic: population mentioned in text.

Summarizing results from correlation of the mode of peritoneal tumor spread and cell frequencies as assessed by flow cytometry, cells expressing CD44 (and EpCAM) are

significantly enriched in ascites of patients with no or few big implants in the peritoneum, suggesting an important role for CD44+ cells in tumor spread.

Table 15. Correlation of spheroids with the mode of peritoneal tumor spread

		Tumor spread		total	Sign. (Fischer)
		no/few	miliary		
Spheroids	no	2	0	2	0.152
	yes	3	7	10	

Significance (2-tailed) computed with Fischer's exact tests.

Ascites without filterable spheroids was observed only in patients without or with few big implants, whereas all patients with ascites and miliary spread had spheroids (p=0.152). Probably a higher sample number will show this association to be statistically significant.

3.3.7 Correlation with presence of ascites

In both, peritoneal and ovarian tumor tissues the abundance of CD45+ cells was enriched in patients presenting without ascites (n=4), although without statistical significance if analyzed alone (peritoneal tumor: p=0.209; ovarian tumor: p=0.33). Mutual analysis of the ovarian and peritoneal tumors resulted in a p-value of 0.054 for exact significance supporting a strong trend towards a higher CD45+ cell abundance in tumor tissues of patients without ascites.

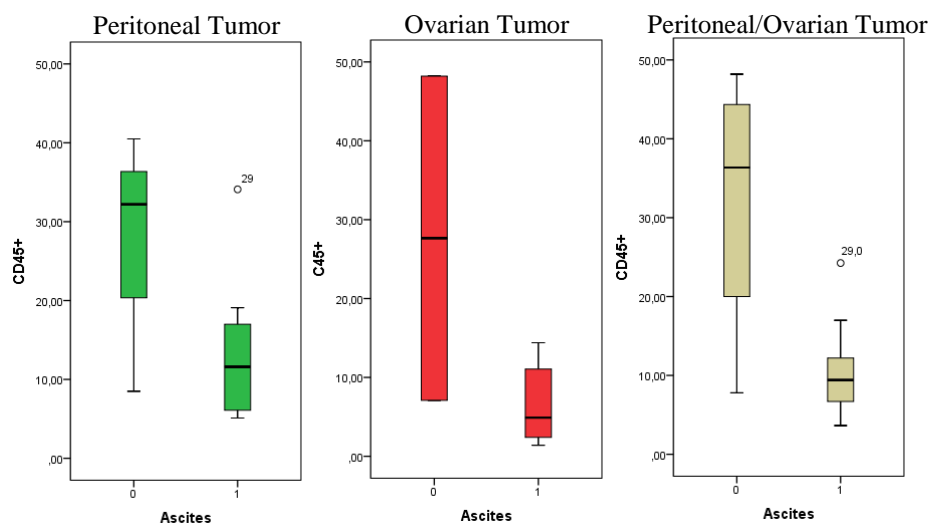


Figure 26. CD45+ cells are enriched in tumor tissues of patients without (0) ascites. Left= peritoneal tumors, middle= ovarian tumors; right= peritoneal and ovarian tumors together; if data for both were available for one patient, mean values were used.

Moreover, cells from peritoneal tumors co-expressing L1CAM and CD44 (but no EpCAM) were significantly enriched in patients without ascites ($p=0.032$). In contrast, the population with the same characteristics in ovarian primary tumor tissue is nearly as abundant in patients with ascites as in patients without ($p=0.417$). Taking together the data for ovarian and peritoneal tumors, the frequency of EpCAM-L1CAM+CD44+ cells correlates with the abundance of ascites ($p=0.039$).

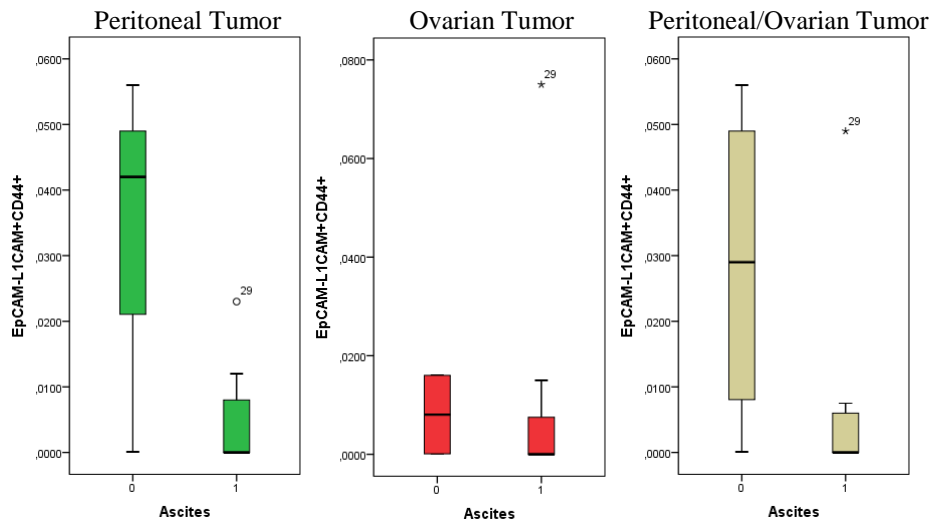


Figure 27. CD44+L1CAM+ cells are enriched in tumor tissues of patients without (0) ascites, (left) peritoneal tumor, (middle) ovarian tumor, (right) peritoneal and ovarian tumors together; if data for both were available for one patient, mean values were used.

3.3.8 Correlation with mutation status

The results from flow cytometry and gating were also correlated with functional mutations in the genes *TP53* and *KRAS*. The biggest differences between these groups were the highly increased numbers of L1CAM+ (54.6 %), CD44+ (65.5 %), and EpCAM+ (59.6 %) cells in the ascites (single cell fraction) of the patient harboring a *KRAS* gene mutation resulting in an amino acid substitution from glycine (G) to aspartic acid (D) at position 12 in *KRAS* (G12D). In contrast to other examined markers, the number of CD45+ cells accounted for 10.2 % of the events in this patient, whereas ascites single cell samples from other patients contained around 67.4 % CD45+ cells.

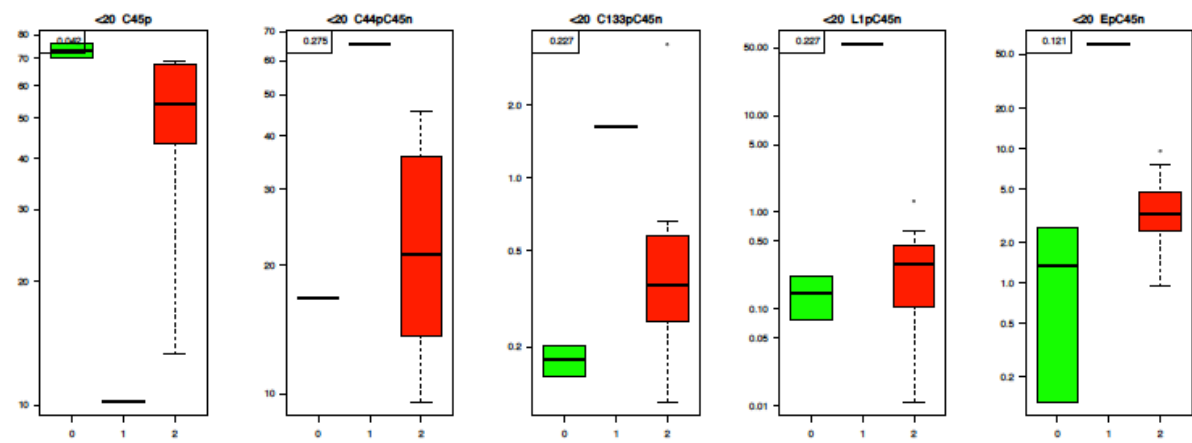


Figure 28. Frequency of surface markers in different mutation types: 0= no *TP53* or *KRAS* mutation observed (n=2), 1= *KRAS* mutated (n=1), 2= functional *TP53* mutation (n=12).

For a more informative correlation of the mutation status with the frequency of distinct cell populations, p53 mutated samples were compared to non-p53 mutated (including the only *KRAS* mutated patient). Results for spheroids as well as single cells were similar: both showed little differences in cell populations from the two cohorts, only CD44+/EpCAM- cells in spheroids were slightly enriched in the group of p53 mutated patients (p=0.117; Fig. 29).

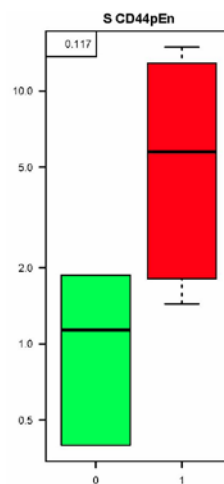


Figure 29. Frequency of CD44+EpCAM- cell populations in spheroids of non-p53 mutated (0), and p53 mutated tumors (1)

Considering other EpCAM positive and negative subpopulations, the two groups do not significantly differ in any of the observed marker combinations. Nevertheless, EpAM+CD44+CD133- and EpCAM+ CD44+L1CAM- cells showed a trend towards less frequency in p53 mutated ascites cells (p=0.644 in single cells, and p=0.117 in spheroids for CD133- and p=0.926, and p=0.296 for L1CAM-, respectively) but were also slightly enriched in the same group in tumor tissue (p=0.425 in ovarian, and 0.405 in ovarian tissue for CD133- and p=0.425, and p=0.405 for L1CAM-, respectively).

3.4 Transcriptome Analysis

3.4.1 RNA Preparation

Isolation of RNA from ascites and tissue samples yielded in a mean RNA amount of 627 ng (EpCAM+ single cell fraction) and 3 052 ng (spheroid fraction) RNA per sample. Large RNAs mostly had RNA integrity numbers (RIN) over 9 and only mRNA samples with high concentrations and good quality as determined by Agilent Bioanalyzer analysis and Nanodrop concentration measurements were used for RNA-seq. Figure 30 shows the Bioanalyzer electropherogram of an EpCAM+ sorted single cell ascites sample. The two peaks (corresponding to the two black bands on the pseudo-gel representation shown on the right side of Fig. 30) represent the amount of 28S and 18S rRNA in the sample and the sharp shape of these peaks demonstrate little or no RNA degradation, resulting in a high RIN.

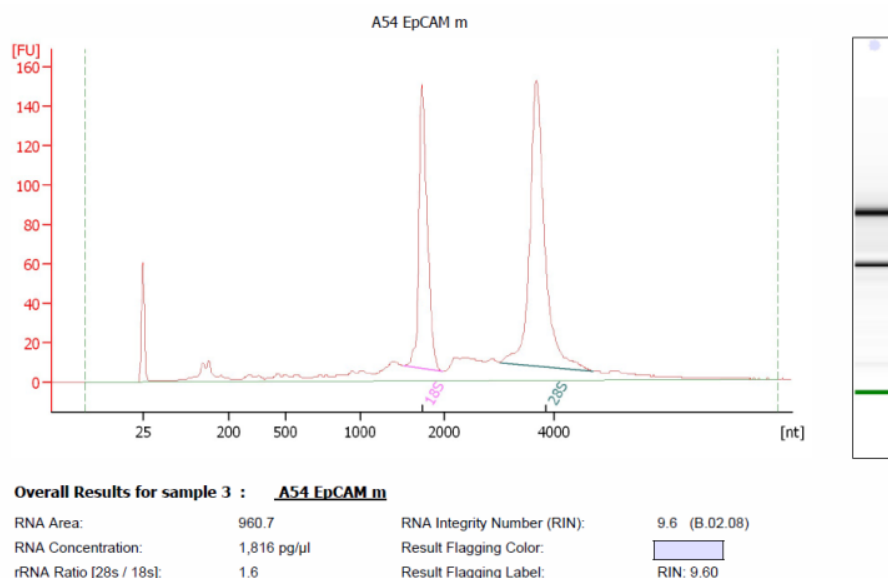


Figure 30. Electropherogram of large RNAs from EpCAM sorted ascites cells analyzed on the Agilent bioanalyzer

3.4.2 RNA-Seq and Functional Annotation

Eight paired samples of ascites single cells and spheroids were sequenced to a median depth of 20.4 million basepair paired-end reads (range: 10.6-33.1 million). Subsequently reads were counted into a gene model (gencode v16) and finally 26 480 reliably expressed genes were used for further analysis (counts per million over 0.1 in at least eight samples). To avoid expression bias by highly abundant circular RNAs (Memczak, Jens et al. 2013), these RNAs were predicted by a recently published pipeline searching for back-spliced exon-exon junctions and all pairs of reads putatively belonging to such circular RNAs were excluded from further analysis. The R-package limma was used for

differential gene expression analysis, modeling single cell and spheroid samples as biological replicates except for the analysis of differences between these samples.

3.4.2.1 Aggregation status

3.4.2.1.1 limma

Interestingly, hardly any significant differences between single cells and spheroids were found using limma, and only five genes showed a FDR below 10 %: *POU3F1*, *NEFH*, *REXO1L1*, *RAB31*, and *CD79A*.

3.4.2.1.2 pairedBayes

But using a more sensitive approach, pairedBayes (R-package), found 1 103 genes differentially expressed with a posterior probability for differentially expressed of 1.0, 590 of them down- and 513 up-regulated in spheroids (Fig. 31).

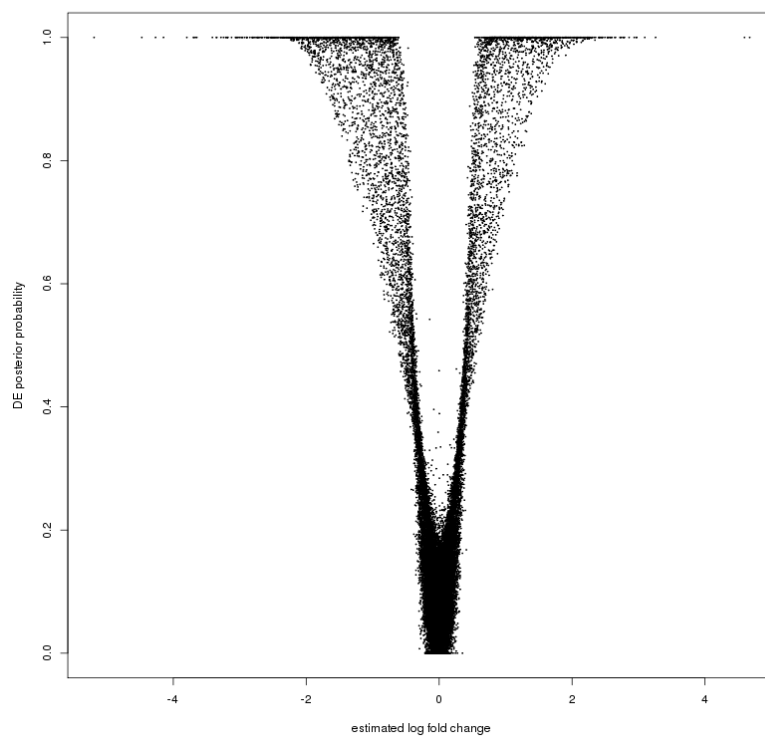


Figure 31. pairedBayes revealing 1103 genes to be differentially expressed between EpCAM+ sorted single cells and spheroids from ascites with a posterior probability of 1.0.

3.4.2.1.3 SPIA

A SPIA analysis (Fig. 32) using these 1 103 genes and their log-2 fold change values revealed eight pathways activated or inhibited between spheroids and single cells. Activated pathways in spheroids were ECM-receptor interaction (Fig. 33), focal adhesion, calcium signaling, staphylococcus aureus infection, systemic lupus erythematosus, long-term depression, and complement and coagulation cascades. The only inhibited pathway in spheroids was the B-cell receptor signaling pathway.

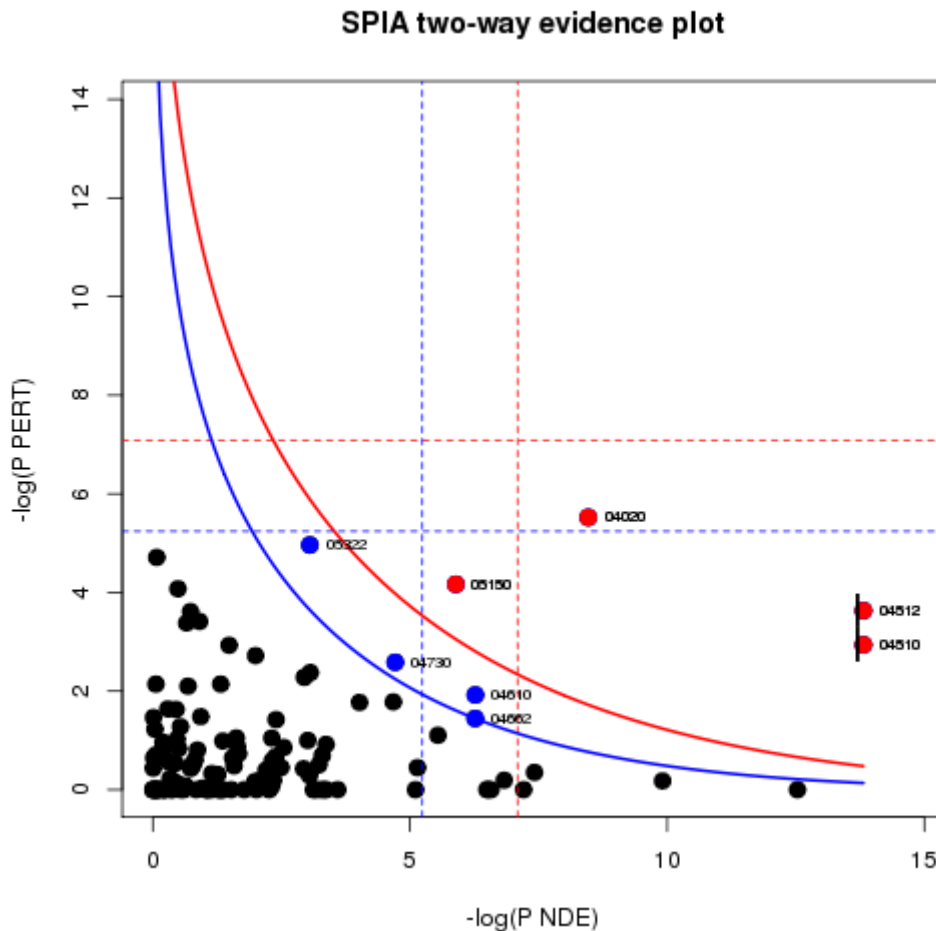


Figure 32. SPIA plot showing inhibited and activated pathways between single cells and spheroids (FDR of 10 %). All points on and above the blue line indicate activated or inhibited pathways. The x-axis represents the p-value (minus log of) corresponding to the probability of obtaining at least the observed number of genes (NDE) on the given pathway just by chance. The y-axis represents the p-value (minus log of) corresponding to the probability of obtaining the observed total accumulation (tA) or more extreme on the given pathway just by chance.

A KEGG pathway as obtained through SPIA analysis depicts the differentially expressed genes between ascites spheroids and single cells in this pathway (Fig. 33). The pathway most prominently activated in spheroids was the ECM interaction pathway. Within this pathway consisting of 85 gene products, 18 differentially expressed genes as computed by pairedBayes analysis of RNA-seq data could be annotated.

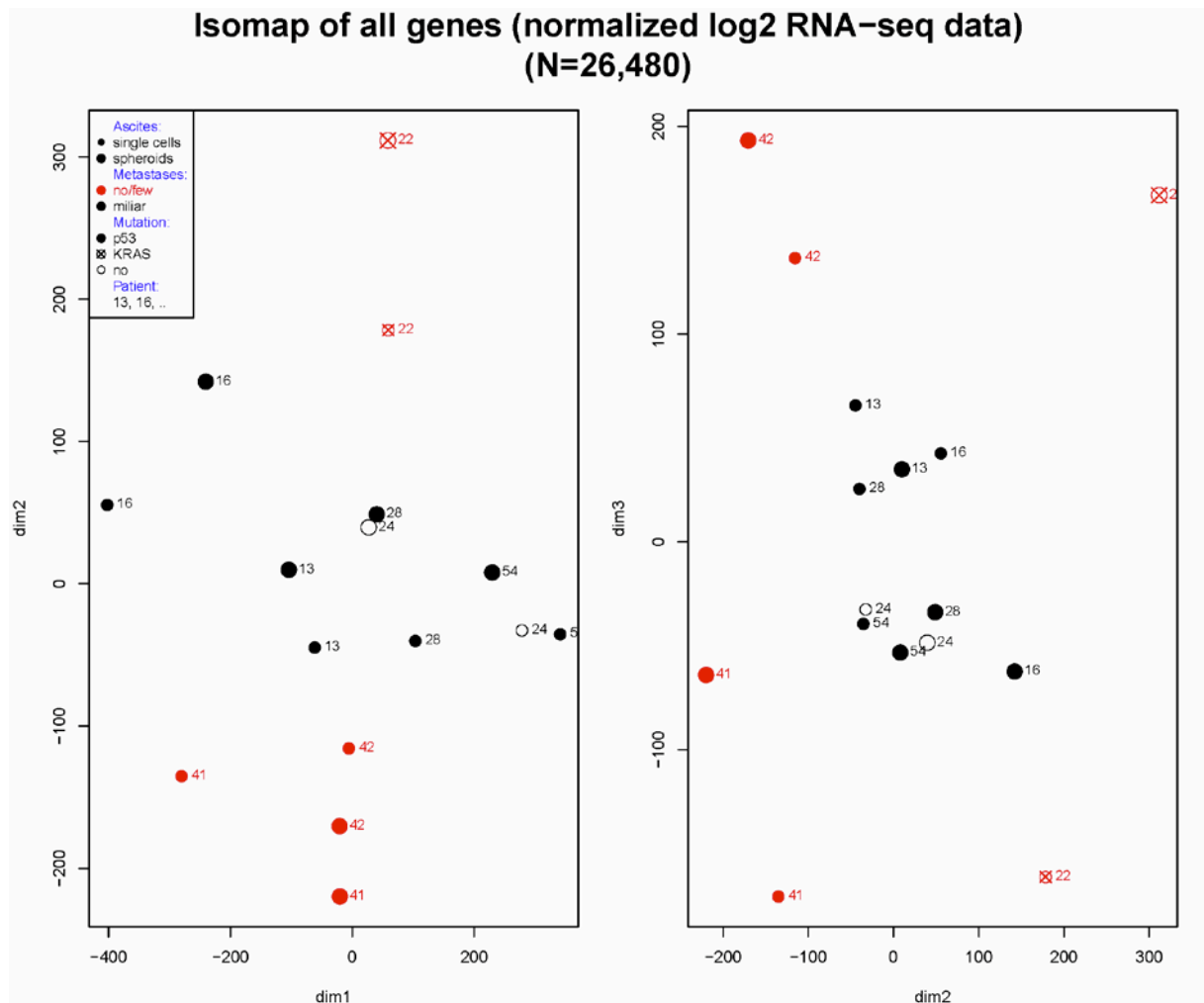


Figure 34. Isomap of transcriptome data of 8 paired ascites spheroid and EpCAM+ single cell samples

3.4.2.2 Mode of peritoneal tumor spread

3.4.2.2.1 limma

Using the mode of tumor spread as dependent variable in the differential gene expression analysis, 460 genes were found to be differentially expressed ($FDR < 10\%$) between the two groups miliary and no/few implants, 260 are down-, and 180 up-regulated in the miliary subtype. Among the 280 down-regulated genes were prominent mediators of EMT like *SNAIL2*, encoding a transcription factor and associated with repression of E-cadherin in breast carcinoma, or *BMP7*, a member of the TGF-beta superfamily (see Supplement Tab. S1 for gene list).

3.4.2.2.2 heatmap

In figure 35 hierarchical clustering and a heatmap of all differentially expressed genes between subtypes of different tumor spread is depicted. The upper-most bar shows that samples from miliary spread and no/few big implants cluster together, except for sam-

ples from patient 13. Also, both ascites samples (single EpCAM+ and aggregated cells) of patients cluster together, except for patients' samples 16 and 41. The heatmap, showing the pattern of up- and down-regulated genes for each sample, reveals, that the expression pattern of the spheroid fraction from patient 41 resembled those from patient 42 and hardly any similarities can be found between the expression patterns from ascites samples of patient 16 and others.

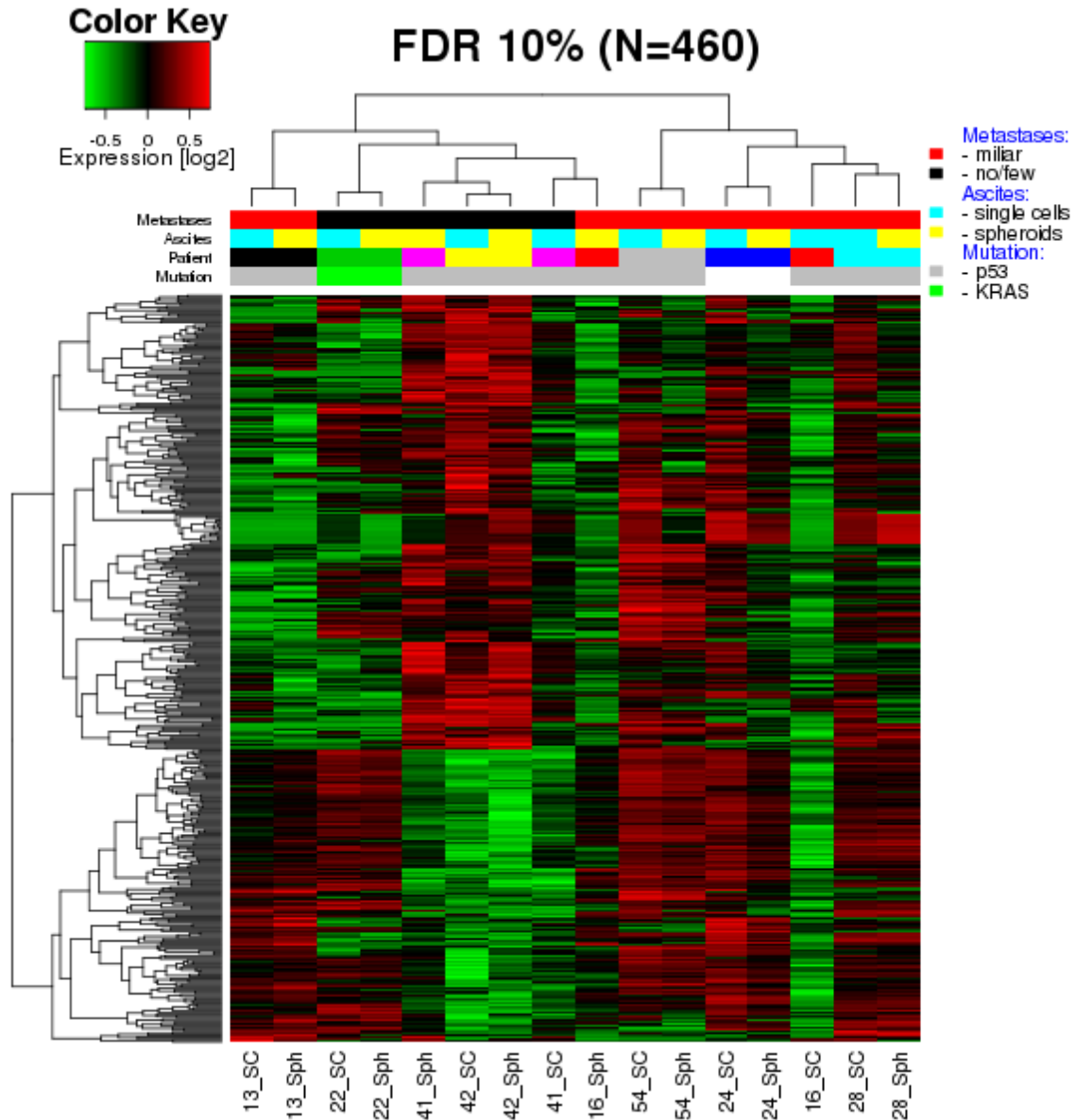


Figure 35. Heatmap and clustering of 460 differentially expressed genes between patients with miliary tumor spread and no/few big implants in the peritoneum

3.4.2.2.3 SPIA and DAVID

Functional annotation of RNA-seq data about differentially expressed genes between patients with and without miliary peritoneal tumor spread was conducted with the Database for Annotation, Visualization and Integrated Discovery (DAVID), revealing an overrepresentation of glycoproteins, extracellular matrix proteins, cell adhesion proteins and pathways responsive to wounding from Go-term and SP_Pir-Keywords. A SPIA analysis revealed four over-represented and perturbed pathways (Fig. 36): cytokine-cytokine receptor interaction, ECM-receptor interaction, focal adhesion, and melanogenesis (Figs. 37-40).

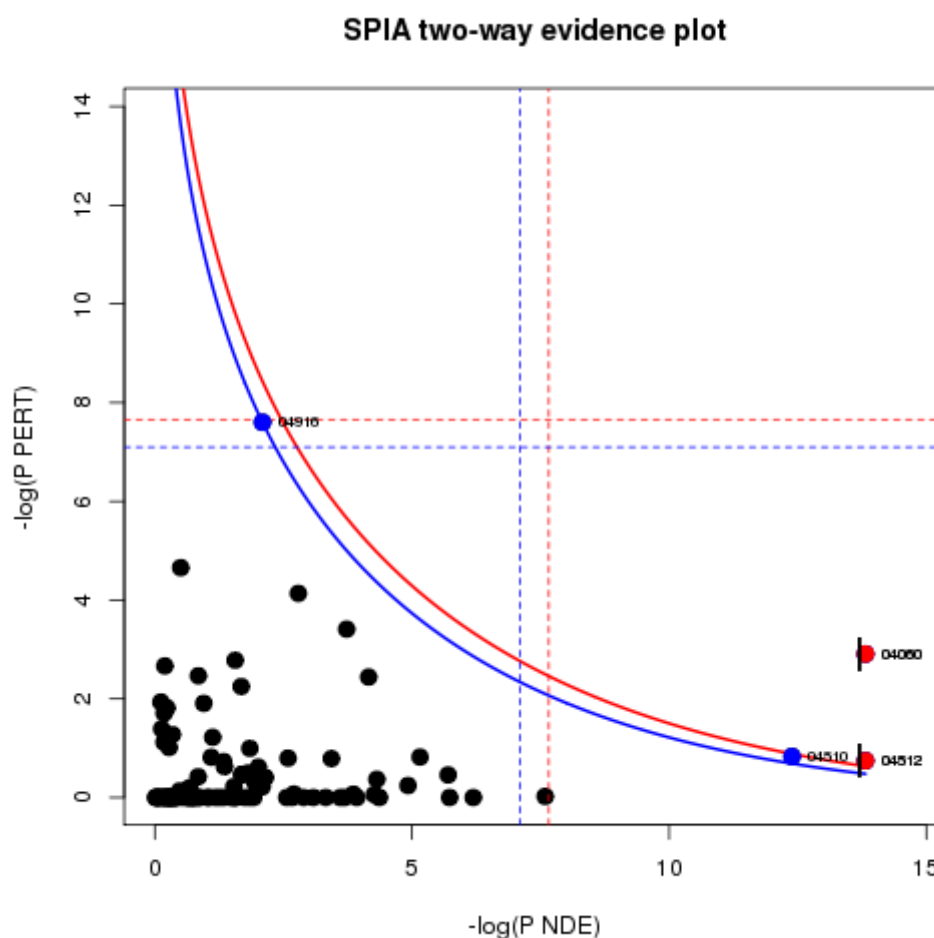
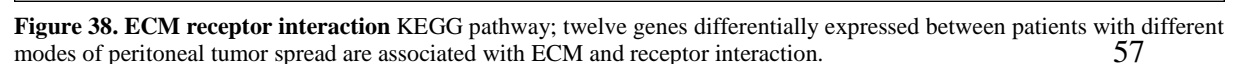
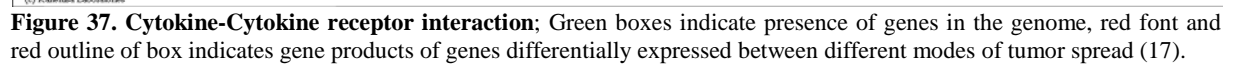


Figure 36. SPIA analysis of 460 differentially expressed genes between patients without or with few big implants and a miliary tumor spread revealed three pathways significantly deregulated and one activated using a FDR of 10 % (blue line). Each dot represents a pathway; the pathways right and over the blue curve are considered statistically significant.



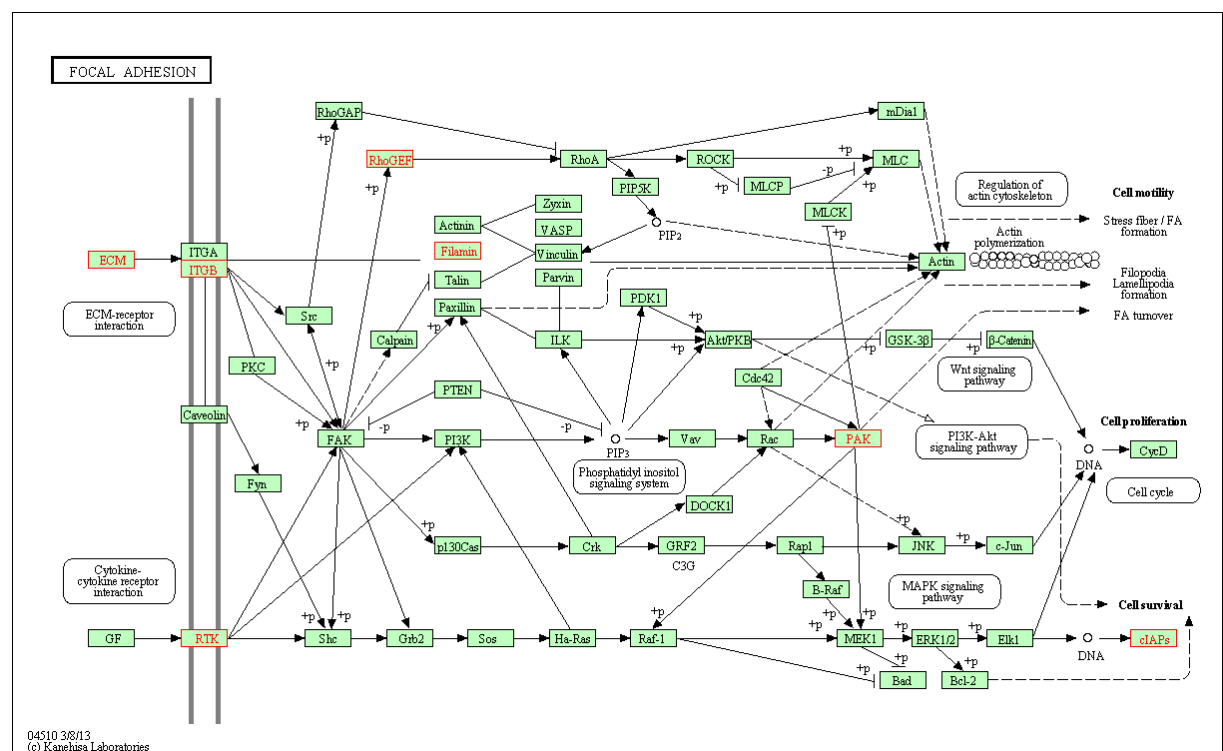


Figure 39. Focal Adhesion KEGG pathway; sixteen genes differentially expressed between patients with different modes of peritoneal tumor spread are associated with focal adhesion.

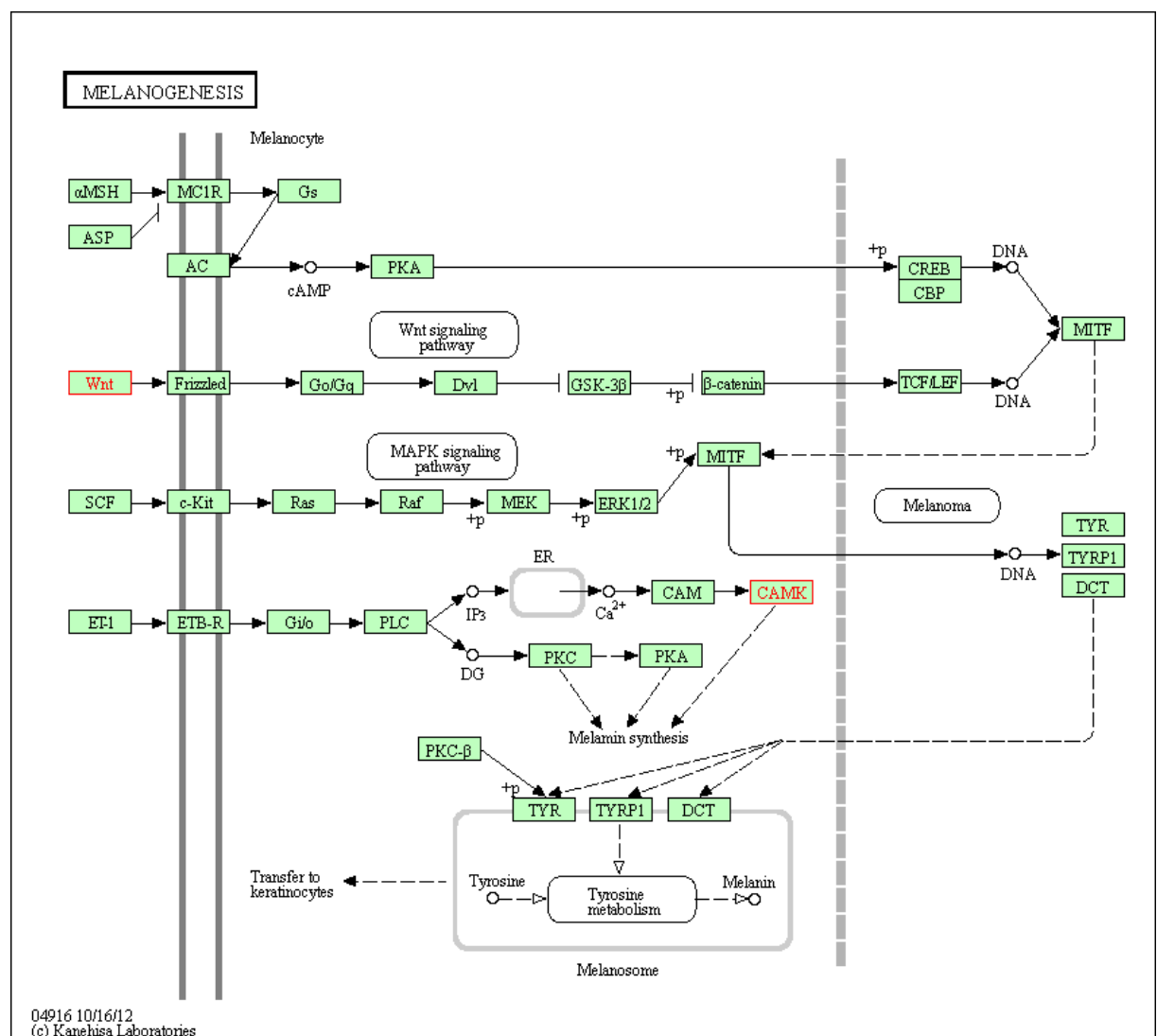


Figure 40. Melanogenesis KEGG pathway; four genes differentially expressed between patients with different modes of peritoneal tumor spread are associated with melanogenesis.

3.4.2.3 Molecular subclassification

Using the 112 gene-signature for molecular subclassification (Yoshihara, Tajima et al. 2009) or all reliably expressed genes, a NMF based unsupervised classification approach revealed a stable classification of the samples, shown in Fig. 41. Both samples of each patient accounted for the same subclass, except for patient 16 with spheroid sample in subclass 1 and EpCAM+ ascites single cell sample in subclass 2.

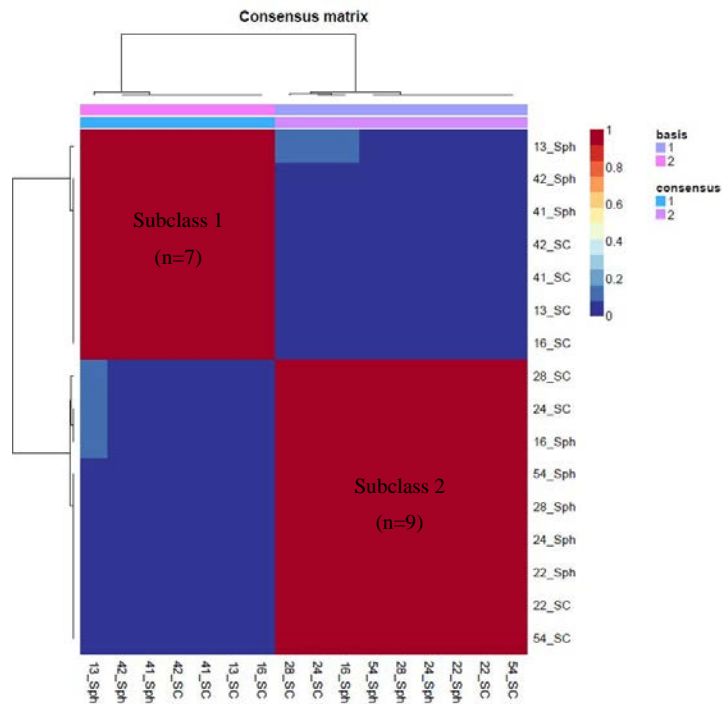


Figure 41. Subclassification of patients' samples shown in NMF clustered matrix (K=2) Number stands for patient; SC for EpCAM+ single cells ascites fraction; Sph for spheroid fraction.

3.4.2.3.1 Isomap

An isomap of all samples with reliably expressed genes colored according to this molecular subclassification (Fig. 42), indicates a complete separation of the two subclasses along dimension one. Between these two subclasses, 7 250 genes were significantly differentially expressed (FDR 5 %), 6 827 of them up-regulated in subclass 2 and 423 of them down-regulated.

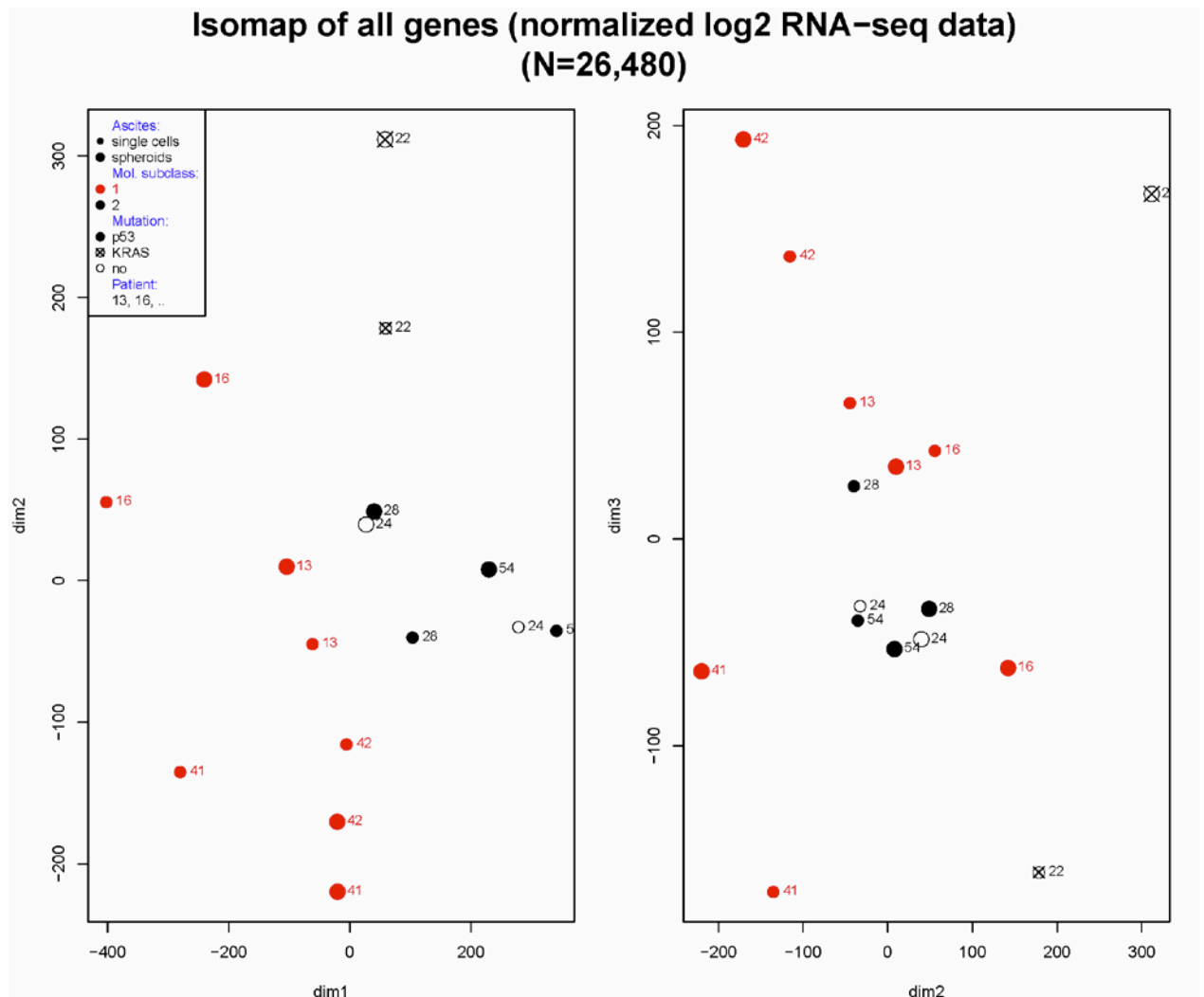


Figure 42. Isomap dimension reduction of NGS data for 8 patients; molecular subclasses as calculated by NMF with 112 genes are marked as filled red circles (subclass 1) and black circles (subclass 2). CAVE: Spheroid sample of patient 16 is colored red, although calculated in subclass 2 by NMF.

3.4.2.3.2 SPIA and DAVID

DAVID analysis using this differentially expressed genes up to a p-value of 0.01 (2 943 genes) revealed an overrepresentation of protein clusters associated with cell adhesion, extracellular matrix proteins, signal peptides, proteins involved in cell-cell junction, and associated with EGF. SPIA analysis revealed 23 overrepresented and perturbed pathways (Tab. 16):

Table 16. SPIA analysis revealed 23 pathways activated or inhibited between the two NMF based subgroups, 9 were activated and 14 inhibited in subclass 2.

Pathways	ID	pGFdr	Status
Focal adhesion	4510	<0.001	Activated
Small cell lung cancer	5222	<0.001	Activated
ECM-receptor interaction	4512	<0.001	Activated
Basal cell carcinoma	5217	<0.001	Activated
Pathways in cancer	4670	<0.001	Activated

Melanogenesis	5200	<0.001	Activated
Hedgehog signaling pathway	5146	<0.001	Activated
Glioma	5150	<0.001	Activated
Wnt signaling pathway	5322	<0.001	Activated
Leukocyte transendothelial migration	4110	<0.001	Inhibited
Amoebiasis	4916	0.002	Inhibited
Staphylococcus aureus infection	5140	0.004	Inhibited
Systemic lupus erythematosus	4666	0.009	Inhibited
Cell cycle	5133	0.009	Inhibited
Leishmaniasis	4340	0.015	Inhibited
Fc gamma R-mediated phagocytosis	5214	0.028	Inhibited
Pertussis	5100	0.028	Inhibited
Bacterial invasion of epithelial cells	4940	0.028	Inhibited
Type I diabetes mellitus	4810	0.029	Inhibited
Regulation of actin cytoskeleton	4530	0.029	Inhibited
Tight junction	4310	0.038	Inhibited
Toxoplasmosis	5145	0.039	Inhibited
Maturity onset diabetes of the young	4950	0.041	Inhibited

ID: corresponding to points in Fig 43; pGFdr: false discovery rate

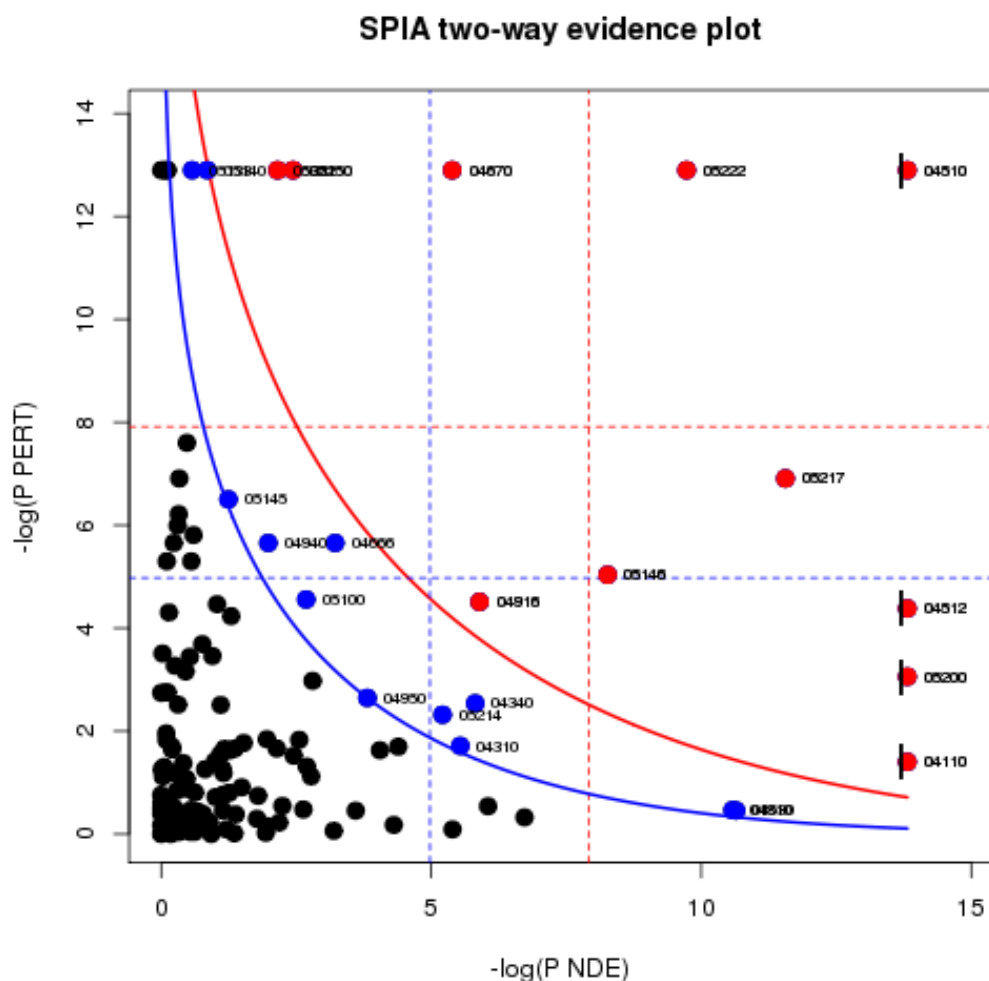


Figure 43. SPIA plot showing inhibited and activated pathways between NMF based subclass 1 and subclass 2 (FDR of 10 %).

3.4.2.4 Summary of RNA-seq and annotation results

Summarized, following significant molecular differences were found between ascites single cells and spheroids, between patients without or with few, big implants and a miliary tumor spread, and between patients of subclass 1 and subclass 2 determined with the NMF approach (Tab. 17):

Table 17. Results from statistical analysis of RNA-seq data.

Compared groups		Statistical method		Direction (Group 2 vs. Group 1)		SPIA	
Group 1	Group 2	limma	pairedBayes	Up	Down	Acti- vated	In- hibited
Cell aggregation							
Single cells	Spheroids	5 (FDR 10 %)	-				
Single cells	Spheroids	-	1 103 (posterior prob. 1.0)	513	590	7	1
Tumor spread							
no/few	miliary	460 (FDR 10 %)	-	180	280	1	3
Molecular subclass							
Subclass 1	Subclass 2	7 250 (FDR 5 %)	-	6 827	423	9	14

3.5 Immunofluorescence

Immunofluorescent stainings of embedded ascites pellets showed the distribution of CD45+ immune cells, EpCAM+ tumor cells and CD44+ cells within spheroidal cell aggregates and single cells. Figure 44 demonstrates an overview of ascites cells of the epithelial ovarian cancer patient 28, FIGO IIIC, grade 3, carrying a functional p53 mutation in the tumor. The primary tumor, residing on both ovaries, was relatively small; nonetheless the patient had miliary tumor implants all over the peritoneum together with partial adhesions of the organs. The ascites showed a high abundance of filterable sphe-roids, which upon immunofluorescent staining with antibodies directed against Ep-CAM, CD44 and CD45, where shown to be EpCAM positive (Fig. 44, red). Also visible in the micrograph are CD45 positive immune cells (white), residing as single cells in the

ascites or, to a fewer extend, infiltrating the spheroids. Note that all CD45+ cells are also positive for CD44 (green), but there are also EpCAM/CD44 double positives, predominantly residing in the single cell population or adjacent to cell aggregates.

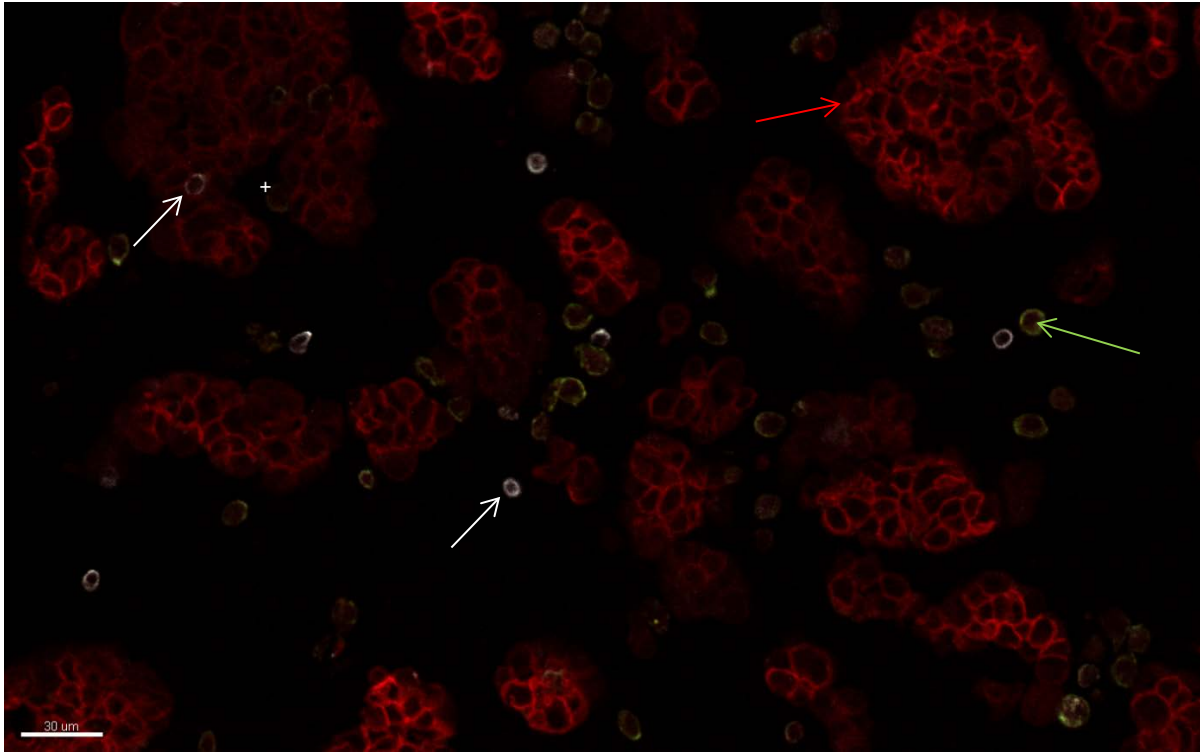


Figure 44. Spheroids and single cells in ascites of ovarian cancer patients. Intense CD45 staining (white arrows) visible on membrane of leukocytes residing as single cells and within the spheroid on the upper left CD44 staining (green arrow) is observed on the membrane of single cells. The membrane of aggregated cells is stained for EpCAM (red arrow).

4 Discussion

Although some improvements in the 5-year survival rate of ovarian cancer patients were achieved over the past twenty years due to improved surgical practice and treatment with optimized drug combinations, the best prognostic factor for woman suffering from EOC is still a clinical factor: the amount of residual tumor mass in the peritoneal cavity after debulking surgery. Chemotherapy is only partly effective and a large number of patients develop platinum resistance in the course of the disease (Bast, Hennessy et al. 2009). In the last years it became obvious, that due to the heterogeneous composition of high grade serous epithelial ovarian tumors, consisting of highly proliferating tumor cells as well as lower numbers of tumor initiating stem cells, it is unlikely to fight all subtypes of cancerous cells with one strategy (Zhan, Wang et al. 2013). But to find the best strategies for each of the challenges (highly proliferating cells, tumor initiation) a very comprehensive and still detailed understanding of the tumor composition from different tumor cell types, its mode to spread, and mechanisms for developing resistance is necessary. Recently, a molecular subclassification was published (Yoshihara, Tajima et al. 2009) helping to further divide the most common ovarian cancer in the western world, i.e. the high grade serous EOC, into molecular subclasses with substantial impact on outcome.

This work aimed to contribute to the understanding of the composition and characteristics of the tumor and its “metastases” in the ascites (spheroids) and the intraperitoneal cavity (tumor implants). The major goal was to investigate the role of cellular subclasses in the formation of spheroids in ascitic fluid, distribution of tumor lesions in the peritoneum, and the accumulation of ascitic fluid in the abdomen.

4.1 Sample preparation and spheroid digest

The immediate receiving and processing of the ascites, intended to get live cells in good quality for FC and transcriptome analysis, allowed to obtain both: i) fractions of filtered single cell samples and ii) intact spheroids. Single cell suspensions of supernatants from EpCAM and CD45 enrichment approaches of digested tumor tissue samples were likewise collected. Immediate lysis and freezing of lysates granted RNA samples with good quality although sometimes the amount of nucleic acid yield was lower than expected in some magnetat separated ascites single cell and tissue samples. But since the amount of tumor and immune cells in patients’ tissues differed and only a restricted amount of specimens was available, accomplished optimizations of the sampling process could not improve this so far. For FC analysis cells were frozen alive and although this always

diminishes the amount of cells with intact cell membranes, it was necessary to guarantee reproducibility as direct staining was not possible in all cases. However, a pilot test showed, that after slow and cautious thawing the composition of ascitic fluid resembled those of directly stained ascites. Thawed spheroids needed to be partly digested first in order to obtain single cells for staining. This procedure with enzymatic and mechanical disruption of cell aggregates worked at varying degrees of success in different ascites samples. If the spheroid cells were very strongly attached to each other up to four repeats were necessary to obtain single cells with the side effect that also a large number of cells was destroyed.

4.2 Flow cytometry

After excessive testing on different cell lines and blood cells, all six colors or five antibodies of the flow cytometry panel could be confirmed to work properly. Staining ascites single cells and digested spheroids worked fine but in the gating process lower cell numbers of EpCAM positive tumor cells and higher amounts of leukocytes (mostly lymphocytes, see Supp. Fig. S1) than expected were observed. Also a population of cells expressing CD44 but neither EpCAM nor CD45 was unexpected but present in all ascites samples, especially in the single cell fraction with a median of 46.6 % (range: 1.44 % - 69.9 %) of all CD45 negative cells. The origin of this cell population is so far unclear but it's speculated to consist of reactive cells from the mesothelium, cancer associated fibroblasts, or even tumor cells that have lost their EpCAM expression on the surface (due to EMT associated processes). Interestingly, in spheroids only minor numbers of CD44 single positive cells were observed. As erythrocytes also express CD44 but neither EpCAM nor CD45 it could be speculated that filtered ascites single cell fractions were contaminated with red blood cells, but a FC experiment comparing a sample of filtered ascites with visible amounts of red blood cells (red pellet) with and without lysis of erythrocytes showed very similar results for the CD44+ population (see Supp. Fig. S2).

Leukocytes were abundant in the spheroid fraction also, but to a smaller extent. Cell aggregates were observed to mostly consist of EpCAM+ cells, consistent with our theory that spheroids are free floating cell aggregates or "micrometastases" of the solid tumor; leukocytes could infiltrate these aggregates or at least adhere to the surface. This would explain the detection of CD45+ cells in the spheroid fraction. Another explanation might be aggregates of lymphocytes that, upon filtration, were treated as spheroids. To answer this, paraffin embedded ascites pellets were stained for CD45 and EpCAM

(immunofluorescence) and both could be observed, albeit aggregates of leukocytes were rare (not shown).

Also significant enrichment of cells expressing the marker CD133 was observed in spheroids. The function of this pentaspan transmembrane molecule is still under debate, but together with other markers like CD44 or CD24 it had been shown to characterize tumor initiating stem cells in breast cancer (Wright, Calcagno et al. 2008) and is also proposed to define tumor initiating cells in ovarian cancer (Kryczek, Liu et al. 2012), (Wintzell, Hjerpe et al. 2012).

L1CAM positive cells were also more abundant in the spheroid fraction, but in total only minor numbers of cells expressed L1CAM on the surface. As this molecule was found to be overexpressed in ovarian carcinomas (Stoeck, Schlich et al. 2006), we also expected elevated abundance in cells shed off from solid tumors in the patient cohort. But except for one patient (Patient 22) levels of L1CAM expressing cells were much lower than expected (median of 0.25 % in single cells and 0.87 % in spheroids). A possible explanation for this could be the low grade of the tumor (grade 1), describing tumor cells that are still well differentiated in contrast to higher grades (lower differentiation of cells) and possibly goes hand in hand with less surface expression of distinct markers like L1CAM. Furthermore it is known, that L1CAM can be cleaved and forms a soluble molecule present in ascites of ovarian cancer patients (Bondong, Kiefel et al. 2012). But also cells from tumor tissues of the ovaries and the peritoneum were examined for L1CAM expression by flow cytometry and similarly low levels of membranous L1CAM were found in CD45 negative cell populations (see Tab. 9f.).

Taking a look at the EpCAM⁺ and EpCAM⁻ subpopulations (combinations of L1CAM, CD44, and CD133 expressing cells) often double negative cells seemed to be statistically significantly enriched in the spheroid fraction, but this was probably an artifact of the gating procedure, where a broad gate is drawn around all cell populations (Fig 12, 2) including some debris from disruption of spheroids that could not be completely washed away before fixation.

Analyzed patients could be separated in groups according to their differential expression of surface markers analyzed with FC. In the plots generated by PCA (Fig. 18) a cluster of patients sharing a miliary tumor spread (outlier Patient 16) and a wider distribution of patients without or with few big implants can be observed. As conclusion, patients with miliary peritoneal tumor spread resemble each other in relations of their cell surface markers expressed on ascites and solid tumor cells and patients with other modes of

tumor spread are more diverse in their cell marker profile. Anyway, more patients are needed to strengthen this preliminary finding.

4.3 Presence of spheroids in ascites

No difference between the two patients without filterable spheroids in the malignant ascites and the ten patients with confirmed spheroids could be observed from FC data in the PCA. For a more detailed view regarding cell populations and abundance of spheroids, the two groups were compared using statistical analysis of FC data from primary ovarian and peritoneal tumors, and the single cell fraction of all ascites. Results showed only trends regarding the distribution of CD44+EpCAM+ cells in ovarian tumor tissue and ascites single cells (Fig. 19 f.). An explanation for the presence of spheroidal tumor cell aggregates in the ascites could be overexpression of the hyaluronic acid receptor CD44, thus promoting cell-cell adhesion. CD44 plays an important role in adhesion, migration and metastasis (Marhaba and Zoller 2004), but still a lot of CD44 single positive cells were found in the ascites single cell fraction. Hyaluronic acid (HA) is a glucosaminoglycan produced by the membrane bound enzyme hyaluronan synthase (HAS). Ovarian cancer patients with tumors negative for HAS1 were shown to have a prolonged overall survival time compared to patients with HAS-1 positive tumors (Yabushita, Noguchi et al. 2004). Binding of CD44 to HA results in up-regulation of EMT-markers like N-cadherin, vimentin, alpha-actin, and fibronectin and down-regulation of E-cadherin (Cho, Park et al. 2012), so it may be speculated that high expression of CD44 on tumor cells may promote tumor cell dissemination and spread in the peritoneal fluid as a result of EMT. Furthermore cells still expressing EpCAM together with CD44 may have found a way to overcome anoikis without changing to a mesenchymal subtype by maintaining cell-cell contacts. This remains to be elucidated by staining ascites cells for CD44, vimentin, and other mesenchymal cell markers.

A more detailed view at the EpCAM positive and negative subpopulations by combined gating of the markers CD44, CD133, and L1CAM revealed no further differentially expressed surface marker combinations between patients with and without spheroids in ascites. This might be a consequence of large heterogeneity in cell composition and/or low patient numbers.

RNA-seq results also showed that variation between patients might be bigger than the differences between EpCAM+ single cells and spheroids, as limma analysis found only five genes differentially expressed between these two cell populations.

4.4 Mode of peritoneal tumor spread

To my knowledge, the type of peritoneal tumor spread is not regarded important in the clinical routine. But when comparing ascites samples of patients with different modes of tumor spread it becomes obvious that the ones of the first group (miliary spread) tend to have high numbers of leukocytes in the ascites. This is consistent with our theory that an over-reactive immune system leads to damage of the mesothelium, making it easier for tumor cells to adhere on multiple sides to the underlying ECM and spread planar all over the peritoneum. A significantly higher number of CD44 positive cells could be observed in the group with no or only a few big nodular implants. This was astonishing as speculations were made that tumor cells with more CD44 are prone to migrate and adhere to components of the ECM resulting in more implants. Nevertheless, it would be also reasonable that if tumor cells adhere to the mesothelial lining of the peritoneum, big tumors result without initial invasion of the underlying ECM. Taking a closer look at the CD44+ subpopulations, both EpCAM+ and EpCAM- cells were enriched, especially in spheroids. An explanation for this would either be a gradually lower EpCAM level in tumor cells undergoing EMT in the ascites and therefore both populations would account to the tumor cell population or CD44+ cells like reactive mesothelial cells or cancer associated fibroblasts that can also affect cancer spread and adhesion in the peritoneal cavity. Unfortunately more information could not be drawn from flow cytometric analyses of the 17 patients, as neither in tumor tissues nor in ascites samples did any other subpopulation significantly differ between the two cohorts.

All patients with ascites and a miliary tumor spread had spheroids, in contrast to the two patients without spheroids, that showed no or only few big implants. This supports the theory of spheroids being micrometastases that adhere to the peritoneal wall. However, this finding has to be taken with care because of the low patient number, with only two patients that had ascites without spheroids.

But also in the PCA using all ascites FC data the separation of patients with miliary tumor spread from patients with other modes of tumor spread (no or few big) became obvious (Fig. 18), which further strengthened our hypothesis of molecular differences in tumors showing these different modes of peritoneal tumor spread.

The RNA-seq results of ascites cell samples further support this interpretation, as in the isomap (non-linear dimension reduction) a cluster of patients with miliary peritoneal tumor spread can be observed (Fig. 34). Only patient 16 showed a complex picture: Clinically we classified the peritoneal lesions of this patient as miliary which is in ac-

cordance with the isomap of expressed genes, whereas PCA of FC data clearly showed a relation to the group of no/few big implants (Fig. 18). But as the patient presented at a very advanced stage of the disease with large peritoneal tumor nodules but also tumor implants all over the peritoneum, classification in either miliary type or the type with of few big exophytically growing implants was difficult. . We have also seen patients at an advanced stage with miliar tumor spread all over the peritoneum, still not showing an exophytic nodular tumor growth but presenting with mainly planar lesions. Patient 16 might combine both types of local peritoneal tumor spread. Moreover, the heatmap of all differentially expressed genes between both modes of tumor spread was inconsistent in classifying this patient: The spheroid fraction clustered with the no/few implants pattern and the EpCAM+ single cell fraction with the miliary pattern. Also the molecular subclassification was inconsistent for this patient: the spheroid fraction clustered with subclass 2 whereas the single cell fraction clustered with subclass 1.

The *KRAS* mutation of patient 22 accounted for a lot of variability compared to all other patients with functional *TP53* mutation or *KRAS/TP53* wildtype tumors. The *KRAS* mutation leads to a constitutively active GTPase KRas which serves as oncogene (Bos 1989) and has obviously a large impact on the whole transcriptome.

4.5 Presence of ascites

The finding of enhanced CD45+ cell abundance in tumor tissue from patients without ascites seemed contra-intuitive, as elevated rates of inflammatory cells would be expected in the tumor tissue surrounded by ascites harboring these cells. However, the type of leukocytes infiltrating tumor tissues and floating free in ascitic fluid remains to be elucidated. The elevated presence of CD44/L1CAM double positive cells in metastatic (peritoneal) tumor tissues of patients without ascites is also surprising but might be explained by the fact that both molecules can be shed into ascites, hence might be more frequently found as membrane bound form in patients that did not develop ascites (Lee, Schramme et al. 2010).

4.6 Mutation status

As expected at least 70.6 % (missing data for two patients) of high grade serous EOC patients in this study carried a functional mutation in the *TP53* gene, pointing out the importance of the tumor suppressor gene in ovarian cancer development. One of the 17 patients observed (5.9 %), carried a mutation in the codon 12 of the *KRAS* gene resulting in substitution of the amino acid glycine to aspartic acid. This is consistent with the findings of Auner et al. describing an approximate frequency of 9% of serous ovarian

cancer patients carrying a *KRAS* mutation, of which 92 % affect codon 12 (Auner, Kriegshauser et al. 2009). As stated by Lalwani, Prasad et al., ovarian carcinomas harboring a *KRAS* mutation can be classified as type I, characterized by low grade and large adnexal manifestation (Lalwani, Prasad et al. 2011). All this is true for the *KRAS* mutated carcinoma included in the study showing a good differentiation (G1) and even borderline portions of the large ovarian tumor. The high differentiation grade could be an explanation for the big amount of cells positive for EpCAM, L1CAM, CD44 and CD133 in the tumor and ascites samples of this patient. The low abundance of CD45+ cells could be explained by absent inflammation in the peritoneum, because of unaggressive and slow tumor growth. Enrichment of CD44+EpCAM- cells in corresponding ascites of the *TP53* mutated tumors may be explained by an experiment of Godar S. et al, who found, that p53 inhibits the expression of CD44 and derepression by mutated p53 aids the survival of premalignant immortalized cells (Godar, Ince et al. 2008).

4.7 Molecular subclassification

A molecular subclassification approach of serous ovarian carcinoma using NMF as published by Yoshihara et al. (Yoshihara, Tajima et al. 2009) and validated by Pils et al. (Pils, Hager et al. 2012), revealed two stable subclasses of tumor cell samples from eight patients analyzed by RNA-seq. Of these, four patients accounted for subclass 1 and three for subclass 2, whereas ascites samples of patient 16 were separated in subclass 1 (spheroid sample) and subclass 2 (single cells). The isomap approach using all expressed genes (RNA-seq) showed a separation of molecular subclasses along dimension 1 and a separation of the mode of peritoneal tumor spread along dimension 2, indicating two independent molecular subclassifications of EOC patients. Furthermore, both samples of patient 16 were shown to cluster to subclass 1. Upon inspection of FC data a significantly increased population of CD133+ cells was observed in the ascites of this patient, indicating a molecular distinctiveness of this sample. As patients in subclass 1 were shown to have an increased overall survival rate, tumor cell populations accounting for this molecular signature (CD133?) are of interest for potential therapeutic targets and further research is needed to understand different molecular mechanisms separating these two subclasses. Furthermore, genes differentially expressed in the two subclasses could be tested with immunohistochemical stainings to establish an easy subclassification approach of ovarian tumor tissues.

Finally, characteristics regarding the mode of peritoneal tumor spread and the molecular subclassification are compared for the eight patients analyzed with RNA-seq and flow cytometry so far (Tab. 18):

Table 18. Summary of flow cytometry and RNA-sequencing data of eight patients with high grade serous EOC

Patient	Mutation	Tumor spread (clinically)	Flow cytometry (5 marker)	RNA-seq (Clustering with 460 sign. genes)	Subclass (NMF with 112 genes)
13	p53	miliar	miliar	miliar	1
16	p53	miliar ? ¹	few big	miliar ? ²	1/2
22	KRAS	few big	few big	few big	2
24	no	miliar	miliar	miliar	2
28	p53	miliar	miliar	miliar	2
41	p53	few big	few big	few big	1
42	p53	few big	few big	few big	1
54	p53	miliar	miliar	miliar	2

¹ Probably due to the very late stage of this patient with a large number of big implants wrongly classified. ² Ascitic cancer cell aggregates clustered with few big implants and ascitic EpCAM+ single cells with miliary implants (data not shown).

4.8 Immunofluorescence

Immunofluorescence experiments were conducted in order to validate and visualize FC results. Although EpCAM staining varied in intensity in ascites samples from different patients, spheroids could be shown to express the molecule especially at the membrane, whereas most single cells stained very weakly for EpCAM. Furthermore, CD45 stainings showed that leukocytes predominantly reside in the single cell fraction as observed by flow cytometry, but also, albeit only rare, invade spheroids. The characterization of these immune cells with antibodies against specific groups of leukocytes such as monocyte/macrophage, granulocyte or lymphocyte markers would probably prove their origin. Also the major population of cells staining for the anti-CD44 antibody could be found residing as single cells, but a smaller amount of CD44+ cells was observed isolated within or at the edge of cell aggregates. This supports theories of CD44 positive cells being cancer associated fibroblasts (CAFs) with pro-tumorigenic effects, originating from epithelial or endothelial cells that underwent mesenchymal transition (Ostman and Augsten 2009). Another explanation are CD44+ tumor initiating stem cells, that either just reside within or also contribute to the growth of spheroids, but the latter seems unlikely since not every cell aggregate was observed to contain a CD44+ cell. It would be more likely that tumor cells undergo EMT, gain stem cell-like properties, and subsequently evade the cell aggregate.

5 Conclusion

The use of a multicolor flow-cytometry panel to distinguish cells with different surface markers in a cell suspension like the malignant ascites of ovarian cancer patients or disintegrated spheroids or tumor tissues is, once established, a quick and easy method to screen a lot of different patient samples. It is an adequate method for the often limited sample amount, since a relatively low number of cells is needed for analysis. This method was chosen to study different tumor cell populations in the ascitic fluid in order to add to the characterization of the heterogeneous disease epithelial ovarian cancer on the basis of individual patients.

The results obtained from this analysis allowed for a new subclassification of patients according to their mode of peritoneal tumor spread. This subclassification was further confirmed by transcriptome analysis using RNA sequencing, which revealed an overrepresentation of genes involved in cell adhesion and ECM interaction pathways in patients that show a miliary mode of peritoneal tumor spread. This new subclassification of patients with either miliary spread from patients without or with only few, bigger, more exophytic growing implants was independent of the molecular subclassification defined by a 112 gene signature. Whether this mode of tumor spread causes independent differences in outcome of EOC patients remains to be elucidated employing a larger cohort of patients and a longer follow up. Understanding the molecular characteristics that allow the tumor to spread easily in the peritoneal cavity could help to find targeted approaches to inhibit this behavior and thus prevent patients from getting recurrences in the peritoneum. Impairing the tumors ability to spread locally would even improve their survival time.

5.1 Limitations of the study/outlook

One restriction for biostatistical analysis was the small patient number. Although several samples of each patient were obtained and could be used as biological replica, a larger patient cohort would definitely contribute to statistical power. Also non-uniform classification of the mode of peritoneal tumor spread as observed in patient 16 might benefit from a larger sample size, making it possible to compare more patients with many large implants in the peritoneum to allocate them to one of the previously defined subgroups (miliary; no/few big implants) or to define a new subgroup for this tumor spread.

Furthermore, cell numbers from disintegration of tumor tissues and spheroids were sometimes very low, due to aggressive enzymatic and mechanical methods necessary to disrupt cell-cell contacts. Subsequent flow cytometric analysis on these samples suf-

ferred from blurred population borders, making the gating process difficult at first. To circumvent this problem a gating template was set up with cell-rich ascites and tissue samples. However, for future tests, an improvement in the tissue disruption process would be beneficial, possibly by adding DNase to the sample during the process to prevent DNA from broken cells to clump and trap living cells.

The definite classification of cells as tumor cells both in flow cytometry and immunofluorescent stainings relied on EpCAM positivity. But many ascites samples showed only minor numbers of EpCAM⁺ cells and high numbers of CD44⁺/CD45⁻ cells (distinguishing these cells from leukocytes). To determine the nature of these cells an immunofluorescent staining panel was established, consisting of anti-EpCAM, -CD45, -CD44 and -vimentin antibodies. The staining of the latter one was not evaluable as the stained samples could not be distinguished from the unstained control (not shown). For subsequent studies vimentin antibodies from other companies should be tested with varying antigen retrieval methods (EDTA/citrate buffer) and in combination with the existing three-color panel of anti-EpCAM, -CD45, and -CD44 antibodies. Also other mesenchymal makers like alpha smooth muscle actin, fibronectin, and n-cadherin could be tested as well as phalloidin to determine the formation of actin stress fibers and depolarization of the cells, associated with EMT.

6 List of Abbreviations

AKH	Allgemeines Krankenhaus
BRAF	V-Raf murine sarcoma viral oncogene homolog B1
BRCA	Breast Cancer (gene)
BSA	Bovine serum albumin
CA-125	Cancer antigen 125
CAF	Cancer associated fibroblast
CD133	Cluster of differentiation 133
CD44	Cluster of differentiation 44
CD45	Cluster of differentiation 45
CO ₂	Carbon dioxide
CSC	Cancer stem cell
CSF	Campus Science Support Facilities GmbH
Cy7	Cyanine 7
DNA	Deoxyribonucleic acid
DAVID	Database for Annotation, Visualization and Integrated Discovery
ddH ₂ O	Double-distilled water
DMEM	Dulbecco's Modified Eagle Medium modi
DMSO	Dimethylsulfoxide
ECM	Extracellular matrix
EDTA	Ethylenediaminetetraacetic acid
EGF	Epidermal growth factor
EMT	Epithelial-mesenchymal transition
EOC	Epithelial ovarian cancer
EpCAM	Epithelial cell adhesion molecule
FASAY	Functional analysis of separated alleles in yeast
FC	Flow cytometry
FCS	Fetal calf serum
FDR	False discovery rate
FIGO	International Federation of Obstetricians and Gynaecologists
FITC	Fluorescein isothiocyanate
FSC	Forward scatter channel
G (1-3)	Grade
GA-733-2	Gastrointestinal tumor-associated antigen 2
HEPES	4-(2-hydroxyethyl)-1-piperazineethanesulfonic acid
IgG	Immunoglobulin G
IQR	Interquartile range
KEGG	Kyoto Encyclopedia of Genes and Genomes

KHCO ₃	Potassium bicarbonate
KRAS	V-Ki-ras2 Kirsten rat sarcoma viral oncogene homolog
L1CAM	L1-cell adhesion molecule
MAP	Mitogen-activated protein
mRNA	Messenger RNA
NF-kB	Nuclear factor kappa-light-chain-enhancer of activated B cells
NGS	Next generation sequencing
NH ₄ Cl	Ammonium chloride
NMF	Non-negative matrix factorization
NOD/SCID	Non-Obese Diabetic/Severe Combined Immunodeficiency
p53	Tumor protein 53 (protein)
PBMC	Peripheral blood mononuclear cell
PBS	Phosphate buffered saline,
PBS-T	1x PBS/0.05 % Tween
PC	Principal Component
PCA	Principal Component Analysis
PE	Phycoerythrin
PerCP	Peridinin
PMT	Photomultiplier tube
PROM1	Prominin-1
PTP	Protein tyrosine phosphatase
PTPRC	Protein tyrosine phosphatase, receptor type, C
RIN	RNA integrity number
RNA	Ribonucleic acid
RNA-Seq	RNA sequencing
rRNA	ribosomal RNA
RT	Room temperature
RUM	RNA-Seq Unified Mapper
SC	Single cells
Sph	Spheroids
SPIA	Signaling pathway impact analysis
SSC	Side scatter channel
TGF-beta	Transforming growth factor beta
TP53	Tumor protein 53 (gene)
VEGF	Vascular endothelial growth factor

7 References

- Al-Hajj, M., M. S. Wicha, A. Benito-Hernandez, S. J. Morrison and M. F. Clarke (2003). "Prospective identification of tumorigenic breast cancer cells." Proc Natl Acad Sci U S A **100**(7): 3983-3988.
- Allen, H. J., C. Porter, M. Gamarra, M. S. Piver and E. A. Johnson (1987). "Isolation and morphologic characterization of human ovarian carcinoma cell clusters present in effusions." Exp Cell Biol **55**(4): 194-208.
- Auner, V., G. Kriegshauser, D. Tong, R. Horvat, A. Reinthaller, A. Mustea and R. Zeillinger (2009). "KRAS mutation analysis in ovarian samples using a high sensitivity biochip assay." BMC Cancer **9**: 111.
- Bast, R. C., Jr., B. Hennessy and G. B. Mills (2009). "The biology of ovarian cancer: new opportunities for translation." Nat Rev Cancer **9**(6): 415-428.
- Benedet, J. L., H. Bender, H. Jones, 3rd, H. Y. Ngan and S. Pecorelli (2000). "FIGO staging classifications and clinical practice guidelines in the management of gynecologic cancers. FIGO Committee on Gynecologic Oncology." Int J Gynaecol Obstet **70**(2): 209-262.
- Berns, E. M., I. L. van Staveren, M. P. Look, M. Smid, J. G. Klijn and J. A. Foekens (1998). "Mutations in residues of TP53 that directly contact DNA predict poor outcome in human primary breast cancer." Br J Cancer **77**(7): 1130-1136.
- Bondong, S., H. Kiefel, T. Hielscher, A. G. Zeimet, R. Zeillinger, D. Pils, E. Schuster, D. C. Castillo-Tong, I. Cadron, I. Vergote, I. Braicu, J. Sehouli, S. Mahner, M. Fogel and P. Altevogt (2012). "Prognostic significance of L1CAM in ovarian cancer and its role in constitutive NF-kappaB activation." Ann Oncol **23**(7): 1795-1802.
- Bos, J. L. (1989). "ras oncogenes in human cancer: a review." Cancer Res **49**(17): 4682-4689.
- Bristow, R. E., R. S. Tomacruz, D. K. Armstrong, E. L. Trimble and F. J. Montz (2002). "Survival effect of maximal cytoreductive surgery for advanced ovarian carcinoma during the platinum era: a meta-analysis." J Clin Oncol **20**(5): 1248-1259.
- Brummendorf, T., S. Kenwrick and F. G. Rathjen (1998). "Neural cell recognition molecule L1: from cell biology to human hereditary brain malformations." Curr Opin Neurobiol **8**(1): 87-97.
- Bruno, S., B. Bussolati, C. Grange, F. Collino, M. E. Graziano, U. Ferrando and G. Camussi (2006). "CD133+ renal progenitor cells contribute to tumor angiogenesis." Am J Pathol **169**(6): 2223-2235.
- Cho, S. H., Y. S. Park, H. J. Kim, C. H. Kim, S. W. Lim, J. W. Huh, J. H. Lee and H. R. Kim (2012). "CD44 enhances the epithelial-mesenchymal transition in association with colon cancer invasion." Int J Oncol **41**(1): 211-218.
- Chung, L. M., J. P. Ferguson, W. Zheng, F. Qian, V. Bruno, R. R. Montgomery and H. Zhao (2013). "Differential expression analysis for paired RNA-Seq data." BMC Bioinformatics **14**: 110.

- Clark, T. G., M. E. Stewart, D. G. Altman, H. Gabra and J. F. Smyth (2001). "A prognostic model for ovarian cancer." Br J Cancer **85**(7): 944-952.
- Colombo, N., T. Van Gorp, G. Parma, F. Amant, G. Gatta, C. Sessa and I. Vergote (2006). "Ovarian cancer." Crit Rev Oncol Hematol **60**(2): 159-179.
- Curley, M. D., V. A. Therrien, C. L. Cummings, P. A. Sergent, C. R. Koulouris, A. M. Friel, D. J. Roberts, M. V. Seiden, D. T. Scadden, B. R. Rueda and R. Foster (2009). "CD133 expression defines a tumor initiating cell population in primary human ovarian cancer." Stem Cells **27**(12): 2875-2883.
- De Cecco, L., L. Marchionni, M. Gariboldi, J. F. Reid, M. S. Lagonigro, S. Caramuta, C. Ferrario, E. Bussani, D. Mezzanzanica, F. Turatti, D. Delia, M. G. Daidone, M. Oggionni, N. Bertuletti, A. Ditto, F. Raspagliesi, S. Pilotti, M. A. Pierotti, S. Canevari and C. Schneider (2004). "Gene expression profiling of advanced ovarian cancer: characterization of a molecular signature involving fibroblast growth factor 2." Oncogene **23**(49): 8171-8183.
- Fujita, Y., M. Kitagawa, S. Nakamura, K. Azuma, G. Ishii, M. Higashi, H. Kishi, T. Hiwasa, K. Koda, N. Nakajima and K. Harigaya (2002). "CD44 signaling through focal adhesion kinase and its anti-apoptotic effect." FEBS Lett **528**(1-3): 101-108.
- Godar, S., T. A. Ince, G. W. Bell, D. Feldser, J. L. Donaher, J. Bergh, A. Liu, K. Miu, R. S. Watnick, F. Reinhardt, S. S. McAllister, T. Jacks and R. A. Weinberg (2008). "Growth-inhibitory and tumor-suppressive functions of p53 depend on its repression of CD44 expression." Cell **134**(1): 62-73.
- Gosein, M. A., D. Narinesingh, G. V. Narayansingh, N. A. Bhim and P. A. Sylvester (2013). "Peritoneal tuberculosis mimicking advanced ovarian carcinoma: an important differential diagnosis to consider." BMC Res Notes **6**: 88.
- Herr, D., A. Sallmann, I. Bekes, R. Konrad, I. Holzheu, R. Kreienberg and C. Wulff (2012). "VEGF induces ascites in ovarian cancer patients via increasing peritoneal permeability by downregulation of Claudin 5." Gynecol Oncol **127**(1): 210-216.
- Hofseth, L. J., S. P. Hussain and C. C. Harris (2004). "p53: 25 years after its discovery." Trends Pharmacol Sci **25**(4): 177-181.
- Hollstein, M., D. Sidransky, B. Vogelstein and C. C. Harris (1991). "p53 mutations in human cancers." Science **253**(5015): 49-53.
- Hristozova, T., R. Korschak, V. Budach and I. Tinhofer (2012). "A simple multicolor flow cytometry protocol for detection and molecular characterization of circulating tumor cells in epithelial cancers." Cytometry A **81**(6): 489-495.
- International Collaborative Ovarian Neoplasm, G. (2002). "Paclitaxel plus carboplatin versus standard chemotherapy with either single-agent carboplatin or cyclophosphamide, doxorubicin, and cisplatin in women with ovarian cancer: the ICON3 randomised trial." Lancet **360**(9332): 505-515.
- Jemal, A., F. Bray, M. M. Center, J. Ferlay, E. Ward and D. Forman (2011). "Global cancer statistics." CA Cancer J Clin **61**(2): 69-90.
- Kiefel, H., S. Bondong, N. Erbe-Hoffmann, J. Hazin, S. Riedle, J. Wolf, M. Pfeifer, A. Arlt, H. Schafer, S. S. Muerkoster and P. Altevogt (2010). "L1CAM-integrin interaction

- induces constitutive NF-kappaB activation in pancreatic adenocarcinoma cells by enhancing IL-1beta expression." Oncogene **29**(34): 4766-4778.
- Kiefel, H., S. Bondong, M. Pfeifer, U. Schirmer, N. Erbe-Hoffmann, H. Schafer, S. Sebens and P. Altevogt (2012). "EMT-associated up-regulation of L1CAM provides insights into L1CAM-mediated integrin signalling and NF-kappaB activation." Carcinogenesis **33**(10): 1919-1929.
- Kindelberger, D. W., Y. Lee, A. Miron, M. S. Hirsch, C. Feltmate, F. Medeiros, M. J. Callahan, E. O. Garner, R. W. Gordon, C. Birch, R. S. Berkowitz, M. G. Muto and C. P. Crum (2007). "Intraepithelial carcinoma of the fimbria and pelvic serous carcinoma: Evidence for a causal relationship." Am J Surg Pathol **31**(2): 161-169.
- Kryczek, I., S. Liu, M. Roh, L. Vatan, W. Szeliga, S. Wei, M. Banerjee, Y. Mao, J. Kotarski, M. S. Wicha, R. Liu and W. Zou (2012). "Expression of aldehyde dehydrogenase and CD133 defines ovarian cancer stem cells." Int J Cancer **130**(1): 29-39.
- Kurman, R. J. and M. Shih Ie (2010). "The origin and pathogenesis of epithelial ovarian cancer: a proposed unifying theory." Am J Surg Pathol **34**(3): 433-443.
- Lalwani, N., S. R. Prasad, R. Vikram, A. K. Shanbhogue, P. C. Huettner and N. Fasih (2011). "Histologic, molecular, and cytogenetic features of ovarian cancers: implications for diagnosis and treatment." Radiographics **31**(3): 625-646.
- Latifi, A., R. B. Luwor, M. Bilandzic, S. Nazaretian, K. Stenvers, J. Pyman, H. Zhu, E. W. Thompson, M. A. Quinn, J. K. Findlay and N. Ahmed (2012). "Isolation and characterization of tumor cells from the ascites of ovarian cancer patients: molecular phenotype of chemoresistant ovarian tumors." PLoS One **7**(10): e46858.
- Lee, S. B., A. Schramme, K. Doberstein, R. Dummer, M. S. Abdel-Bakky, S. Keller, P. Altevogt, S. T. Oh, J. Reichrath, D. Oxmann, J. Pfeilschifter, D. Mihic-Probst and P. Gutwein (2010). "ADAM10 is upregulated in melanoma metastasis compared with primary melanoma." J Invest Dermatol **130**(3): 763-773.
- Lengyel, E. (2010). "Ovarian cancer development and metastasis." Am J Pathol **177**(3): 1053-1064.
- Marhaba, R. and M. Zoller (2004). "CD44 in cancer progression: adhesion, migration and growth regulation." J Mol Histol **35**(3): 211-231.
- Mazur, P. (1984). "Freezing of living cells: mechanisms and implications." Am J Physiol **247**(3 Pt 1): C125-142.
- Melichar, B. and R. S. Freedman (2002). "Immunology of the peritoneal cavity: relevance for host-tumor relation." Int J Gynecol Cancer **12**(1): 3-17.
- Memczak, S., M. Jens, A. Elefsinioti, F. Torti, J. Krueger, A. Rybak, L. Maier, S. D. Mackowiak, L. H. Gregersen, M. Munschauer, A. Loewer, U. Ziebold, M. Landthaler, C. Kocks, F. le Noble and N. Rajewsky (2013). "Circular RNAs are a large class of animal RNAs with regulatory potency." Nature **495**(7441): 333-338.
- Miraglia, S., W. Godfrey, A. H. Yin, K. Atkins, R. Warnke, J. T. Holden, R. A. Bray, E. K. Waller and D. W. Buck (1997). "A novel five-transmembrane hematopoietic stem

cell antigen: isolation, characterization, and molecular cloning." Blood **90**(12): 5013-5021.

Nakayama, N., K. Nakayama, S. Yeasmin, M. Ishibashi, A. Katagiri, K. Iida, M. Fukumoto and K. Miyazaki (2008). "KRAS or BRAF mutation status is a useful predictor of sensitivity to MEK inhibition in ovarian cancer." Br J Cancer **99**(12): 2020-2028.

Naor, D., R. V. Sionov and D. Ish-Shalom (1997). "CD44: structure, function, and association with the malignant process." Adv Cancer Res **71**: 241-319.

Nielsen, T. O., J. S. Parker, S. Leung, D. Voduc, M. Ebbert, T. Vickery, S. R. Davies, J. Snider, I. J. Stijleman, J. Reed, M. C. Cheang, E. R. Mardis, C. M. Perou, P. S. Bernard and M. J. Ellis (2010). "A comparison of PAM50 intrinsic subtyping with immunohistochemistry and clinical prognostic factors in tamoxifen-treated estrogen receptor-positive breast cancer." Clin Cancer Res **16**(21): 5222-5232.

O'Brien, C. A., A. Pollett, S. Gallinger and J. E. Dick (2007). "A human colon cancer cell capable of initiating tumour growth in immunodeficient mice." Nature **445**(7123): 106-110.

Odicino, F., S. Pecorelli, L. Zigliani and W. T. Creasman (2008). "History of the FIGO cancer staging system." Int J Gynaecol Obstet **101**(2): 205-210.

Ostman, A. and M. Augsten (2009). "Cancer-associated fibroblasts and tumor growth--bystanders turning into key players." Curr Opin Genet Dev **19**(1): 67-73.

Perou, C. M., T. Sorlie, M. B. Eisen, M. van de Rijn, S. S. Jeffrey, C. A. Rees, J. R. Pollack, D. T. Ross, H. Johnsen, L. A. Akslen, O. Fluge, A. Pergamenschikov, C. Williams, S. X. Zhu, P. E. Lonning, A. L. Borresen-Dale, P. O. Brown and D. Botstein (2000). "Molecular portraits of human breast tumours." Nature **406**(6797): 747-752.

Piek, J. M., P. Kenemans and R. H. Verheijen (2004). "Intraperitoneal serous adenocarcinoma: a critical appraisal of three hypotheses on its cause." Am J Obstet Gynecol **191**(3): 718-732.

Piek, J. M., P. J. van Diest, R. P. Zweemer, J. W. Jansen, R. J. Poort-Keesom, F. H. Menko, J. J. Gille, A. P. Jongsma, G. Pals, P. Kenemans and R. H. Verheijen (2001). "Dysplastic changes in prophylactically removed Fallopian tubes of women predisposed to developing ovarian cancer." J Pathol **195**(4): 451-456.

Pils, D., G. Hager, D. Tong, S. Aust, G. Heinze, M. Kohl, E. Schuster, A. Wolf, J. Sehouli, I. Braicu, I. Vergote, I. Cadron, S. Mahner, G. Hofstetter, P. Speiser and R. Zeillinger (2012). "Validating the impact of a molecular subtype in ovarian cancer on outcomes: a study of the OVCAD Consortium." Cancer Sci **103**(7): 1334-1341.

Poplawski, G. H., A. K. Tranziska, I. Leshchyn'ska, I. D. Meier, T. Streichert, V. Sytnyk and M. Schachner (2012). "L1CAM increases MAP2 expression via the MAPK pathway to promote neurite outgrowth." Mol Cell Neurosci **50**(2): 169-178.

Rao, C. G., D. Chianese, G. V. Doyle, M. C. Miller, T. Russell, R. A. Sanders, Jr. and L. W. Terstappen (2005). "Expression of epithelial cell adhesion molecule in carcinoma cells present in blood and primary and metastatic tumors." Int J Oncol **27**(1): 49-57.

- Rasmussen, D. H. and A. P. MacKenzie (1968). "Phase diagram for the system water-dimethylsulphoxide." Nature **220**(5174): 1315-1317.
- Raveh, S., N. Gavert and A. Ben-Ze'ev (2009). "L1 cell adhesion molecule (L1CAM) in invasive tumors." Cancer Lett **282**(2): 137-145.
- Schachner, M. (1997). "Neural recognition molecules and synaptic plasticity." Curr Opin Cell Biol **9**(5): 627-634.
- Silva, J. L., L. P. Rangel, D. C. Costa, Y. Cordeiro and C. V. De Moura Gallo (2013). "Expanding the Prion Concept to Cancer Biology: Dominant-Negative Effect of Aggregates of Mutant p53 Tumor Suppressor." Biosci Rep.
- Smith-Sorensen, B., J. Kaern, R. Holm, A. Dorum, C. Trope and A. L. Borresen-Dale (1998). "Therapy effect of either paclitaxel or cyclophosphamide combination treatment in patients with epithelial ovarian cancer and relation to TP53 gene status." Br J Cancer **78**(3): 375-381.
- Stoeck, A., S. Schlich, Y. Issa, V. Gschwend, T. Wenger, I. Herr, A. Marme, S. Bourbie, P. Altevogt and P. Gutwein (2006). "L1 on ovarian carcinoma cells is a binding partner for Neuropilin-1 on mesothelial cells." Cancer Lett **239**(2): 212-226.
- Taddei, M. L., E. Giannoni, T. Fiaschi and P. Chiarugi (2012). "Anoikis: an emerging hallmark in health and diseases." J Pathol **226**(2): 380-393.
- Tarca, A. L., S. Draghici, P. Khatri, S. S. Hassan, P. Mittal, J. S. Kim, C. J. Kim, J. P. Kusanovic and R. Romero (2009). "A novel signaling pathway impact analysis." Bioinformatics **25**(1): 75-82.
- Tarin, D., J. E. Price, M. G. Kettlewell, R. G. Souter, A. C. Vass and B. Crossley (1984). "Mechanisms of human tumor metastasis studied in patients with peritoneovenous shunts." Cancer Res **44**(8): 3584-3592.
- Tothill, R. W., A. V. Tinker, J. George, R. Brown, S. B. Fox, S. Lade, D. S. Johnson, M. K. Trivett, D. Etemadmoghadam, B. Locandro, N. Traficante, S. Fereday, J. A. Hung, Y. E. Chiew, I. Haviv, G. Australian Ovarian Cancer Study, D. Gertig, A. DeFazio and D. D. Bowtell (2008). "Novel molecular subtypes of serous and endometrioid ovarian cancer linked to clinical outcome." Clin Cancer Res **14**(16): 5198-5208.
- van der Gun, B. T., L. J. Melchers, M. H. Ruiters, L. F. de Leij, P. M. McLaughlin and M. G. Rots (2010). "EpCAM in carcinogenesis: the good, the bad or the ugly." Carcinogenesis **31**(11): 1913-1921.
- Wintzell, M., E. Hjerpe, E. Avall Lundqvist and M. Shoshan (2012). "Protein markers of cancer-associated fibroblasts and tumor-initiating cells reveal subpopulations in freshly isolated ovarian cancer ascites." BMC Cancer **12**: 359.
- Wright, M. H., A. M. Calcagno, C. D. Salcido, M. D. Carlson, S. V. Ambudkar and L. Varticovski (2008). "Brca1 breast tumors contain distinct CD44+/CD24- and CD133+ cells with cancer stem cell characteristics." Breast Cancer Res **10**(1): R10.
- Yabushita, H., M. Noguchi, T. Kishida, K. Fusano, Y. Noguchi, N. Itano, K. Kimata and M. Noguchi (2004). "Hyaluronan synthase expression in ovarian cancer." Oncol Rep **12**(4): 739-743.

Yin, S., J. Li, C. Hu, X. Chen, M. Yao, M. Yan, G. Jiang, C. Ge, H. Xie, D. Wan, S. Yang, S. Zheng and J. Gu (2007). "CD133 positive hepatocellular carcinoma cells possess high capacity for tumorigenicity." Int J Cancer **120**(7): 1444-1450.

Yoshihara, K., A. Tajima, D. Komata, T. Yamamoto, S. Kodama, H. Fujiwara, M. Suzuki, Y. Onishi, M. Hatae, K. Sueyoshi, H. Fujiwara, Y. Kudo, I. Inoue and K. Tanaka (2009). "Gene expression profiling of advanced-stage serous ovarian cancers distinguishes novel subclasses and implicates ZEB2 in tumor progression and prognosis." Cancer Sci **100**(8): 1421-1428.

Zhan, Q., C. Wang and S. Ngai (2013). "Ovarian cancer stem cells: a new target for cancer therapy." Biomed Res Int **2013**: 916819.

8 Supplementary data

Table S1. Differentially expressed genes between patients with miliary and no/few, big implants.

ID= ensembl gene ID; FC= fold change in expression between modes of tumor spread; adj P.Val = adjusted p- value; Transcripts= number of transcripts annotated; Length= length of annotated transcript.

GeneName	logFC	P.Value	adj.P.Val	Length	Exons	Type	ID
C19orf59	-7.078	1.713E-07	2.430E-04	1730	7	protein_coding	ENSG00000183019
GSTT1	-6.997	7.735E-08	1.576E-04	2066	5	protein_coding	ENSG00000184674
P2RY12	-6.827	3.201E-07	3.685E-04	1766	3	protein_coding	ENSG00000169313
AC104135.3	-6.824	5.642E-07	5.335E-04	3662	4	lincRNA	ENSG00000204792
HLA-V	-6.601	6.001E-07	5.480E-04	4814	4	pseudogene	ENSG00000181126
MGP	-6.583	7.492E-07	6.399E-04	1405	5	protein_coding	ENSG00000111341
RP11-172E10.1	-6.531	2.033E-06	1.224E-03	545	3	lincRNA	ENSG00000254060
AIM2	-6.496	8.018E-07	6.635E-04	1529	7	protein_coding	ENSG00000163568
SV2B	-6.430	2.029E-06	1.224E-03	11279	15	protein_coding	ENSG00000185518
HAS2	-6.327	5.749E-06	2.415E-03	4190	4	protein_coding	ENSG00000170961
ZFHX4	-6.322	2.324E-06	1.338E-03	14019	12	protein_coding	ENSG00000091656
SDPR	-6.275	1.138E-06	8.467E-04	3229	2	protein_coding	ENSG00000168497
USP17L30	-6.261	4.456E-06	2.269E-03	1593	1	protein_coding	ENSG00000228856
U6	-6.248	5.781E-06	2.415E-03	107	1	snRNA	ENSG00000202081
PRDM16	-6.215	7.917E-06	2.953E-03	8721	18	protein_coding	ENSG00000142611
RGS13	-6.199	8.817E-06	3.243E-03	5119	7	protein_coding	ENSG00000127074
USP17L29	-6.186	6.280E-06	2.550E-03	1593	1	protein_coding	ENSG00000231637
USP17L28	-6.146	7.538E-06	2.852E-03	1593	1	protein_coding	ENSG00000231051
RP1-206D15.5	-6.135	1.193E-05	3.829E-03	100	1	pseudogene	ENSG00000234604
PKDCC	-6.123	2.514E-06	1.387E-03	2502	8	protein_coding	ENSG00000162878
INHBA	-6.108	5.580E-06	2.415E-03	6064	3	protein_coding	ENSG00000122641
USP17L27	-6.099	9.271E-06	3.318E-03	1593	1	protein_coding	ENSG00000235780
SNAI2	-6.086	1.345E-05	3.958E-03	2204	4	protein_coding	ENSG00000019549
SLCO5A1	-6.059	1.447E-05	4.119E-03	3790	10	protein_coding	ENSG00000137571
MEDAG	-6.059	5.202E-06	2.415E-03	2374	5	protein_coding	ENSG00000102802
HOXA5	-6.000	1.594E-05	4.351E-03	1657	2	protein_coding	ENSG00000106004
USP17L5	-5.994	1.398E-05	4.025E-03	1593	1	protein_coding	ENSG00000227140
USP17L26	-5.989	1.486E-05	4.166E-03	1593	1	protein_coding	ENSG00000229579
RP11-467H10.2	-5.939	2.277E-05	5.743E-03	617	3	processed_transcript	ENSG00000259628
DPYS	-5.936	2.497E-05	6.122E-03	2127	10	protein_coding	ENSG00000147647
USP17L25	-5.926	1.938E-05	5.031E-03	1593	1	protein_coding	ENSG00000230430
FABP4	-5.900	6.660E-06	2.593E-03	941	4	protein_coding	ENSG00000170323
ABCA8	-5.888	1.261E-05	3.838E-03	5677	40	protein_coding	ENSG00000141338
BNC1	-5.882	3.871E-06	2.010E-03	4610	5	protein_coding	ENSG00000169594
AP000350.6	-5.858	2.869E-05	6.548E-03	1763	3	pseudogene	ENSG00000225282
USP17L24	-5.854	2.611E-05	6.230E-03	1593	1	protein_coding	ENSG00000232264
PAMR1	-5.794	4.246E-05	8.472E-03	3143	13	protein_coding	ENSG00000149090
FAM19A3	-5.792	4.192E-05	8.472E-03	1282	5	protein_coding	ENSG00000184599
USP17L9P	-5.789	3.122E-05	6.846E-03	1593	1	pseudogene	ENSG00000251694
PCBP3	-5.781	4.348E-05	8.528E-03	2202	16	protein_coding	ENSG00000183570
LINC00607	-5.757	1.304E-05	3.923E-03	3690	10	processed_transcript	ENSG00000235770
CHL1	-5.745	1.223E-05	3.829E-03	8013	28	protein_coding	ENSG00000134121
CALB2	-5.738	9.991E-06	3.436E-03	1466	11	protein_coding	ENSG00000172137
FCRL3	-5.703	1.226E-05	3.829E-03	4725	16	protein_coding	ENSG00000160856

CR2	-5.698	2.844E-05	6.548E-03	4240	20	protein_coding	ENSG00000117322
GPC3	-5.675	7.299E-05	1.212E-02	2568	9	protein_coding	ENSG00000147257
USP17L22	-5.660	5.244E-05	9.779E-03	1593	1	protein_coding	ENSG00000248933
BDKRB1	-5.653	7.888E-05	1.289E-02	1687	5	protein_coding	ENSG00000100739
IDO1	-5.647	5.706E-06	2.415E-03	2097	12	protein_coding	ENSG00000131203
SLITRK2	-5.634	6.776E-05	1.180E-02	7672	5	protein_coding	ENSG00000185985
USP17L21	-5.620	6.623E-05	1.179E-02	1593	1	protein_coding	ENSG00000249811
VCAM1	-5.566	1.338E-06	9.084E-04	3083	9	protein_coding	ENSG00000162692
LINC00189	-5.560	9.134E-05	1.457E-02	989	4	processed_transcript	ENSG00000215533
USP17L20	-5.547	7.935E-05	1.289E-02	1593	1	protein_coding	ENSG00000250745
KLHL4	-5.538	1.154E-04	1.652E-02	5818	11	protein_coding	ENSG00000102271
RP11-15J10.8	-5.500	3.232E-05	6.846E-03	1263	5	pseudogene	ENSG00000236252
LIPN	-5.499	1.912E-05	5.031E-03	1197	9	protein_coding	ENSG00000204020
SERPINB2	-5.485	1.151E-06	8.467E-04	2155	9	protein_coding	ENSG00000197632
CXCL6	-5.482	5.724E-05	1.053E-02	1718	4	protein_coding	ENSG00000124875
USP17L19	-5.474	1.045E-04	1.554E-02	1593	1	protein_coding	ENSG00000248920
RP11-89H19.1	-5.467	1.344E-04	1.863E-02	1287	4	antisense	ENSG00000205537
ACSM1	-5.452	1.397E-04	1.927E-02	2147	14	protein_coding	ENSG00000166743
RP11-381O7.3	-5.439	1.496E-04	2.042E-02	2566	5	lincRNA	ENSG00000182021
PLA2G2A	-5.419	1.124E-04	1.635E-02	1306	6	protein_coding	ENSG00000188257
MCCC1-AS1	-5.411	3.945E-05	8.225E-03	765	2	antisense	ENSG00000243368
USP17L18	-5.404	1.316E-04	1.835E-02	1593	1	protein_coding	ENSG00000250844
Metazoa_SRP	-5.375	1.913E-04	2.378E-02	281	1	misc_RNA	ENSG00000265411
Metazoa_SRP	-5.371	1.935E-04	2.383E-02	281	1	misc_RNA	ENSG00000265315
OR2B11	-5.367	4.430E-05	8.626E-03	1054	1	protein_coding	ENSG00000177535
MAOB	-5.350	9.667E-05	1.497E-02	2566	16	protein_coding	ENSG00000069535
USP17L17	-5.335	1.735E-04	2.253E-02	1593	1	protein_coding	ENSG00000249104
ELAVL3	-5.326	1.672E-04	2.202E-02	4727	7	protein_coding	ENSG00000196361
RGS5	-5.312	2.394E-04	2.732E-02	5862	6	protein_coding	ENSG00000143248
AC114730.2	-5.292	1.649E-04	2.194E-02	571	2	antisense	ENSG00000235151
BCHE	-5.287	2.509E-04	2.839E-02	2527	5	protein_coding	ENSG00000114200
BEND4	-5.284	1.630E-04	2.179E-02	8765	6	protein_coding	ENSG00000188848
RP11-669B18.1	-5.281	2.247E-04	2.625E-02	591	1	pseudogene	ENSG00000257199
CFHR1	-5.254	2.139E-04	2.552E-02	1271	6	protein_coding	ENSG00000244414
CCL24	-5.248	1.597E-04	2.147E-02	585	4	protein_coding	ENSG00000106178
USP17L6P	-5.234	2.241E-04	2.625E-02	1197	1	pseudogene	ENSG00000205946
RP5-1163L11.2	-5.209	3.234E-04	3.439E-02	285	1	pseudogene	ENSG00000258930
XPNPEP2	-5.202	2.024E-04	2.461E-02	3270	21	protein_coding	ENSG00000122121
CPA4	-5.192	6.711E-05	1.180E-02	2797	11	protein_coding	ENSG00000128510
LGR5	-5.183	3.163E-04	3.391E-02	4611	20	protein_coding	ENSG00000139292
SHROOM4	-5.173	2.110E-04	2.528E-02	9556	10	protein_coding	ENSG00000158352
PDGFRA	-5.167	3.146E-05	6.846E-03	6576	23	protein_coding	ENSG00000134853
OSR1	-5.156	5.662E-05	1.049E-02	4175	3	protein_coding	ENSG00000143867
USP17L15	-5.134	3.294E-04	3.474E-02	1590	1	protein_coding	ENSG00000223569
ASIC3	-5.121	3.720E-04	3.704E-02	2232	11	protein_coding	ENSG00000213199
MARCH3	-5.113	6.029E-05	1.093E-02	4196	5	protein_coding	ENSG00000173926
CBLN2	-5.107	4.122E-04	3.999E-02	3336	5	protein_coding	ENSG00000141668
CCL20	-5.090	1.241E-04	1.757E-02	831	4	protein_coding	ENSG00000115009
USP17L23	-5.081	3.692E-04	3.691E-02	551	1	protein_coding	ENSG00000250913
IFNK	-5.076	1.749E-04	2.256E-02	1140	2	protein_coding	ENSG00000147896

DONSON	-5.072	2.499E-06	1.387E-03	2332	11	protein_coding	ENSG00000159147
HEY1	-5.071	2.549E-04	2.873E-02	2296	5	protein_coding	ENSG00000164683
HP	-5.064	4.287E-05	8.472E-03	3024	8	protein_coding	ENSG00000257017
RASGRF1	-5.064	3.056E-04	3.317E-02	6294	28	protein_coding	ENSG00000058335
OGN	-5.061	1.781E-04	2.268E-02	2971	7	protein_coding	ENSG00000106809
PDGFR	-5.054	3.997E-04	3.891E-02	1905	7	protein_coding	ENSG00000104213
DGAT2	-5.048	9.390E-05	1.471E-02	2452	8	protein_coding	ENSG00000062282
ADH1B	-5.042	5.464E-04	4.828E-02	4072	10	protein_coding	ENSG00000196616
RP11-51M18.1	-5.036	5.338E-04	4.792E-02	1521	2	lincRNA	ENSG00000253898
RIMBP2	-5.032	5.433E-04	4.828E-02	6321	19	protein_coding	ENSG00000060709
ATP1B3-AS1	-5.029	2.026E-04	2.461E-02	376	2	antisense	ENSG00000244124
CADM3	-5.007	7.289E-05	1.212E-02	3745	10	protein_coding	ENSG00000162706
CDC42EP5	-5.005	3.140E-04	3.390E-02	864	3	protein_coding	ENSG00000167617
AL049758.2	-5.004	5.546E-04	4.844E-02	397	1	pseudogene	ENSG00000226989
ADAMTS9-AS1	-4.995	5.848E-04	4.963E-02	1727	3	antisense	ENSG00000241158
PDZRN4	-4.990	6.626E-04	5.402E-02	3411	10	protein_coding	ENSG00000165966
RP11-252I13.1	-4.990	2.887E-04	3.186E-02	2157	1	pseudogene	ENSG00000248827
EFEMP1	-4.986	5.282E-06	2.415E-03	3024	12	protein_coding	ENSG00000115380
AC140076.1	-4.962	7.066E-04	5.601E-02	361	1	pseudogene	ENSG00000227309
HAS1	-4.960	1.095E-04	1.602E-02	2110	5	protein_coding	ENSG00000105509
RP11-16K12.1	-4.953	5.758E-04	4.947E-02	1900	2	antisense	ENSG00000177699
PHYHIP	-4.931	6.693E-04	5.430E-02	3200	6	protein_coding	ENSG00000168490
IGJ	-4.919	8.597E-05	1.380E-02	1438	6	protein_coding	ENSG00000132465
RP3-355L5.3	-4.918	7.524E-04	5.877E-02	747	1	pseudogene	ENSG00000216639
FAM5B	-4.915	3.877E-04	3.788E-02	3558	8	protein_coding	ENSG00000198797
MT1X	-4.908	4.168E-05	8.472E-03	1727	3	protein_coding	ENSG00000187193
LHCGR	-4.899	8.155E-04	6.223E-02	3044	11	protein_coding	ENSG00000138039
TMEM200B	-4.896	5.950E-04	5.034E-02	2553	2	protein_coding	ENSG00000253304
DCN	-4.895	5.335E-06	2.415E-03	2924	9	protein_coding	ENSG00000011465
CD248	-4.880	7.679E-05	1.263E-02	2558	1	protein_coding	ENSG00000174807
RP11-318K12.1	-4.867	4.329E-04	4.153E-02	1452	10	pseudogene	ENSG00000228991
RP11-48O20.4	-4.859	8.230E-04	6.263E-02	1113	3	lincRNA	ENSG00000224259
EZR-AS1	-4.829	8.826E-04	6.621E-02	217	2	antisense	ENSG00000233893
AC026202.3	-4.827	4.220E-04	4.079E-02	672	4	antisense	ENSG00000233912
CH25H	-4.818	2.592E-05	6.230E-03	1378	1	protein_coding	ENSG00000138135
AC007386.4	-4.814	1.037E-03	7.443E-02	1018	3	antisense	ENSG00000232613
GNA14	-4.805	1.031E-03	7.419E-02	2482	7	protein_coding	ENSG00000156049
ST6GALNAC3	-4.795	4.533E-04	4.274E-02	6861	5	protein_coding	ENSG00000184005
Y_RNA	-4.791	7.027E-04	5.601E-02	102	1	misc_RNA	ENSG00000201501
LIN7A	-4.789	3.744E-04	3.713E-02	6112	7	protein_coding	ENSG00000111052
TRH	-4.788	6.229E-04	5.171E-02	1978	3	protein_coding	ENSG00000170893
CTLA4	-4.785	3.485E-04	3.605E-02	1977	4	protein_coding	ENSG00000163599
BCKDHA	-4.778	1.047E-03	7.496E-02	2103	9	protein_coding	ENSG00000248098
AC005785.2	-4.759	1.209E-03	8.206E-02	1771	2	processed_transcript	ENSG00000268189
CNN1	-4.751	7.654E-04	5.909E-02	1848	8	protein_coding	ENSG00000130176
AK8	-4.751	1.141E-03	8.010E-02	2465	15	protein_coding	ENSG00000165695
COL9A3	-4.740	2.964E-04	3.243E-02	2485	32	protein_coding	ENSG00000092758
RP11-141P6.1	-4.733	1.310E-03	8.509E-02	799	1	pseudogene	ENSG00000250076
EMR3	-4.732	5.104E-04	4.665E-02	2254	16	protein_coding	ENSG00000131355
PAK3	-4.725	1.291E-03	8.509E-02	2638	19	protein_coding	ENSG00000077264

TPH2	-4.724	1.292E-03	8.509E-02	2992	11	protein_coding	ENSG00000139287
SMTNL2	-4.705	4.536E-04	4.274E-02	2280	8	protein_coding	ENSG00000188176
CTD-3037G24.4	-4.704	1.237E-03	8.354E-02	563	2	antisense	ENSG00000259876
AP000857.1	-4.704	9.843E-04	7.260E-02	871	1	pseudogene	ENSG00000213305
CAMK2A	-4.702	1.458E-03	9.086E-02	5322	19	protein_coding	ENSG00000070808
PFN1P3	-4.688	1.477E-03	9.086E-02	402	1	pseudogene	ENSG00000234367
RPS12P20	-4.688	1.396E-03	8.802E-02	380	1	pseudogene	ENSG00000244134
HEATR4	-4.686	1.324E-03	8.509E-02	3523	18	protein_coding	ENSG00000187105
PIGR	-4.684	1.929E-04	2.383E-02	4279	11	protein_coding	ENSG00000162896
RP11-38P22.2	-4.676	3.506E-04	3.613E-02	2050	1	lincRNA	ENSG00000241732
RP11-290F5.2	-4.667	1.556E-03	9.406E-02	2153	3	processed_transcript	ENSG00000180712
Metazoa_SRP	-4.664	1.477E-03	9.086E-02	294	1	misc_RNA	ENSG00000243227
RP5-1115A15.1	-4.656	1.131E-03	8.007E-02	516	4	antisense	ENSG00000232912
CTC-268N12.2	-4.647	1.618E-03	9.583E-02	718	3	antisense	ENSG00000266895
CTC-265F19.2	-4.642	1.641E-03	9.677E-02	1708	1	sense_intronic	ENSG00000267412
SNCAIP	-4.629	7.038E-04	5.601E-02	4986	14	protein_coding	ENSG00000064692
RP11-81H14.3	-4.624	1.661E-03	9.730E-02	1162	1	pseudogene	ENSG00000256075
Metazoa_SRP	-4.608	1.002E-03	7.341E-02	268	1	misc_RNA	ENSG00000242330
PTPRB	-4.606	3.637E-04	3.691E-02	11332	34	protein_coding	ENSG00000127329
WDR69	-4.605	1.204E-03	8.194E-02	2476	14	protein_coding	ENSG00000123977
AC027612.6	-4.604	9.896E-04	7.279E-02	1104	4	pseudogene	ENSG00000143429
HOXC6	-4.603	1.671E-03	9.768E-02	2943	3	protein_coding	ENSG00000197757
HSPA4L	-4.597	7.150E-04	5.618E-02	4128	20	protein_coding	ENSG00000164070
ADAMTS12	-4.596	1.059E-03	7.558E-02	8774	24	protein_coding	ENSG00000151388
CXCL9	-4.594	2.987E-05	6.760E-03	2740	4	protein_coding	ENSG00000138755
PLA2G2D	-4.576	5.835E-04	4.963E-02	2672	4	protein_coding	ENSG00000117215
CDA	-4.564	1.383E-03	8.795E-02	963	4	protein_coding	ENSG00000158825
PKHD1L1	-4.562	1.149E-04	1.652E-02	13076	78	protein_coding	ENSG00000205038
GPR116	-4.560	1.171E-03	8.097E-02	5810	21	protein_coding	ENSG00000069122
ACSM3	-4.557	6.359E-04	5.246E-02	2845	14	protein_coding	ENSG00000005187
GPR124	-4.545	3.760E-04	3.715E-02	6270	19	protein_coding	ENSG00000020181
CNR2	-4.544	4.927E-04	4.546E-02	5350	3	protein_coding	ENSG00000188822
RP4-791M13.4	-4.534	1.591E-03	9.513E-02	573	3	antisense	ENSG00000255148
AC007365.3	-4.525	1.581E-03	9.493E-02	627	2	lincRNA	ENSG00000226756
PAPPA	-4.516	2.479E-04	2.817E-02	10959	22	protein_coding	ENSG00000182752
LILRA3	-4.500	1.356E-03	8.676E-02	1880	11	protein_coding	ENSG00000170866
CACNA1G	-4.498	1.485E-03	9.101E-02	7848	38	protein_coding	ENSG00000006283
RP3-455J7.4	-4.497	1.315E-03	8.509E-02	2523	2	processed_transcript	ENSG00000241666
RP11-925D8.3	-4.496	9.099E-04	6.806E-02	1481	1	pseudogene	ENSG00000259600
GRIA2	-4.483	5.794E-04	4.949E-02	5621	17	protein_coding	ENSG00000120251
PDK4	-4.483	7.435E-07	6.399E-04	3576	11	protein_coding	ENSG00000004799
SPARCL1	-4.462	6.124E-04	5.100E-02	2994	12	protein_coding	ENSG00000152583
IGHM	-4.455	1.212E-06	8.677E-04	1461	4	IG_C_gene	ENSG00000211899
CXCL10	-4.453	3.272E-05	6.875E-03	1173	4	protein_coding	ENSG00000169245
DIRAS1	-4.452	7.681E-04	5.912E-02	3424	3	protein_coding	ENSG00000176490
GNAT2	-4.433	4.683E-04	4.382E-02	1339	8	protein_coding	ENSG00000134183
GLI2	-4.426	1.272E-03	8.464E-02	6799	14	protein_coding	ENSG00000074047
DNMBP-AS1	-4.425	1.415E-03	8.900E-02	2034	5	antisense	ENSG00000227695
FAM101A	-4.425	8.543E-04	6.427E-02	2148	3	protein_coding	ENSG00000178882
SEMA3D	-4.424	3.687E-04	3.691E-02	6265	17	protein_coding	ENSG00000153993

P2RY14	-4.397	1.143E-03	8.010E-02	2513	4	protein_coding	ENSG00000174944
FFAR3	-4.382	2.611E-04	2.917E-02	1796	2	protein_coding	ENSG00000185897
UCP3	-4.376	1.289E-03	8.509E-02	2623	7	protein_coding	ENSG00000175564
RP11-464O2.2	-4.362	1.301E-03	8.509E-02	1491	3	antisense	ENSG00000233334
CPE	-4.360	1.462E-04	2.006E-02	2421	9	protein_coding	ENSG00000109472
SVEP1	-4.358	2.393E-04	2.732E-02	12341	48	protein_coding	ENSG00000165124
MTND5P14	-4.348	1.608E-03	9.571E-02	1267	1	pseudogene	ENSG00000230225
GPR42	-4.345	5.226E-04	4.739E-02	1795	2	protein_coding	ENSG00000126251
COL4A3	-4.310	6.018E-04	5.059E-02	8097	52	protein_coding	ENSG00000169031
PTGR2	-4.303	1.202E-03	8.194E-02	4859	10	protein_coding	ENSG00000140043
EGFL6	-4.284	1.855E-04	2.328E-02	2398	12	protein_coding	ENSG00000198759
RP11-796E2.4	-4.276	1.442E-03	9.021E-02	5699	3	antisense	ENSG00000245904
PTPRQ	-4.261	1.385E-03	8.795E-02	7201	50	protein_coding	ENSG00000139304
NR4A3	-4.260	5.837E-06	2.415E-03	4982	8	protein_coding	ENSG00000119508
AREGB	-4.210	2.277E-05	5.743E-03	1239	6	protein_coding	ENSG00000205595
STRA6	-4.203	1.240E-03	8.354E-02	2887	19	protein_coding	ENSG00000137868
L1TD1	-4.201	1.271E-03	8.464E-02	3849	4	protein_coding	ENSG00000240563
FCAR	-4.198	7.047E-05	1.196E-02	1619	6	protein_coding	ENSG00000186431
AREG	-4.191	1.749E-05	4.677E-03	1240	6	protein_coding	ENSG00000109321
DLC1	-4.190	5.501E-04	4.840E-02	7447	18	protein_coding	ENSG00000164741
GPAT2	-4.168	1.252E-03	8.396E-02	4407	23	protein_coding	ENSG00000186281
ISLR	-4.155	1.570E-03	9.446E-02	2371	2	protein_coding	ENSG00000129009
POSTN	-4.131	7.116E-04	5.608E-02	3373	23	protein_coding	ENSG00000133110
FPR2	-4.101	1.031E-04	1.543E-02	2621	4	protein_coding	ENSG00000171049
ABI3BP	-4.056	1.670E-04	2.202E-02	6783	67	protein_coding	ENSG00000154175
ANKRD22	-3.999	9.139E-04	6.817E-02	1596	6	protein_coding	ENSG00000152766
RHOH	-3.997	4.422E-04	4.228E-02	1999	5	protein_coding	ENSG00000168421
GFPT2	-3.996	1.605E-03	9.569E-02	3093	19	protein_coding	ENSG00000131459
SORBS2	-3.993	1.614E-03	9.582E-02	6050	24	protein_coding	ENSG00000154556
COL1A2	-3.971	2.330E-05	5.766E-03	5993	52	protein_coding	ENSG00000164692
APOBEC3A	-3.959	4.144E-05	8.472E-03	1478	6	protein_coding	ENSG00000128383
RGS2	-3.951	1.244E-05	3.829E-03	1344	5	protein_coding	ENSG00000116741
CDH11	-3.908	4.859E-04	4.499E-02	6874	14	protein_coding	ENSG00000140937
SIK1	-3.902	3.160E-05	6.846E-03	4712	14	protein_coding	ENSG00000142178
KDR	-3.902	1.199E-03	8.194E-02	5831	30	protein_coding	ENSG00000128052
LRRN4	-3.899	3.808E-04	3.741E-02	2692	5	protein_coding	ENSG00000125872
NEFH	-3.898	1.526E-03	9.267E-02	3783	4	protein_coding	ENSG00000100285
IGHV3-30	-3.862	1.376E-03	8.781E-02	431	2	IG_V_gene	ENSG00000211953
SDC2	-3.812	3.149E-04	3.390E-02	3751	5	protein_coding	ENSG00000169439
P2RY13	-3.759	9.349E-04	6.931E-02	2764	2	protein_coding	ENSG00000181631
MS4A1	-3.759	2.578E-04	2.893E-02	3475	7	protein_coding	ENSG00000156738
PIEZO2	-3.749	1.679E-03	9.788E-02	9356	54	protein_coding	ENSG00000154864
FLRT2	-3.739	5.395E-04	4.810E-02	7943	5	protein_coding	ENSG00000185070
LUM	-3.729	5.324E-04	4.792E-02	3008	3	protein_coding	ENSG00000139329
LAMP3	-3.675	7.574E-04	5.899E-02	3375	6	protein_coding	ENSG00000078081
COL6A2	-3.662	1.015E-04	1.543E-02	3461	28	protein_coding	ENSG00000142173
ALDH1A3	-3.620	7.981E-04	6.108E-02	3924	13	protein_coding	ENSG00000184254
DES	-3.611	1.127E-03	7.998E-02	2248	9	protein_coding	ENSG00000175084
CXCR7	-3.602	6.066E-04	5.083E-02	2203	2	protein_coding	ENSG00000144476
RNA28S5	-3.602	1.072E-04	1.585E-02	432	1	pseudogene	ENSG00000226958

CX3CR1	-3.601	2.251E-04	2.625E-02	3255	2	protein_coding	ENSG00000168329
OLR1	-3.597	6.818E-05	1.180E-02	2460	6	protein_coding	ENSG00000173391
PDE4B	-3.587	7.323E-05	1.212E-02	4546	17	protein_coding	ENSG00000184588
CD36	-3.570	6.988E-05	1.194E-02	6179	17	protein_coding	ENSG00000135218
AQP1	-3.519	1.296E-03	8.509E-02	2752	10	protein_coding	ENSG00000240583
CCDC80	-3.476	1.869E-04	2.335E-02	4664	8	protein_coding	ENSG00000091986
COL1A1	-3.468	1.717E-04	2.246E-02	6727	51	protein_coding	ENSG00000108821
MT2A	-3.447	2.086E-04	2.510E-02	903	3	protein_coding	ENSG00000125148
COL3A1	-3.424	2.728E-04	3.023E-02	5543	51	protein_coding	ENSG00000168542
EREG	-3.423	4.796E-04	4.472E-02	4619	5	protein_coding	ENSG00000124882
ZNF331	-3.405	1.850E-04	2.328E-02	5042	7	protein_coding	ENSG00000130844
TIMP1	-3.392	3.652E-04	3.691E-02	1415	6	protein_coding	ENSG00000102265
COBLL1	-3.360	6.790E-04	5.482E-02	9367	17	protein_coding	ENSG00000082438
CCRN4L	-3.359	6.826E-04	5.494E-02	1767	3	protein_coding	ENSG00000151014
BANK1	-3.343	1.465E-03	9.086E-02	3544	21	protein_coding	ENSG00000153064
THBS1	-3.333	5.688E-04	4.907E-02	7775	22	protein_coding	ENSG00000137801
FLT1	-3.292	1.310E-03	8.509E-02	7084	30	protein_coding	ENSG00000102755
CD79A	-3.263	1.632E-03	9.644E-02	1258	5	protein_coding	ENSG00000105369
IL10	-3.238	6.324E-04	5.233E-02	1630	5	protein_coding	ENSG00000136634
FAM65B	-3.210	4.836E-04	4.493E-02	5471	23	protein_coding	ENSG00000111913
NLRP3	-3.187	3.814E-04	3.741E-02	4318	11	protein_coding	ENSG00000162711
COL6A1	-3.168	7.809E-04	5.993E-02	4238	35	protein_coding	ENSG00000142156
NAMPTL	-3.160	6.013E-04	5.059E-02	2514	2	protein_coding	ENSG00000229644
LRRK2	-3.149	6.470E-04	5.321E-02	9158	51	protein_coding	ENSG00000188906
WARS	-3.148	9.302E-04	6.919E-02	3092	12	protein_coding	ENSG00000140105
CASS4	-3.081	1.470E-03	9.086E-02	3155	7	protein_coding	ENSG00000087589
CFP	-3.053	8.285E-04	6.286E-02	4040	10	protein_coding	ENSG00000126759
GRASP	-2.994	1.031E-03	7.419E-02	1933	8	protein_coding	ENSG00000161835
FLNC	-2.985	1.560E-03	9.407E-02	9188	48	protein_coding	ENSG00000128591
BIRC3	-2.973	1.165E-03	8.075E-02	5197	10	protein_coding	ENSG00000023445
CXCR4	-2.952	1.014E-03	7.356E-02	1895	2	protein_coding	ENSG00000121966
EGR3	-2.928	1.530E-03	9.273E-02	4336	3	protein_coding	ENSG00000179388
CD300E	-2.915	1.191E-03	8.188E-02	3501	4	protein_coding	ENSG00000186407
PTGIS	-2.902	1.723E-03	9.934E-02	5579	10	protein_coding	ENSG00000124212
SAMSN1	-2.888	1.345E-03	8.624E-02	2185	9	protein_coding	ENSG00000155307
C5AR1	-2.885	1.395E-03	8.802E-02	2311	4	protein_coding	ENSG00000197405
LAPTM4B	3.085	1.726E-03	9.934E-02	3173	7	protein_coding	ENSG00000104341
CD24P4	3.107	1.431E-03	8.977E-02	243	1	pseudogene	ENSG00000185275
MSLN	3.118	1.479E-03	9.086E-02	2418	18	protein_coding	ENSG00000102854
EPB41L1	3.172	1.590E-03	9.513E-02	6266	22	protein_coding	ENSG00000088367
CLDN4	3.184	1.316E-03	8.509E-02	4163	4	protein_coding	ENSG00000189143
PLXNB1	3.289	5.579E-04	4.844E-02	7308	39	protein_coding	ENSG00000164050
SPP1	3.325	8.454E-04	6.378E-02	1664	8	protein_coding	ENSG00000118785
BMP7	3.394	1.503E-03	9.189E-02	4013	7	protein_coding	ENSG00000101144
EPPK1	3.408	6.124E-04	5.100E-02	7997	2	protein_coding	ENSG00000227184
CDH1	3.440	7.085E-04	5.601E-02	4875	16	protein_coding	ENSG00000039068
CTD-2314B22.3	3.456	1.521E-03	9.267E-02	4264	8	lincRNA	ENSG00000244306
RNF150	3.513	1.322E-03	8.509E-02	4535	8	protein_coding	ENSG00000170153
TRIM29	3.540	1.118E-03	7.956E-02	3328	10	protein_coding	ENSG00000137699
LCN2	3.559	1.478E-03	9.086E-02	1109	8	protein_coding	ENSG00000148346

PTPRU	3.577	6.505E-04	5.333E-02	5579	31	protein_coding	ENSG00000060656
SOX17	3.614	5.689E-04	4.907E-02	2342	2	protein_coding	ENSG00000164736
PCDH1	3.620	1.161E-03	8.073E-02	4530	5	protein_coding	ENSG00000156453
RIMS4	3.702	1.722E-03	9.934E-02	5203	6	protein_coding	ENSG00000101098
TMPRSS3	3.704	1.162E-03	8.073E-02	3193	13	protein_coding	ENSG00000160183
KCNK15	3.750	7.626E-04	5.905E-02	1320	2	protein_coding	ENSG00000124249
AIF1L	3.756	9.371E-04	6.931E-02	3515	7	protein_coding	ENSG00000126878
ELF3	3.760	2.287E-04	2.657E-02	4994	9	protein_coding	ENSG00000163435
AL589743.1	3.782	4.465E-04	4.238E-02	4676	8	lincRNA	ENSG00000225210
VWA1	3.810	3.200E-04	3.416E-02	4511	3	protein_coding	ENSG00000179403
ZBED2	3.902	1.646E-03	9.684E-02	2311	2	protein_coding	ENSG00000177494
TJP3	3.909	1.522E-03	9.267E-02	3350	21	protein_coding	ENSG00000105289
ARHGEF28	3.930	7.405E-04	5.802E-02	8285	37	protein_coding	ENSG00000214944
FRK	3.936	1.323E-03	8.509E-02	2849	8	protein_coding	ENSG00000111816
RIPK4	3.962	5.573E-04	4.844E-02	4017	9	protein_coding	ENSG00000183421
KRT7	3.964	6.634E-05	1.179E-02	1754	9	protein_coding	ENSG00000135480
SLPI	4.024	4.679E-05	9.021E-03	596	4	protein_coding	ENSG00000124107
LMO3	4.025	1.134E-03	8.007E-02	3759	7	protein_coding	ENSG00000048540
TMEM132B	4.030	1.722E-03	9.934E-02	10906	9	protein_coding	ENSG00000139364
NPR1	4.052	1.233E-04	1.755E-02	4236	22	protein_coding	ENSG00000169418
MLPH	4.110	1.004E-03	7.341E-02	3823	17	protein_coding	ENSG00000115648
GLDC	4.132	3.306E-04	3.474E-02	3767	25	protein_coding	ENSG00000178445
FMO2	4.141	1.654E-03	9.711E-02	5181	10	protein_coding	ENSG00000094963
KRT15	4.147	1.819E-04	2.304E-02	5237	10	protein_coding	ENSG00000171346
EPS8L1	4.166	4.242E-05	8.472E-03	2536	20	protein_coding	ENSG00000131037
CLDN7	4.186	5.967E-05	1.090E-02	1923	5	protein_coding	ENSG00000181885
CACNG4	4.213	7.599E-04	5.901E-02	3380	4	protein_coding	ENSG00000075461
TMEM125	4.233	5.121E-04	4.665E-02	1850	4	protein_coding	ENSG00000179178
ITGB4	4.264	3.049E-05	6.842E-03	5919	40	protein_coding	ENSG00000132470
RASIP1	4.265	6.706E-04	5.430E-02	3308	12	protein_coding	ENSG00000105538
FOXJ1	4.296	2.674E-04	2.976E-02	2641	3	protein_coding	ENSG00000129654
KCND2	4.312	1.712E-03	9.934E-02	5331	6	protein_coding	ENSG00000184408
TMC4	4.313	8.224E-05	1.328E-02	2412	15	protein_coding	ENSG00000167608
ADAM32	4.322	6.630E-04	5.402E-02	6871	25	protein_coding	ENSG00000197140
LRR1Q1	4.326	1.682E-03	9.788E-02	5394	27	protein_coding	ENSG00000133640
WNT11	4.343	5.773E-04	4.947E-02	1930	5	protein_coding	ENSG00000085741
TMEM45B	4.345	1.178E-03	8.126E-02	2234	6	protein_coding	ENSG00000151715
OGDHL	4.354	3.694E-04	3.691E-02	3704	23	protein_coding	ENSG00000197444
FLJ14082	4.362	1.196E-03	8.194E-02	3541	1	protein_coding	ENSG00000229689
BMPR1B	4.394	3.632E-04	3.691E-02	5567	13	protein_coding	ENSG00000138696
TCTEX1D1	4.432	1.389E-03	8.798E-02	2001	7	protein_coding	ENSG00000152760
CRTAC1	4.433	1.310E-03	8.509E-02	2890	15	protein_coding	ENSG00000095713
SLC27A6	4.435	1.218E-03	8.250E-02	3219	11	protein_coding	ENSG00000113396
SCNN1A	4.444	1.394E-05	4.025E-03	3545	13	protein_coding	ENSG00000111319
CDR2L	4.471	1.136E-04	1.644E-02	3536	5	protein_coding	ENSG00000109089
EPN3	4.502	3.054E-04	3.317E-02	4071	10	protein_coding	ENSG00000049283
RP11-156K13.1	4.518	1.152E-03	8.048E-02	510	2	antisense	ENSG00000253944
CP	4.551	5.471E-06	2.415E-03	4676	19	protein_coding	ENSG00000047457
FGF12	4.609	5.035E-04	4.629E-02	3058	6	protein_coding	ENSG00000114279
LINC00086	4.625	1.138E-03	8.010E-02	2913	2	lincRNA	ENSG00000178947

WBSR17	4.657	5.470E-04	4.828E-02	3884	11	protein_coding	ENSG00000185274
CPSF1P1	4.664	1.444E-03	9.021E-02	3730	1	pseudogene	ENSG00000214076
CTD-2114J12.1	4.679	2.052E-04	2.482E-02	1464	1	pseudogene	ENSG00000253525
AL035610.1	4.683	1.755E-04	2.256E-02	1754	5	lincRNA	ENSG00000232079
PNMA6D	4.686	5.541E-04	4.844E-02	1479	2	protein_coding	ENSG00000257088
CSPG5	4.713	1.017E-03	7.356E-02	4161	5	protein_coding	ENSG00000114646
FOXQ1	4.735	2.153E-04	2.556E-02	2318	1	protein_coding	ENSG00000164379
SOWAHA	4.738	1.249E-03	8.394E-02	3456	1	protein_coding	ENSG00000198944
SERPINA5	4.756	1.259E-03	8.421E-02	2312	7	protein_coding	ENSG00000188488
WFDC2	4.763	4.666E-06	2.331E-03	818	5	protein_coding	ENSG00000101443
DBNDD2	4.766	1.014E-03	7.356E-02	1537	4	protein_coding	ENSG00000244274
C10orf67	4.772	1.317E-03	8.509E-02	2799	9	protein_coding	ENSG00000179133
MYH14	4.794	6.507E-06	2.572E-03	6910	43	protein_coding	ENSG00000105357
CLGN	4.801	2.364E-04	2.722E-02	3043	16	protein_coding	ENSG00000153132
UGT2B7	4.805	1.540E-04	2.092E-02	1887	6	protein_coding	ENSG00000171234
GTSF1	4.807	5.127E-04	4.665E-02	1621	10	protein_coding	ENSG00000170627
LYPD1	4.846	1.575E-04	2.128E-02	1891	3	protein_coding	ENSG00000150551
ATP6V1B1	4.852	1.334E-05	3.958E-03	1905	14	protein_coding	ENSG00000116039
EMX2OS	4.856	1.775E-04	2.268E-02	1924	4	antisense	ENSG00000229847
TCN1	4.859	1.015E-03	7.356E-02	1582	9	protein_coding	ENSG00000134827
CPLX1	4.870	5.359E-04	4.794E-02	2181	5	protein_coding	ENSG00000168993
PDZK1IP1	4.894	9.263E-05	1.464E-02	846	5	protein_coding	ENSG00000162366
TMEM30B	4.904	9.618E-05	1.497E-02	4471	2	protein_coding	ENSG00000182107
DKK2	4.943	8.331E-04	6.303E-02	3638	6	protein_coding	ENSG00000155011
PRAME	4.947	1.232E-05	3.829E-03	2831	6	protein_coding	ENSG00000185686
AJAP1	4.950	3.410E-04	3.555E-02	2922	6	protein_coding	ENSG00000196581
KLRG2	4.966	5.325E-04	4.792E-02	2197	5	protein_coding	ENSG00000188883
NUS1P2	4.992	7.080E-04	5.601E-02	873	1	pseudogene	ENSG00000234685
C2orf54	5.011	1.258E-04	1.772E-02	2017	5	protein_coding	ENSG00000172478
TSPAN12	5.017	2.802E-05	6.548E-03	2796	9	protein_coding	ENSG00000106025
PNMA6A	5.024	1.092E-04	1.602E-02	2236	2	protein_coding	ENSG00000224201
FGF12-AS2	5.026	6.956E-04	5.582E-02	580	2	antisense	ENSG00000230126
RP6-109B7.2	5.030	4.451E-04	4.238E-02	1181	2	lincRNA	ENSG00000231010
RP3-439F8.1	5.065	3.656E-04	3.691E-02	2949	2	antisense	ENSG00000234869
PNMA6C	5.070	9.934E-05	1.529E-02	2255	2	protein_coding	ENSG00000235961
ADRA2C	5.113	5.150E-05	9.671E-03	2127	2	protein_coding	ENSG00000184160
LIX1	5.115	6.915E-05	1.189E-02	4023	6	protein_coding	ENSG00000145721
LINC00516	5.118	4.667E-04	4.382E-02	783	3	lincRNA	ENSG00000215394
VWA2	5.149	1.023E-04	1.543E-02	2875	14	protein_coding	ENSG00000165816
CYP4F31P	5.160	4.292E-04	4.133E-02	2249	5	protein_coding	ENSG00000178206
GPR39	5.162	3.299E-04	3.474E-02	2784	3	protein_coding	ENSG00000183840
EYA2	5.195	4.820E-06	2.360E-03	2702	16	protein_coding	ENSG00000064655
MUC4	5.200	9.173E-06	3.318E-03	17110	25	protein_coding	ENSG00000145113
LY6D	5.203	3.635E-04	3.691E-02	1423	3	protein_coding	ENSG00000167656
PCDHA13	5.209	3.366E-04	3.523E-02	5260	5	protein_coding	ENSG00000239389
ERBB4	5.217	1.204E-05	3.829E-03	12132	28	protein_coding	ENSG00000178568
NPTXR	5.236	6.355E-06	2.550E-03	5784	5	protein_coding	ENSG00000221890
SPINK5	5.238	3.445E-04	3.577E-02	3656	34	protein_coding	ENSG00000133710
MYOM3	5.249	1.030E-04	1.543E-02	5809	37	protein_coding	ENSG00000142661
RP11-1094H24.4	5.256	2.354E-04	2.722E-02	2533	3	processed_transcript	ENSG00000246640

UCA1	5.267	4.716E-05	9.021E-03	2313	3	processed_transcript	ENSG00000214049
AC012123.1	5.278	2.920E-04	3.208E-02	1661	4	protein_coding	ENSG00000228835
KLK6	5.280	4.902E-06	2.360E-03	1708	7	protein_coding	ENSG00000167755
IBSP	5.296	4.736E-05	9.021E-03	1033	7	protein_coding	ENSG00000029559
USH2A	5.300	3.134E-05	6.846E-03	18955	73	protein_coding	ENSG00000042781
CNTN3	5.311	1.276E-04	1.787E-02	4948	22	protein_coding	ENSG00000113805
KRT23	5.340	1.028E-05	3.491E-03	1987	9	protein_coding	ENSG00000108244
INHBB	5.365	1.161E-05	3.829E-03	3204	2	protein_coding	ENSG00000163083
RP11-296I10.5	5.379	2.175E-04	2.571E-02	106	1	pseudogene	ENSG00000261145
RP11-445F12.1	5.392	1.951E-04	2.392E-02	1462	4	antisense	ENSG00000255509
CTCFL	5.395	3.212E-05	6.846E-03	3996	12	protein_coding	ENSG00000124092
GJB3	5.397	2.328E-05	5.766E-03	2217	2	protein_coding	ENSG00000188910
VGLL1	5.412	4.955E-05	9.371E-03	1215	5	protein_coding	ENSG00000102243
RP3-416H24.1	5.415	1.921E-05	5.031E-03	1693	2	processed_transcript	ENSG00000257671
NTF3	5.415	1.722E-04	2.246E-02	1167	5	protein_coding	ENSG00000185652
CLIC5	5.443	1.411E-06	9.338E-04	2713	6	protein_coding	ENSG00000112782
HTR3A	5.456	2.828E-05	6.548E-03	2432	9	protein_coding	ENSG00000166736
FAM3B	5.520	6.730E-05	1.180E-02	2742	10	protein_coding	ENSG00000183844
TMEM132C	5.529	7.322E-05	1.212E-02	4947	9	protein_coding	ENSG00000181234
GRIN2A	5.529	1.564E-05	4.315E-03	9335	14	protein_coding	ENSG00000183454
EFHD1	5.536	9.288E-05	1.464E-02	2259	5	protein_coding	ENSG00000115468
HCN4	5.542	1.029E-04	1.543E-02	7228	8	protein_coding	ENSG00000138622
BCAM	5.543	3.957E-08	1.364E-04	2686	15	protein_coding	ENSG00000187244
BIK	5.556	1.620E-05	4.377E-03	953	5	protein_coding	ENSG00000100290
CLDN3	5.560	5.505E-07	5.335E-04	1273	1	protein_coding	ENSG00000165215
OVOL2	5.568	2.258E-05	5.743E-03	1555	4	protein_coding	ENSG00000125850
DNAH5	5.675	9.706E-06	3.382E-03	15633	79	protein_coding	ENSG00000039139
MAL	5.689	9.894E-07	7.705E-04	1108	4	protein_coding	ENSG00000172005
VSTM2L	5.710	3.244E-06	1.718E-03	1959	4	protein_coding	ENSG00000132821
CYP4F43P	5.726	6.541E-05	1.178E-02	2248	5	pseudogene	ENSG00000239402
SLC34A2	5.753	2.945E-08	1.300E-04	4122	13	protein_coding	ENSG00000157765
LINC00284	5.815	2.721E-05	6.434E-03	3208	5	lincRNA	ENSG00000233725
CYP4F30P	5.836	4.264E-05	8.472E-03	2250	5	pseudogene	ENSG00000214081
FOXA2	5.897	3.215E-05	6.846E-03	2422	3	protein_coding	ENSG00000125798
NLRP7	5.899	9.471E-06	3.344E-03	3826	13	protein_coding	ENSG00000167634
CLDN16	5.912	1.420E-07	2.350E-04	3273	5	protein_coding	ENSG00000113946
ALDH3B2	5.945	1.802E-06	1.136E-03	2649	10	protein_coding	ENSG00000132746
MYT1	6.027	2.554E-05	6.205E-03	5614	23	protein_coding	ENSG00000196132
ST6GALNAC1	6.068	8.446E-07	6.777E-04	2657	10	protein_coding	ENSG00000070526
DCDC2	6.077	2.099E-07	2.647E-04	4707	10	protein_coding	ENSG00000146038
DCHS2	6.108	1.495E-05	4.166E-03	8912	25	protein_coding	ENSG00000197410
AP000525.1	6.203	1.053E-05	3.530E-03	633	1	protein_coding	ENSG00000206252
ZFP57	6.305	7.499E-06	2.852E-03	1980	6	protein_coding	ENSG00000204644
IRX3	6.479	2.884E-06	1.559E-03	2601	4	protein_coding	ENSG00000177508
KLK5	6.506	3.785E-09	2.506E-05	1563	7	protein_coding	ENSG00000167754
PROM1	6.536	4.847E-07	4.936E-04	4349	28	protein_coding	ENSG00000007062
WNT9A	6.553	4.780E-07	4.936E-04	3971	4	protein_coding	ENSG00000143816
MAGEA11	6.588	2.258E-06	1.329E-03	3370	7	protein_coding	ENSG00000185247
GLDCP1	6.594	1.695E-06	1.094E-03	2678	1	pseudogene	ENSG00000248590
PI3	6.647	1.307E-06	9.084E-04	577	3	protein_coding	ENSG00000124102

CKMT1B	6.664	1.782E-07	2.430E-04	2396	10	protein_coding	ENSG00000237289
NTN4	6.676	4.205E-08	1.364E-04	3615	11	protein_coding	ENSG00000074527
C1orf172	6.690	3.383E-07	3.733E-04	1793	4	protein_coding	ENSG00000175707
KRT4	6.725	2.632E-07	3.169E-04	2576	10	protein_coding	ENSG00000170477
POU2F3	6.734	1.627E-07	2.430E-04	3013	14	protein_coding	ENSG00000137709
SLC9A2	6.737	5.323E-08	1.364E-04	5410	12	protein_coding	ENSG00000115616
XDH	6.746	1.311E-07	2.315E-04	5688	36	protein_coding	ENSG00000158125
PRSS22	6.765	1.211E-07	2.290E-04	1386	6	protein_coding	ENSG00000005001
LHX1	7.095	5.667E-08	1.364E-04	4121	5	protein_coding	ENSG00000132130
AC141928.1	7.147	1.835E-07	2.430E-04	4525	2	processed_transcript	ENSG00000250986
SLC4A11	7.226	2.930E-09	2.506E-05	3229	20	protein_coding	ENSG00000088836
CBLC	7.243	7.857E-09	4.161E-05	1579	11	protein_coding	ENSG00000142273
BTC	7.264	5.497E-08	1.364E-04	2816	6	protein_coding	ENSG00000174808
POTEC	7.313	7.628E-08	1.576E-04	6556	11	protein_coding	ENSG00000183206
C1orf116	7.882	1.765E-10	2.337E-06	5493	4	protein_coding	ENSG00000182795
WNT7A	8.054	3.440E-11	9.110E-07	4041	4	protein_coding	ENSG00000154764

Table S2. Frequencies (in percent) of cell populations as analyzed with FC. A: filtrate from ascites, S_AC: spheroids from ascites, P: ovarian tumor tissue, M: peritoneal tumor tissue.

Patient	12	13	16	21	22	24	25	27	28	29	30	31	35	41	42	53	54
A_Alive	85.600	96.800	80.900	94.900	81.100	89.200	92.500		78.000	99.400				99.800	96.800		99.700
A_C45n	73.900	45.600	56.200	32.600	89.800	29.600	56.500		31.900	24.100				86.700	32.500		31.300
A_C45p	26.100	54.400	43.800	67.400	10.200	70.400	43.500		68.100	75.900				13.300	67.500		68.700
A_C44pC45n	37.500	9.580	14.000	21.200	65.500	16.600	35.900		13.100	16.800				45.500	23.000		13.600
A_C133pC45n	0.421	0.662	3.560	0.359	1.630	0.202	0.119		0.141	0.152				0.260	0.574		0.255
A_L1pC45n	0.105	1.300	0.628	0.285	54.600	0.078	0.011		0.154	0.218				0.029	0.400		0.449
A_EpC45n	3.250	1.750	4.750	9.520	59.600	2.560	0.941		2.400	0.131				2.980	4.090		7.480
A_EpC133pC44n	0.332	0.678	1.170	0.152	0.069	0.340	0.153		0.160	0.317				0.000	0.329		0.098
A_EpC133pC44p	0.111	0.387	2.190	0.379	1.540	0.227	0.019		0.120	0.000				0.007	1.260		0.424
A_EpC133nC44p	3.000	0.484	0.447	18.600	64.100	4.950	1.210		2.730	0.090				1.070	4.410		5.740
A_EpC133nC44n	0.948	2.300	0.936	10.000	0.577	3.100	0.287		4.490	0.136				2.360	6.560		17.700
A_EpL1pC44n	0.047	0.581	0.140	0.152	0.247	0.038	0.000		0.160	0.181				0.000	0.710		0.424
A_EpL1pC44p	0.032	0.266	0.084	0.417	57.200	0.189	0.000		0.201	0.000				0.000	0.208		0.131
A_EpL1nC44p	3.080	0.605	2.560	18.500	8.490	4.990	1.220		2.610	0.090				1.130	5.470		6.040
A_EpL1nC44n	1.230	2.400	1.970	10.000	0.398	3.400	0.440		4.530	0.271				2.310	6.180		17.300
A_EpC133pL1n	0.079	0.823	3.320	0.303	56.000	0.189	0.000		0.361	0.045				0.007	0.814		0.489
A_EpC133pL1p	0.000	0.121	0.014	0.265	1.500	0.038	0.000		0.000	0.136				0.000	0.104		0.065
A_EpC133nL1p	0.474	0.993	0.223	0.379	0.288	0.530	0.172		0.361	0.226				0.000	1.510		0.489
A_EpC133nL1n	3.820	1.910	1.190	28.200	8.600	7.870	1.490		6.780	0.136				3.440	10.100		22.900
A_EnC45n	70.700	43.800	51.400	23.100	30.200	27.100	55.600		29.500	23.900				83.700	28.400		23.800
A_EnC133pC44n	0.079	0.266	0.419	0.152	0.069	0.076	0.038		0.080	0.226				0.127	0.104		0.163
A_EnC133pC44p	0.000	0.024	0.000	0.076	0.027	0.000	0.000		0.000	0.000				0.233	0.017		0.033
A_EnC133nC44p	46.600	20.100	10.100	46.600	6.990	50.500	61.500		37.400	69.900				47.300	64.700		41.200
A_EnC133nC44n	48.900	75.800	40.900	24.000	26.600	40.800	36.800		55.000	29.300				48.900	22.600		34.700
A_EnL1pC44n	0.032	0.218	0.293	0.000	0.179	0.000	0.000		0.040	0.498				0.007	0.208		0.718

A_EnL1pC44p	0.016	0.024	0.000	0.038	2.200	0.038	0.000		0.040	0.181				0.027	0.035		0.000
A_EnL1nC44p	46.600	20.100	11.200	46.700	4.820	50.500	61.500		38.100	69.700				47.500	64.700		37.500
A_EnL1nC44n	48.900	75.800	39.900	24.100	26.500	41.000	36.900		54.300	29.000				49.000	22.500		37.900
A_EnC133pL1n	0.047	0.218	0.419	0.000	2.360	0.038	0.000		0.080	0.543				0.033	0.242		0.783
A_EnC133pL1p	0.000	0.024	0.000	0.038	0.014	0.000	0.000		0.000	0.136				0.000	0.017		0.000
A_EnC133nL1p	0.095	0.291	0.363	0.265	0.082	0.113	0.057		0.080	0.136				0.360	0.104		0.228
A_EnC133nL1n	95.500	95.600	50.600	70.500	31.200	91.200	98.300		92.300	98.600				96.200	87.100		75.100
A_CD44pEp	3.111	0.871	2.637	18.979	65.640	5.177	1.229		2.850	0.090				1.077	5.670		6.164
A_CD44pEn	46.600	20.124	1.440	46.676	7.017	50.500	61.500		37.400	69.900				47.533	64.717		41.233
S_AC_Alive		97.100	91.100	99.800	96.900	89.900	98.800		69.700					99.800	96.700		99.800
S_AC_C45n		93.200	95.700	95.800	98.100	88.400	87.400		91.600					82.300	62.900		92.900
S_AC_C45p		6.800	4.300	4.200	1.900	11.600	12.600		8.400					17.700	37.100		7.100
S_AC_C44pC45n		1.590	5.930	4.520	6.610	5.680	12.300		6.140					13.700	23.300		3.980
S_AC_C133pC45n		3.420	8.860	3.330	1.330	2.610	0.921		0.215					0.306	11.700		3.310
S_AC_L1pC45n		2.440	1.100	0.822	3.060	0.159	0.921		0.029					0.071	2.580		1.700
S_AC_EpC45n		4.300	9.260	20.500	9.880	13.000	2.890		8.230					9.840	24.000		13.400
S_AC_EpC133pC44n		1.250	2.820	2.260	0.924	1.380	0.670		0.000					0.164	2.790		0.914
S_AC_EpC133pC44p		0.155	5.580	0.429	0.231	0.992	0.239		0.016					0.035	14.700		1.250
S_AC_EpC133nC44p		0.254	0.139	1.170	5.970	3.180	1.100		1.240					1.980	8.620		1.590
S_AC_EpC133nC44n		2.960	0.730	17.500	2.950	9.110	1.290		7.730					9.780	12.100		10.700
S_AC_EpL1pC44n		0.960	0.295	0.468	0.975	0.000	0.239		0.000					0.026	2.200		0.385
S_AC_EpL1pC44p		0.254	0.070	0.195	1.510	0.000	0.431		0.000					0.009	0.475		0.096
S_AC_EpL1nC44p		0.188	5.650	1.400	4.680	4.100	0.910		1.210					2.010	22.900		2.740
S_AC_EpL1nC44n		3.200	3.250	19.300	2.900	10.600	1.720		7.780					9.910	12.700		11.300
S_AC_EpC133pL1n		0.983	7.930	0.429	1.860	0.000	0.383		0.000					0.207	2.260		0.385
S_AC_EpC133pL1p		0.596	0.382	0.273	0.629	0.000	0.287		0.000					0.009	0.416		0.096
S_AC_EpC133nL1p		0.916	0.139	2.850	0.603	2.550	0.670		0.016					0.043	17.500		2.260

S_AC_EpC133nL1n		2.120	0.817	17.800	6.980	12.100	1.960		8.970					11.700	18.100		11.700
S_AC_EnC45n		88.900	86.500	75.300	88.200	75.400	84.500		83.400					72.400	38.900		79.400
S_AC_EnC133pC44n		1.820	1.230	0.390	0.128	0.293	0.048		0.141					0.095	0.178		0.866
S_AC_EnC133pC44p		0.000	0.017	0.000	0.000	0.000	0.048		0.078					0.000	0.059		0.192
S_AC_EnC133nC44p		1.440	0.070	2.180	0.398	1.870	12.500		5.290					14.900	13.100		5.960
S_AC_EnC133nC44n		92.100	85.200	76.000	89.400	83.200	84.100		85.500					73.000	48.400		78.500
S_AC_EnL1pC44n		0.243	0.487	0.000	0.116	0.113	0.239		0.000					0.026	0.832		0.962
S_AC_EnL1pC44p		0.000	0.000	0.000	0.000	0.000	0.096		0.000					0.000	0.000		0.000
S_AC_EnL1nC44p		1.390	0.139	2.180	0.398	1.870	12.500		5.500					14.700	13.200		1.640
S_AC_EnL1nC44n		93.800	85.900	76.400	89.400	83.400	83.900		85.500					73.300	47.800		82.900
S_AC_EnC133pL1n		0.210	1.220	0.000	0.116	0.113	0.335		0.000					0.035	0.951		1.110
S_AC_EnC133pL1p		0.011	0.035	0.000	0.000	0.000	0.000		0.000					0.000	0.000		0.000
S_AC_EnC133nL1p		2.010	0.504	0.429	0.154	0.316	0.096		0.219					0.164	0.297		1.150
S_AC_EnC133nL1n		93.200	84.700	78.200	89.700	84.900	96.300		90.800					87.800	60.500		83.300
S_AC_CD44pEp		0.409	5.719	1.599	6.201	4.172	1.339		1.256					2.015	23.320		2.840
S_AC_CD44pEn		1.440	4.697	2.180	0.398	1.870	12.548		5.368					14.900	13.159		6.152
P_Alive	94.200		97.800		99.000	94.900	98.300	95.700		99.000	99.700			100.000		99.100	
P_C45n	98.600		90.100		97.400	97.800	95.100	51.800		85.600	92.900			87.800		87.400	
P_C45p	1.400		9.900		2.600	2.200	4.900	48.200		14.400	7.100			12.200		12.600	
P_C44pC45n	9.091		14.776		52.693	4.910	14.360	7.200		14.466	4.608			26.516		20.277	
P_C133pC45n	0.000		1.225		3.204	0.640	0.000	2.471		1.130	0.090			0.000		0.435	
P_L1pC45n	0.043		5.460		0.425	0.201	0.244	1.678		1.464	0.985			0.119		0.678	
P_EpC45n	39.046		38.383		28.343	65.722	40.322	15.954		2.893	9.476			29.325		31.551	
P_EpC133pC44n	0.100		0.377		0.840	0.507	1.120	4.480		0.564	0.495			0.209		0.037	
P_EpC133pC44p	0.044		0.890		2.190	0.111	0.167	3.410		0.113	0.365			0.062		0.251	
P_EpC133nC44p	1.690		11.400		6.990	2.140	2.160	14.700		1.500	1.510			5.100		6.460	
P_EpC133nC44n	38.300		34.600		19.900	65.900	41.200	37.000		1.770	8.650			32.600		34.600	

P_EpL1pC44n	0.033		3.360		0.063	0.049	0.103	3.080		0.338	0.443			0.000		0.429	
P_EpL1pC44p	0.011		2.350		0.190	0.000	0.013	1.760		0.263	0.261			0.031		0.266	
P_EpL1nC44p	1.720		9.410		8.430	2.190	2.310	16.300		1.350	1.620			5.140		6.440	
P_EpL1nC44n	38.400		32.200		21.200	66.400	42.200	38.400		1.990	8.700			32.900		34.200	
P_EpC133pL1n	0.033		4.810		0.127	0.049	0.077	3.310		0.527	0.521			0.031		0.562	
P_EpC133pL1p	0.011		0.302		0.127	0.049	0.039	1.530		0.188	0.182			0.000		0.133	
P_EpC133nL1p	0.167		1.150		3.350	0.594	1.430	6.970		0.489	0.860			0.302		0.362	
P_EpC133nL1n	40.000		41.000		26.300	68.000	43.100	47.700		2.750	9.460			37.700		40.300	
P_EnC45n	59.000		47.500		68.300	30.700	52.600	21.000		82.200	82.600			54.400		51.300	
P_EnC133pC44n	0.022		0.000		0.034	0.049	0.077	0.324		0.827	0.521			0.186		0.007	
P_EnC133pC44p	0.000		0.015		0.007	0.000	0.000	0.106		0.000	0.000			0.101		0.000	
P_EnC133nC44p	7.180		5.290		43.500	2.890	13.000	9.190		17.900	3.200			14.000		18.800	
P_EnC133nC44n	52.600		47.400		26.600	28.400	42.200	30.800		77.300	85.300			47.700		39.800	
P_EnL1pC44n	0.000		0.090		0.004	0.000	0.064	0.037		0.527	0.182			0.000		0.007	
P_EnL1pC44p	0.000		0.015		0.000	0.000	0.000	0.016		0.075	0.000			0.000		0.015	
P_EnL1nC44p	7.290		5.380		43.000	2.890	13.000	9.280		17.900	3.200			14.100		18.800	
P_EnL1nC44n	52.500		47.200		27.100	28.400	42.300	31.100		77.600	85.600			47.800		39.800	
P_EnC133pL1n	0.000		0.106		0.004	0.000	0.077	0.048		0.527	0.182			0.000		0.022	
P_EnC133pL1p	0.000		0.000		0.000	0.000	0.000	0.005		0.038	0.000			0.000		0.000	
P_EnC133nL1p	0.022		0.060		0.022	0.025	0.128	0.477		0.827	0.599			1.110		0.015	
P_EnC133nL1n	59.800		52.500		70.100	31.300	55.200	39.900		94.700	88.200			60.900		58.600	
P_CD44pEp	1.734		12.290		9.180	2.251	2.327	18.110		1.613	1.875			5.162		6.711	
P_CD44pEn	7.180		5.305		43.507	2.890	13.000	9.296		17.900	3.200			14.101		18.800	
M_Alive	99.600		99.800	95.700	99.600	94.600	98.400		99.300	99.500	95.900	96.100	95.000			99.100	98.700
M_C45n	86.800		93.900	83.000	80.900	94.900	94.300		88.400	65.900	91.500	67.800	59.500			73.600	93.300
M_C45p	13.200		6.100	17.000	19.100	5.100	5.700		11.600	34.100	8.500	32.200	40.500			26.400	6.700
M_C44pC45n	54.337		84.510	24.402	34.383	3.578	4.225		18.299	8.106	21.045	8.678	24.336			27.011	1.950

M_C133pC45n	0.000		0.015	0.880	0.000	1.433	3.272		4.155	0.407	0.029	1.797	0.164			0.277	1.502
M_L1pC45n	0.138		0.164	0.156	0.544	0.379	0.775		2.016	0.347	1.427	1.837	0.164			1.546	0.574
M_EpC45n	9.288		2.563	22.576	12.459	42.136	35.834		20.597	7.513	49.502	8.814	3.064			10.893	32.748
M_EpC133pC44n	0.049		0.006	0.573	0.507	1.050	2.280		1.880	0.342	0.424	0.819	0.063			0.111	0.799
M_EpC133pC44p	0.012		0.006	0.322	0.386	0.319	0.402		1.700	0.183	0.580	1.143	0.147			0.085	0.330
M_EpC133nC44p	6.030		0.642	8.910	5.580	1.110	2.900		11.400	2.510	4.760	6.090	2.250			2.570	0.456
M_EpC133nC44n	6.220		2.250	23.000	12.600	44.300	34.700		11.400	14.200	51.400	10.500	6.210			17.300	36.000
M_EpL1pC44n	0.085		0.079	0.084	0.212	0.140	0.308		0.999	0.228	0.063	0.875	0.105			1.690	0.266
M_EpL1pC44p	0.049		0.062	0.036	0.174	0.025	0.094		0.279	0.160	0.182	0.956	0.105			0.434	0.025
M_EpL1nC44p	6.000		0.575	9.200	5.510	1.390	3.210		13.000	2.580	6.140	6.220	2.290			2.220	0.761
M_EpL1nC44n	6.180		2.190	23.500	13.200	45.200	36.700		12.100	14.300	51.800	10.500	6.170			15.700	36.600
M_EpC133pL1n	0.122		0.130	0.060	0.182	0.140	0.295		1.070	0.388	0.118	1.040	0.147			2.010	0.266
M_EpC133pL1p	0.000		0.000	0.072	0.204	0.051	0.148		0.488	0.068	0.120	0.916	0.063			0.119	0.025
M_EpC133nL1p	0.073		0.011	1.050	1.110	1.610	2.780		3.950	0.479	2.080	2.100	0.252			0.179	1.220
M_EpC133nL1n	12.100		2.760	31.600	17.600	45.000	37.000		20.800	16.300	55.800	14.600	8.200			17.800	36.100
M_EnC45n	76.100		91.200	55.800	65.500	50.500	56.300		65.100	54.500	37.400	54.800	54.300			58.800	58.200
M_EnC133pC44n	0.037		0.006	0.227	0.303	0.140	0.188		0.325	0.297	0.042	0.614	0.000			0.153	0.241
M_EnC133pC44p	0.000		0.000	0.000	0.030	0.000	0.000		0.046	0.046	0.000	0.000	0.000			0.000	0.051
M_EnC133nC44p	64.900		94.900	20.700	43.500	2.540	1.220		10.600	15.600	17.700	12.000	66.100			46.600	13.600
M_EnC133nC44n	22.700		2.160	46.300	37.100	50.600	58.300		62.700	66.800	23.100	68.200	25.300			33.100	48.500
M_EnL1pC44n	0.012		0.000	0.036	0.038	0.051	0.107		0.465	0.228	0.028	0.168	0.021			0.034	0.342
M_EnL1pC44p	0.012		0.000	0.000	0.008	0.000	0.000		0.000	0.023	0.000	0.056	0.042			0.051	0.000
M_EnL1nC44p	65.400		95.000	20.300	42.600	2.540	1.220		10.700	15.700	17.700	11.700	66.000			46.600	1.370
M_EnL1nC44n	22.300		2.060	46.900	38.300	50.700	58.400		62.500	66.800	23.100	69.000	25.200			33.200	60.700
M_EnC133pL1n	0.037		0.000	0.036	0.045	0.038	0.107		0.465	0.228	0.028	0.223	0.063			0.085	0.342
M_EnC133pL1p	0.000		0.000	0.000	0.000	0.000	0.000		0.000	0.000	0.000	0.000	0.000			0.000	0.000
M_EnC133nL1p	0.037		0.006	0.227	0.212	0.076	0.255		0.511	0.388	0.049	0.726	0.021			0.187	0.342

M_EnC133nL1n	87.600		97.100	67.000	80.700	53.100	59.400		72.700	82.100	40.800	79.900	91.300			79.600	61.700
M_CD44pEp	6.042		0.648	9.232	5.966	1.429	3.302		13.100	2.693	5.340	7.233	2.397			2.655	0.786
M_CD44pEn	64.900		94.900	20.700	43.530	2.540	1.220		10.646	15.646	17.700	12.000	66.100			46.600	13.651

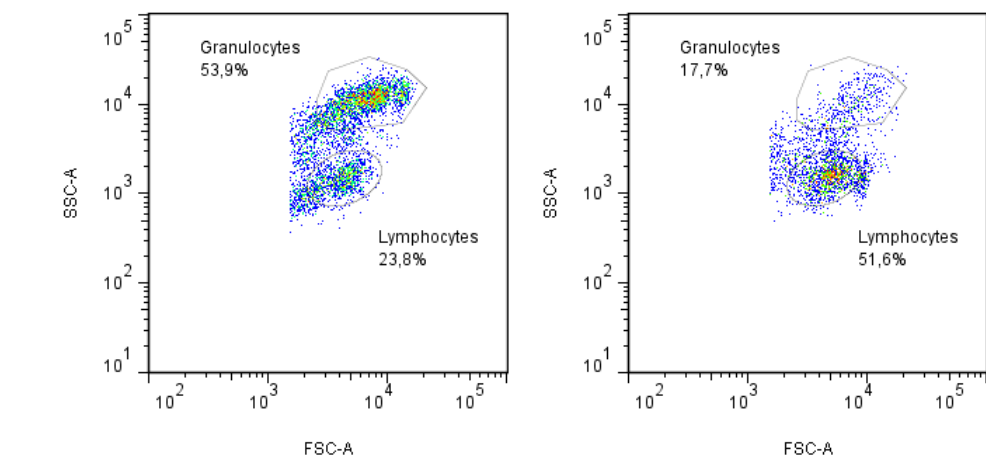


Figure S1 FC pseudo-color plots of peripheral blood mononuclear cell (left) and ascites (right) samples. According to the typical appearance in the FSC-SSC plot lymphocytes in ascites can be separated from granulocytes via gates set up with PBMCs.

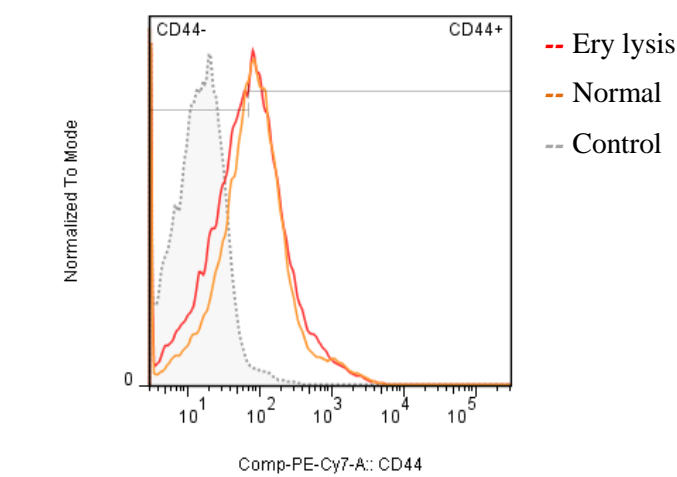


Figure S2 FC histogram comparing CD44+ cell populations of ascites before and after lysis of erythrocytes. Both samples were stained for CD44, control: unstained.

9 Acknowledgements

Many people contributed to the success of this study, my master thesis, and the ongoing project. At first I want to thank Robert Zeillinger for the possibility to work in his laboratory and for providing me with scientific support.

A very special thanks to my supervisor Dietmar Pils, who guided and provided me with everything I needed. Never would I have been able to analyze even one bit or interpret the immense amount of scientific data without his expertise and help in bioinformatics and statistics, and all the hours of fruit-full discussions.

Also, I want to thank my colleagues at the Molecular Oncology Group for the outstanding working atmosphere and the friendly collaborations. Especially, I want to thank Anna Bachmayr-Heyda, Agnes Reiner and Stefanie Aust, each of you has provided me with valuable insights into this project, helped me with the manuscript, and has enriched my time here in a way words cannot express.

Furthermore my dearest appreciation goes to my whole family, my parents Erich and Sylvia, my sisters Johanna, Martina, and Birgit and all of my friends. Special thanks to Rolf for his patience and loving support.

Without all of you this would not have been possible!

10 Abstract

Epithelial ovarian cancer is the leading cause of death from gynecological malignancies in the western world. Reasons for the low 5-year survival rate include diagnosis at advanced stages due to missing or unclear symptoms, massive intraperitoneal tumor load, and chemotherapy resistance after relapse, although initial response to platinum-based therapy is about 80%. Therefore it is of importance to subdivide patients suffering from EOC into subclasses, according to chemotherapy-response, but also other factors including gene mutations to provide the appropriate treatment. The aim of this project was a comprehensive characterization of patients' biomaterials including analysis of expression and frequency of known (tumor) cell markers, to find connections between cell populations and modes of peritoneal tumor spread or other subclasses. Of special interest was the characterization of cell populations in malignant ascites, build up from single cells and cellular aggregates, so called spheroids. To accomplish this, a six-color flow cytometry panel was set up and successfully tested, allowing for simultaneous analysis of the surface markers CD45, EpCAM, CD44, CD133, and L1CAM in each sample. Resulting frequencies of cell population in ascites and tumor tissues were correlated with different peritoneal implantation patterns, including i) miliary and planar tumor spread and ii) no or few, but bigger exophytic and nodular growing implants. The population of cells expressing CD44 was shown to be associated with the subtype of no/few big tumor implants. Furthermore, transcriptome analysis using RNA sequencing and biostatistical methods revealed 460 genes differentially expressed between the different modes of tumor spread, consisting of 180 up- and 280 down-regulated genes in patients with miliary tumor spread. Many of these genes could be annotated to pathways associated with cell adhesion and interaction with extracellular matrix. Moreover, a previously defined molecular subclassification using 112 genes in patients with different overall and progression free survival could be validated in this study, based on expression profiles of eight patients. The new subclassification of patients according to the mode of peritoneal tumor spread does not overlap the more recent molecular subclassification. Both, FC and whole transcriptome data demonstrate the molecular differences of the newly defined subclasses of serous EOC and implications for patients' outcome will be seen in the future.

11 Zusammenfassung

Das epitheliale Ovarialkarzinom ist für die höchste Mortalitätsrate innerhalb von gynäkologischen Krebserkrankungen in der westlichen Welt verantwortlich. Der Hauptgrund dafür ist, dass Eierstockkrebs, aufgrund fehlender Symptomatik in frühen Stadien, oft erst spät erkannt wird und daher meist mit einem ausgeprägten Tumorbefall des Peritoneums bei der Erstdiagnose einhergeht. Ein vielversprechender Ansatz, um Patientinnen optimal behandeln zu können, beziehungsweise neue Therapieansätze zu schaffen, ist die Unterteilung der serös-papillären Ovarialkarzinome in unterschiedliche Subklassen. Diese Einteilung kann im Hinblick auf die Reaktion auf Chemotherapie, aber auch aufgrund anderer Faktoren, wie zum Beispiel der zugrundeliegenden Genmutation, geschehen. Die Grundidee für diese Studie war die möglichst umfassende Charakterisierung von Patientenbiomaterial inklusive der Analyse von Expression und Häufigkeit verschiedener, bekannter (Tumor-) Zellmarker. Insbesondere der zelluläre Anteil der malignen Bauchraumflüssigkeit (Aszites), der sowohl von freischwimmenden Einzelzellen als auch aus aggregierten Tumorzellhaufen, sogenannten Sphäroiden, gebildet wird, wurde genau untersucht. Dazu wurde ein Sechs-Farben-Durchflusszytometrie-Panel entwickelt, mit dem die gleichzeitige Bestimmung der Oberflächenmarker CD45, EpCAM, CD44, CD133 und L1CAM in einer Probe möglich ist. Resultierende Häufigkeiten bestimmter Zellen in den beiden Aszitesfraktionen, sowie im Tumorgewebe, wurden in Folge mit unterschiedlichen Ausbreitungsmustern des Tumors in der Peritonealhöhle, entweder als miliare, über den Bauchraum verteilten, oder wenigen, dafür ausgeprägten Tumorabsiedelungen, korreliert. Unter anderem konnte so ein Zusammenhang zwischen einer Population CD44 positiver Zellen und wenigen, ausgeprägten Absiedelungen, gezeigt werden. Eine zusätzliche Analyse des Transkriptoms mit RNA-Seq und verschiedenen biostatistischen Methoden offenbarte 460 differentiell exprimierte Gene zwischen den beiden Ausbreitungsmustern des Tumors, davon 180 hoch- und 280 runterreguliert im miliaren Subtyp. Viele dieser Gene konnten Genclustern zugeordnet werden, die mit der Interaktion mit extrazellulären Matrixproteinen oder Zelladhäsion assoziiert werden. Außerdem konnte eine zuvor publizierte, molekulare Subklassifizierung basierend auf 112 Genen, in dieser Studie anhand von Genexpressionsprofilen von 8 Patientinnen, nachgewiesen werden. Die neue Subklassifizierung, basierend auf dem intraperitonealen Ausbreitungsmuster des Tumors, überlappt aber nicht mit der vorherigen. Sowohl durchflusszytometrische als auch Transkriptomdaten zeigen molekulare Unterschiede zwischen den neu definierten Subklassen serös-papillärer Ovarialkarzinome. Was dies für das Gesamtüberleben oder dem progressionsfreien Überleben von Patientinnen mit Eierstockkrebs bedeutet, wird sich in den kommenden Jahren zeigen.

12 Curriculum vitae

Personal data

Name: Katharina Auer
Date and place of birth: April 25th 1988, Tamsweg, Salzburg
Nationality: Austrian

Education

2012-2013 **Master thesis** at the Molecular Oncology Group,
Department of Obstetrics and Gynecology, Medical
University of Vienna, Austria
Since 2011 **Master studies** in Genetics and Developmental
Biology, University of Vienna, Austria
2008-2012 **Bachelor studies** in Microbiology and Genetics,
University of Vienna, Austria
2006-2008 **Studies** in Biology, University of Vienna, Austria
2002-2006 **BORG Spittal/Drau**, Austria
Grammar school, focused on science
1998-2002 **BG Porcia**, Spittal/Drau, Austria
Grammar school, focused on languages

Working experience

2011 **Project Employee**. MFPL group Waldsich
2010-2012 **Tutor** in students' laboratory exercises:
Molecular Biology laboratory work, Biochemistry,
Microbiology and Genetics, University of Vienna

Prize

Presentation Award Peritoneal Cavity: the Achilles' Heel for Ovarian Can-
cer, Characterization of Tumor Cells in the Peritoneum,
YSA 2013